INFLUENCE OF PRE-SWIRL AND ECCENTRICITY IN SMOOTH STATOR/GROOVED ROTOR LIQUID ANNULAR SEALS, MEASURED STATIC AND ROTORDYNAMIC CHARACTERISTICS

A Thesis

by

JAMES ALEXANDER MORELAND

Submitted to the Office of Graduate and Professional Studies of
Texas A&M University
in partial fulfillment of the requirements for the degree of

MASTER OF SCIENCE

Chair of Committee,	Dara W. Childs
Committee Members,	Alan Palazzolo
	Lynn Beason
Head of Department,	Andreas Polycarpou

August 2016

Major Subject: Mechanical Engineering

ABSTRACT

Circumferential grooves are machined into the rotor surface of liquid annular seals to reduce leakage. Analyses in the literature regarding rotordynamic coefficients for smooth stator/grooved rotor (SS/GR) seals are scarce, and measured results are absent despite the significant effect of these annular seals on pump rotordynamics. Furthermore, few annular seal test rigs can impose and measure pre-swirl. Consequently, this study aims to quantify the effect of pre-swirl and operating static eccentricity on measured static and dynamic characteristics of the SS/GR seal.

The test seal has a nominal minimum radial clearance of C_r = 203.2 μm (8 mil) and the length-to-diameter ratio of L/D = 0.5. The rotor surface has 15 square grooves with a depth of 1.524 mm (60 mils). This geometry is based on measured dimensions in an Electrical Submersible Pump. The author conducts tests at speeds of 2, 4, 6, and 8 krpm, axial pressure drops of 2.07, 4.14, 6.21, and 8.27 bar (30, 60, 90, and 120 psi), and eccentricity ratios up to ε_0 = 0.80. Pre-swirl is imposed and varied over low, medium, and high values. The lubricant is ISO VG 2 oil at 46.1°C (115°F) to ensure turbulent flow at all operating conditions. Measured grooved seal results are compared to results of a smooth seal of equal length, diameter, and nominal clearance. Note that no published predictions for this seal exist, precluding measurement-versus-prediction comparisons.

Static measurements include leakage rate, applied static load, eccentric position, pre-swirl ratio (PSR), and outlet swirl ratio (OSR). At 2 krpm and 8.27 bar, the SS/GR

seal leakage rate is lower than the smooth seal by a factor of 0.7 for a total reduction of 19 LPM. However, at high speeds and low pressures, grooved seal leakage is 0.8 to 0.9 times that of the smooth seal with reductions in leakage rate on the order of 2 LPM. Consequently, adding rotor grooves to restrict leakage is more advantageous at high pressure drops and low speeds. Outlet swirl is measured for the first time in a liquid-annular-seal test rig. Contrary to expectation, measured OSR is generally lower than 0.5, possibly due to the axial and radial location of the pitot tube within the outlet chamber.

Dynamic measurements include rotor-stator relative displacement, stator acceleration, and applied dynamic excitations. The author calculates dynamic-stiffness values, rotordynamic coefficients, whirl frequency ratio, and effective damping. Most notable of the dynamic results is the negative direct stiffness of the SS/GR seal. Negative direct stiffness would have a detrimental effect on pump rotordynamics, lowering both the natural frequency and the onset speed of instability. Calculated whirl frequency ratio is generally high ($\geq$0.5) with values up to 1.2 for the grooved seal. Finally, effective damping is lower for the grooved seal than the smooth seal indicating that the SS/GR seal has worse stability characteristics than a comparable SS/SR seal.

Overall, increases in PSR have a detrimental effect on SS/GR seal rotordynamic performance leading to modest decreases in direct stiffness, increases in the magnitude of cross-coupled stiffness, and increases in whirl frequency ratio. Additionally, operation at high eccentricity ratios for the SS/GR seal has negative effects. Leakage increases, and direct stiffness decreases as eccentricity ratios approach 0.80.

ACKNOWLEDGEMENTS

First and foremost I would like to thank Dr. Dara Childs for the opportunity to research and pursue a M.S. degree through the Texas A&M Turbomachinery Laboratory and for his generous support throughout the project. Furthermore, I would like to thank Mr. Stephen Phillips for his insight and assistance troubleshooting problems with the test rig. Next I would like to extend thanks to Mr. Ray Matthews for his help in the machine shop and with heavy equipment operation. I would also like to thank Dr. Palazzolo and Dr. Beason for taking the time to be on my committee

Thanks are in order for a number of colleagues and friends from the Turbolab: Andrew, Jesse, Josh, Jennifer, Jose, Jimmy, Clay, Ivan, Patricio, Brian, Min, Matt, Tommy, Travis, Mauricio, Nathan, and Ovais. Not only did you selflessly provide assistance, but you also made the work enjoyable even in times of adversity. I would like to thank my parents for their support throughout this time.

Finally, I would like to thank our Father in Heaven through whom all good things come. It is by His strength alone that I was able to endure and succeed in my research endeavors.

NOMENCLATURE

$\boldsymbol{A_{ij}}$	Frequency domain stator acceleration [L/T^2]
B	Groove depth, illustrated in Fig. 5 [L]
C_{eff}	Seal effective damping [FT/L]
C_{ij}	Seal damping coefficients [FT/L]
C_r	Seal radial clearance [L]
D	Seal diameter [L]
$\boldsymbol{D_{ij}}$	Frequency domain stator displacement [L]
e_0	Static eccentricity [L]
e_{X0}, e_{Y0}	Static eccentricity in X and Y directions [L]
F_r	Fluid-film reaction force [F]
f_{rX}, f_{rY}	Seal reaction forces in X and Y directions [F]
F_s	Applied static load [F]
f_X, f_Y	Applied dynamic loads in X and Y directions [F]
$\boldsymbol{F_X}, \boldsymbol{F_Y}$	Frequency domain excitation forces in X and Y directions [F]
$\boldsymbol{H_{ij}}$	Frequency domain dynamic stiffness [F/L]
$\boldsymbol{j}$	Complex operator [-]
K_{eq}	Equivalent stiffness coefficient [F/L]
K_{ij}	Seal stiffness coefficients [F/L]
L	Seal axial length [L]

L_g	Groove axial length, illustrated in Fig. 5 [L]
L_l	Land axial length, illustrated in Fig. 5 [L]
M_{ij}	Seal virtual mass coefficients [M]
M_s	Stator mass [M]
$\dot{Q}$	Seal volumetric leakage rate [L^3/T]
R	Shaft radius [L]
Re_z	Axial Reynolds number, defined in Eq. (22) [-]
Re_θ	Circumferential Reynolds number, defined in Eq. (24) [-]
Re	Vector Reynolds number, defined in Eq. (25) [-]
u	Circumferential fluid velocity [L/T]
w	Axial fluid velocity [L/T]
$\ddot{X}_s, \ddot{Y}_s$	Stator accelerations in the X and Y directions [-]

Greek symbols

ΔP	Seal differential pressure [F/L^2]
$\Delta X, \Delta Y$	Rotor-stator relative displacement [L]
$\varepsilon_0 = e_0/C_r$	Static eccentricity ratio [-]
$\varepsilon_{X0}, \varepsilon_{Y0}$	Static eccentricity ratio in X and Y directions [-]
μ	Fluid dynamic viscosity [FT/L^2]
ρ	Fluid density [M/L^3]
ω	Rotor speed [1/T]
Ω	Excitation frequency [1/T]

Subscripts

g	Groove section
i, j	Interchangeable X and Y directions
l	Land section
X, Y	X and Y directions

Abbreviations

DE	Drive end
GS/SR	Grooved stator/smooth rotor
NDE	Non drive end
OSR	Outlet swirl ratio
PSR	Pre-swirl ratio
SS/GR	Smooth stator/grooved rotor
SS/SR	Smooth stator/smooth rotor
WFR	Whirl frequency ratio, defined in Eqs. (3)-(5)

TABLE OF CONTENTS

Page

LIST OF FIGURES

Page

LIST OF TABLES

Page

1. INTRODUCTION

Annular seals are non-contacting, mechanical elements designed to restrict the leakage rate, $\dot{Q}$, between two regions of differing pressure. Liquid, gas, and two-phase flow applications use annular seals. Common examples of liquid annular seals are neck-ring (wear-ring), interstage, and balance-piston seals in centrifugal pumps [1]. Flow within these seals, can be laminar, but is generally turbulent due to large axial pressure gradients and reduced viscosity fluids. Unlike bearings, with small clearance-to-radius ratios (C_r/R = 0.001), seals generally have larger clearance-to-radius ratios (C_r/R = 0.003-0.005) [1], [2].

Initially, these larger clearances and low-viscosity working fluids seemed to indicate that annular seals would act as very weak bearings [3]. However, this is not the case as flow is typically turbulent which generates higher effective viscosities. Additionally, inertia effects become important. Henry Black [4] was the first to adequately analyze the rotordynamic impact of annular seals and show their significant effect on pump rotordynamics.

The fluid film within the seal generates reaction forces by two means. The first method is through the hydrodynamic effect typically found in hydrodynamic bearings. This effect is driven by shear flow due to shaft rotation. When the rotor operates eccentrically from the annulus center, lubricant is dragged into a converging, high-pressure region and then passes into a diverging, low-pressure region. This difference in

the circumferential pressure distribution generates the fluid-film reaction force. Pinkus and Sternlicht [5] present a thorough discussion of this phenomenon.

Seals differ from bearings in that they generally have high axial flow rates and large axial pressure drops, ΔP. Fluid at a supply pressure, P_s, suddenly accelerates as it enters the annular clearance causing an inertial pressure drop. The remainder of the pressure drop occurs due to wall friction. Fluid exits the seal at pressure, P_e. Perturbation of the rotor from the centered position decreases the radial clearance on one side, while increasing it on the other. The larger clearance leads to higher $\dot{Q}$ and higher Reynolds numbers which decreases the friction factor. The opposite happens for the smaller clearance side. The resulting change in pressure distribution generates the restoring reaction force, F_r. This phenomenon is known as the Lomakin effect [6]. Figure 1 depicts the Lomakin effect.

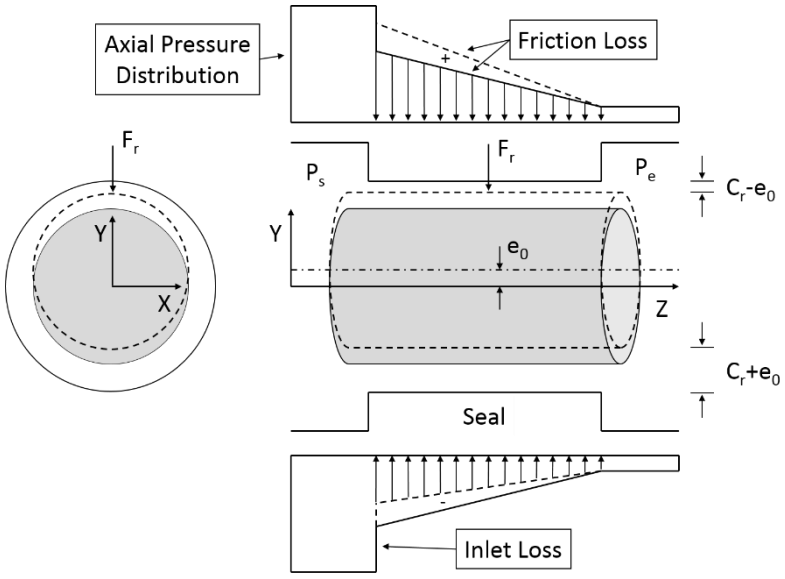

Figure 1. Depiction of centering force generation via the Lomakin effect.

The idealized mechanical elements shown in Fig. 2 represent the fluid-film reaction force. The stiffness coefficients, K_{ij}, are represented as springs while the damping coefficients, C_{ij}, are represented as dashpots. This traditional "KC" model neglects fluid inertia [7].

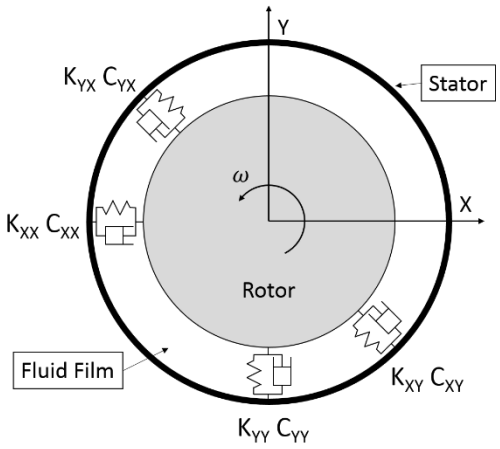

Figure 2. Physical representation of the fluid-film reaction force.

Childs [2] develops a finite-length, bulk-flow solution to express the fluid-film reaction forces in terms of the rotordynamic coefficients. The rotordynamic model represents the centered-seal, reaction forces as

$$-\begin{Bmatrix} f_{rX} \\ f_{rY} \end{Bmatrix} = \begin{bmatrix} K & k \\ -k & K \end{bmatrix} \begin{Bmatrix} \Delta X \\ \Delta Y \end{Bmatrix} + \begin{bmatrix} C & c \\ -c & C \end{bmatrix} \begin{Bmatrix} \Delta \dot{X} \\ \Delta \dot{Y} \end{Bmatrix} + \begin{bmatrix} M & m \\ -m & M \end{bmatrix} \begin{Bmatrix} \Delta \ddot{X} \\ \Delta \ddot{Y} \end{Bmatrix} \quad (1)$$

where f_{rX} and f_{rY} are the seal reaction forces, K is the direct stiffness, k is the cross-coupled stiffness, C is the direct damping, and c is the cross-coupled damping. The ΔX and ΔY terms are the rotor-stator relative displacements. The model accounts for fluid

inertia through the direct virtual mass term, M, and the cross-coupled virtual mass term, m. The solution applies for small perturbations about a centered, zero-eccentricity position. The model is used out to eccentricity ratios of $\varepsilon_0 = 0.5$ under the premise that the dynamic coefficients are relatively independent of static eccentricity.

Nelson and Nguyen [8], [9] developed a new method to calculate rotordynamic coefficients for seals operating eccentrically. Noting that operation at a non-centered position due to loading or misalignment is likely to occur, the authors define the fluid-film reaction forces as

$$-\begin{Bmatrix} f_{rX} \\ f_{rY} \end{Bmatrix} = \begin{bmatrix} K_{XX}(e_0) & K_{XY}(e_0) \\ K_{YX}(e_0) & K_{YY}(e_0) \end{bmatrix} \begin{Bmatrix} \Delta X \\ \Delta Y \end{Bmatrix} + \begin{bmatrix} C_{XX}(e_0) & C_{XY}(e_0) \\ C_{YX}(e_0) & C_{YY}(e_0) \end{bmatrix} \begin{Bmatrix} \Delta \dot{X} \\ \Delta \dot{Y} \end{Bmatrix} + \begin{bmatrix} M_{XX}(e_0) & M_{XY}(e_0) \\ M_{YX}(e_0) & M_{YY}(e_0) \end{bmatrix} \begin{Bmatrix} \Delta \ddot{X} \\ \Delta \ddot{Y} \end{Bmatrix} \tag{2}$$

where e_0 is the static eccentricity. Note the subscripts of the dynamic coefficients, indicating their values need not be equivalent.

As with bearings, the whirl frequency ratio (WFR) of a seal partially characterizes its effect on system stability. WFR is the ratio of the first flexural, natural frequency (ω_{n1}) to the onset speed of instability (OSI), or

$$WFR = \frac{\omega_{n1}}{OSI} \rightarrow OSI = \frac{\omega_{n1}}{WFR} \tag{3}$$

Lund [10] first formulated the WFR for a journal bearing or seal as

$$(WFR)^2 = \frac{\left(K_{eq} - K_{XX}\right)\left(K_{eq} - K_{YY}\right) - K_{XY}K_{YX}}{\omega^2(C_{XX}C_{YY} - C_{XY}C_{YX})} \tag{4}$$

where ω is the running speed and

$$K_{eq} = \frac{K_{XX}C_{YY} + K_{YY}C_{XX} - K_{XY}C_{YX} - K_{YX}C_{XY}}{C_{XX} + C_{YY}} \quad (5)$$

Note that WFR is a function of only rotordynamic coefficients and ω. This model is valid for seals if the magnitude of the cross-coupled virtual mass coefficients are negligible. If $|M_{XY}|$ and $|M_{YX}|$ are not negligible the definition of WFR developed by San Andrés [11] is appropriate. The full definition for San Andrés' WFR is given in Appendix B.

For seals, WFR is only useful for comparing the performance of a single geometry at different operating conditions. For comparing two different seal geometries the appropriate characteristic is effective damping [1]. Effective damping is

$$C_{eff} = C\left(1 - \frac{k}{C\omega}\right) \quad (6)$$

This metric combines the stabilizing impact of C with the destabilizing impact of k. Note that this definition only applies for a seal operating at the centered position where $C_{XX} = C_{YY} = C$ and $K_{XY} = -K_{YX} = k$.

Fluid rotation within the annular clearances of bearings and seals is the leading cause of destabilizing forces [3]. Black et al. [12] present an analysis exploring the effects of the fluid inlet circumferential velocity. They found that the inlet swirl or pre-swirl of the fluid significantly impacts the axial development of the circumferential fluid velocity, $u(Z)$. For seals where the rotor and stator surface roughness is equivalent, $u(Z)$ asymptotically approaches $0.5R\omega$. The analysis also demonstrates that the cross-coupled-stiffness coefficients are significantly affected by pre-swirl. Consequently, pre-swirl's influence extends to WFR and C_{eff}. The authors conclude that through active control of

pre-swirl, such as fluid injection in the direction opposite of shaft rotation, cross coupling can be significantly reduced or eliminated. Another solution is the swirl brake first used by Benckert and Wachter [13] to mitigate the effect of inlet swirl for gas labyrinth seals.

Iwatsubo et al. [14] develop a test rig to study the static and dynamic characteristics of four smooth seals with differing L/D and C_r. The test rig injects water into the seal inlet at varying pre-swirl velocities. The authors use a pitot tube at the seal inlet to measure the pre-swirl velocity. Their measured results agree with the conclusions of Black et al. [12]. Iwatsubo et al. [15] also test helically-grooved seals with this same test rig and measure pre-swirl. The present author is unaware of additional examples of pre-swirl measurements for liquid annular seals in the existing body of literature. Additionally, to the author's knowledge, there are no published measurements of outlet swirl in liquid annular seals.

Pump manufacturers machine grooves into both stators and rotors to further restrict $\dot{Q}$ and increase the efficiency of turbomachines [1]. Grooves can be circumferential or helical. The intent of helical grooves is to act as a pump opposing $\dot{Q}$. Helical grooves are beyond the scope of this study, which will focus on circumferential grooves.

Nordmann et al. [16] develop a bulk-flow theory for circumferentially grooved stator/smooth rotor (GS/SR) seals to calculate $\dot{Q}$ and rotordynamic coefficients. The authors introduce an equivalent clearance, simplifying the analysis, in what is an extension of Childs finite-length solution [2]. Similarly, Iwatsubo et al. [17] perform an

analytical analysis for smooth stator/grooved rotor (SS/GR) seals. The authors introduce average velocities and use a short seal solution. The analysis includes static and dynamic characteristics calculated for turbulent flow along with inertia effects. In an extension of their work, Iwatsubo and Sheng [18] develop a two-control-volume analysis for both SS/GR and GS/SR seals. Calculated results predict an average $u(Z)$ that is greater for the SS/GR seal than for the GS/SR seal. The authors predict cross-coupling to be larger for the SS/GR seal than for the GS/SR seal indicating that the SS/GR seal is worse from a rotordynamics standpoint. Later, Marquette and Childs [19] develop a three-control-volume method for calculating leakage and rotordynamic coefficients of GS/SR seals.

Marquette et al. test two GS/SR seals [20] and a smooth seal [21] all with L/D = 0.457 and C_r/R = 0.0029. The authors conduct tests with water as the lubricant at $\omega =$ 10.2, 17.4, and 24.6 krpm, $\Delta P = 41.4$, 55.2, and 68.9 bar, and ε_0 ranging from 0.0 to 0.5 in increments of 0.1. Figure 3 shows the geometries of their grooved seals.

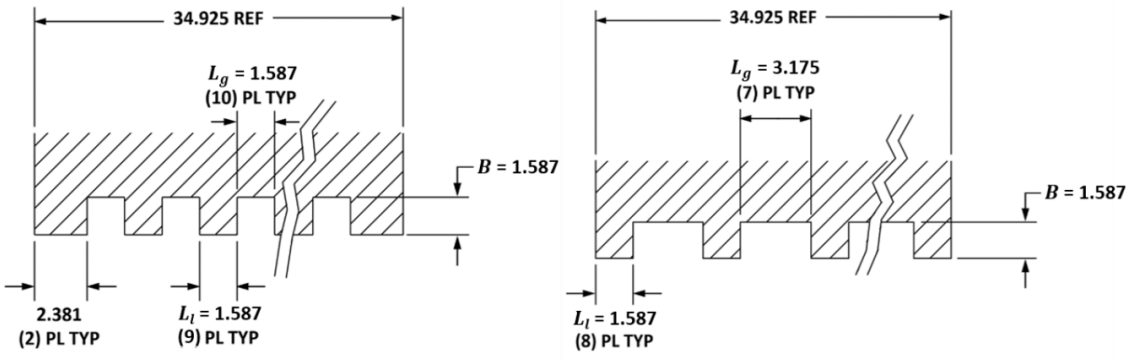

(a) (b)

Figure 3. Groove dimensions (mm) for (a) finely-grooved and (b) coarsely-grooved seals. Adapted from [19].

Marquette et al. present $\dot{Q}$, rotordynamic coefficients (K_{ij}, C_{ij}, and M_{ij}), and WFR. A sample of the measured results is shown in Table 1. Recalling that C_{eff} is the appropriate metric for comparing seal dynamic performance, the present author calculates this characteristic from the results of Marquette et al.

Table 1. Test results from Marquette et al. [20], [21] for ε_0 = 0.0 and ΔP = 55.2 bar

Speed [krpm]	Geometry	$\dot{Q}$ [l/s]	*K* [MN/m]	*k* [MN/m]	*C* [kN-s/m]	*c* [kN-s/m]	WFR [-]	C_{eff} [kN-s/m]
10.2	Smooth	0.99	25.22	9.83	24.34	5.27	0.38	15.14
	Fine groove	0.81	0.05	1.27	6.53	3.42	0.17	5.34
	Coarse groove	0.96	0.30	0.65	5.19	3.69	0.11	4.59
24.6	Smooth	0.83	19.91	36.17	27.16	13.54	0.52	13.12
	Fine groove	0.72	-2.48	5.39	8.19	9.10	0.26	6.10
	Coarse groove	0.90	-2.59	3.82	6.72	8.87	0.22	5.24

At the low ω, the finely-grooved seals leak 10-20% less than the smooth seals. At high ω, leakage is comparable. The authors note that coarse grooves increase the effective clearance of the seal. Consequently, $\dot{Q}$ is similar to the smooth seal at low ω and greater at high ω. Larger effective clearances for both grooved seals affects stiffness, as well. Note particularly, direct stiffness is low and even negative for the grooved seals whereas it is much greater for the smooth. Direct stiffness for the GS/SR seals tends to decrease as ω increases. The authors state that grooved-seal direct stiffness is a weaker function of ε_0 than smooth-seal direct stiffness. Measured cross-coupled stiffness for the grooved

seals is lower in magnitude than smooth seal cross-coupled stiffness. As a result, the WFR is lower for the grooved seals than the smooth seal. This would seem to indicate better stability characteristics. However, the grooved seals' direct damping coefficients are much lower than those of the smooth seal. Comparison of C_{eff} indicates that the smooth seal has more favorable rotordynamic characteristics than the grooved seals.

Marquette et al. [20], [21] test seals out to only ε_0 = 0.5. Measured results at higher eccentricities are scarce in the literature. Kanki and Kawakami [22] test water-lubricated smooth and helically-grooved seals out to $\varepsilon_0 > 0.9$. Measured results for the smooth seal at $\omega = 2$ krpm, ΔP = 10 bar show stiffness and damping coefficients as a strong function of ε_0. Falco et al. [23] produce test results for a short (L/D = 0.25), smooth seal at eccentricities out to $\varepsilon_0 = 0.7$. This seal is also water-lubricated and operates at $\omega = 4000$ and ΔP = 10 bar. Finally, Salas [24] measures static and dynamic characteristics for laminar-flow smooth seals at ε_0 = 0.8.

Aside from the analyses by Iwatsubo et al. in 1987 [17] and in 1990 [18], predictions for smooth stator/circumferentially-grooved rotor seals are limited in the literature. The author was unable to find measured data for a SS/GR seal. Consequently, this study focuses on measured static and dynamic characteristics for a SS/GR seal and comparisons to a smooth seal.

2. STATEMENT OF WORK

The main objective of this study is to measure the static and dynamic characteristics of a SS/GR seal and characterize the effect of pre-swirl and eccentricity. Static measurements include position, $\dot{Q}$, static load, and inlet and outlet swirl ratios. The dynamic measurements include excitation forces, acceleration, and relative displacement. The author uses these measurements to calculate dynamic stiffness, rotordynamic coefficients, WFR, and C_{eff}.

The test seal geometry is based on measured dimensions from an Electrical Submersible Pump. The seal stator is smooth with axial length L = 50.80 mm (2.000 in) and C_r = 203.2 μm (8 mils). A detailed dimensional drawing of the seal stator is shown in Fig. 4.

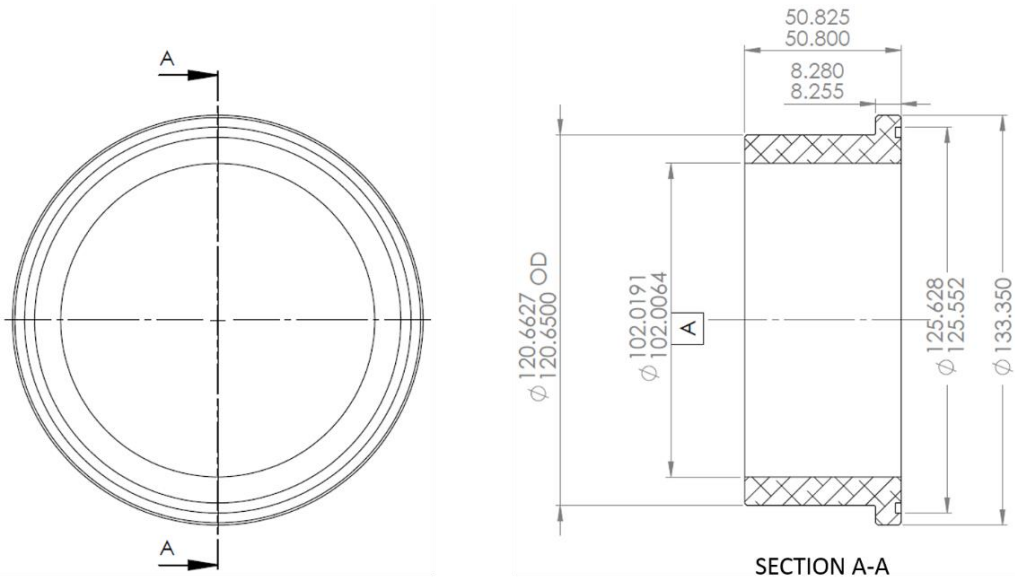

Figure 4. Detailed drawing of seal stator. All dimensions are in mm.

The test rotor has a diameter of D = 101.6 mm (4.000 in) at the location of the seals. From these dimensions, seal length-to-diameter ratio is L/D = 0.5, and clearance-to-radius ratio is C_r/R = 0.004. Each seal has a total of 15 square grooves with $B = L_g = L_l = 1.52$ mm (60 mils). The ratio of groove depth to radial clearance is B/C_r = 7.5. Figure 5 presents the groove detail.

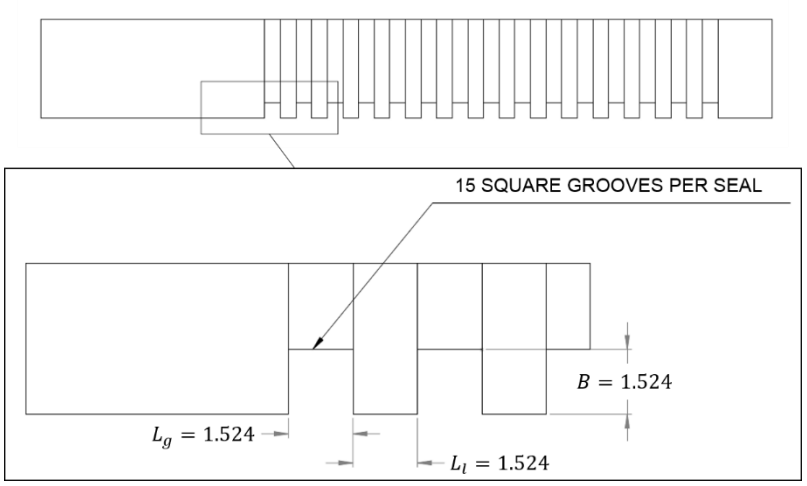

Figure 5. Detailed drawing of rotor grooves. All dimensions are in mm.

Pre-swirl velocity is varied using three different pre-swirl inserts described later in Section 3.1. Tests are completed at speeds of $\omega = 2$, 4, 6, and 8 krpm, axial pressure drops of $\Delta P = 2.07$, 4.14, 6.21, and 8.27 bar (30, 60, 90, and 120 PSI), and $\varepsilon_0 = 0.00$, 0.27, 0.53, and 0.80. ISO VG 2 oil is used as the lubricant to ensure turbulent flow conditions. The target seal inlet temperature is 46.1ºC (115ºF). The author compares measured results to the results of a smooth stator/smooth rotor seal with equivalent C_r, L,

and D. These smooth seal test results are available internally at the Texas A&M Turbomachinery Laboratory and will be the subject of a separate M.S. thesis in Mechanical Engineering. Note that no published predictions exist for this seal precluding measurement-versus-prediction comparisons.

3. TEST RIG DESCRIPTION

The author conducts tests on an existing rig originally designed by Kaul [25] to test annular bushing oil seals. Since then the rig has undergone some modifications. The test apparatus utilizes the rigid rotor and "floating stator" method originally developed by Glienicke [26]. The test rig can be categorized into four main sections: the main test section, the oil supply system, the hydraulic shakers, and the instrumentation and data acquisition system.

3.1 Main Test Section

Welded mild-steel plates form a bed plate to support the main test frame, motor mount, and motor. Figure 6 shows a cross-section view of the main test section.

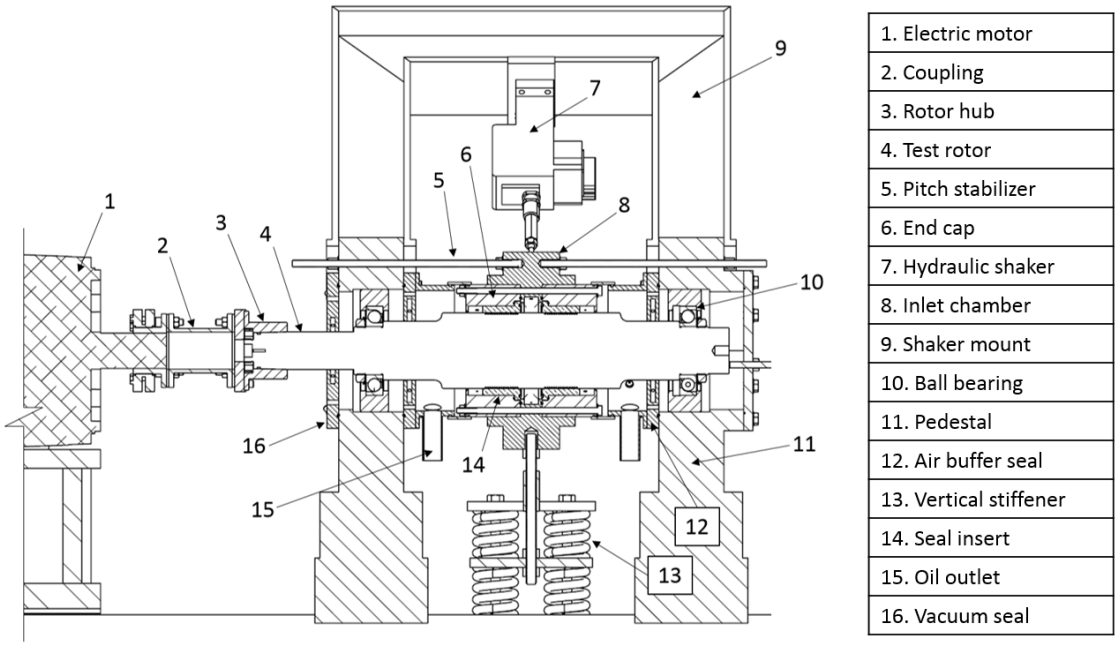

Figure 6. Cross-section view of the main test section.

Two AISI 1040 steel pedestals spaced approximately 380 mm (15 in) apart support the test rotor. They are split into upper and lower halves to allow the rotor and bearing cartridges to be dropped in place. The test rotor is constructed of AISI 4140 steel and is shown in Fig. 7.

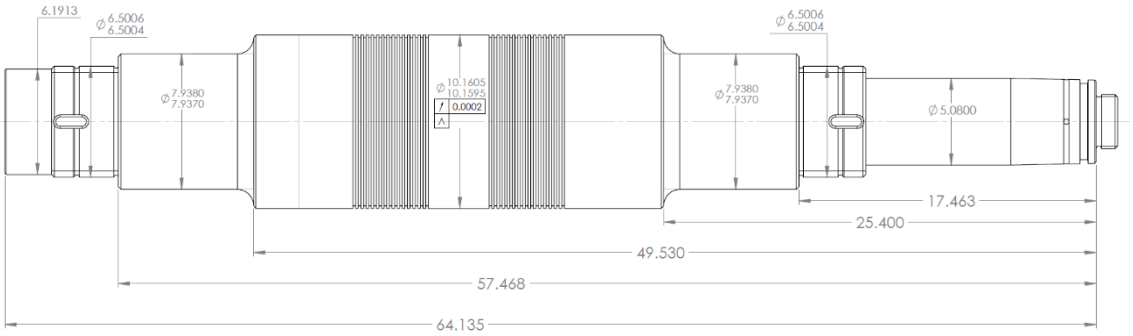

Figure 7. Grooved test rotor. All dimensions are in cm.

Two angular contact ball bearings are fit onto the rotor and span 422 mm (16.6 in). A steel coupling hub is hydraulically mounted on to the rotor. The rotor is driven by a 29.8 kW (40 hp) electric motor with a maximum speed of 8 krpm. The motor is powered and controlled by a variable frequency drive.

As shown in Fig. 6, the stator is positioned between the two pedestals. Two opposing bronze 660 seal inserts are inserted into the 17-4 PH stainless steel end caps. The end caps are positioned back-to-back in the stator inlet chamber and assembled on an alignment mandrel. Figure 8 depicts the assembly process.

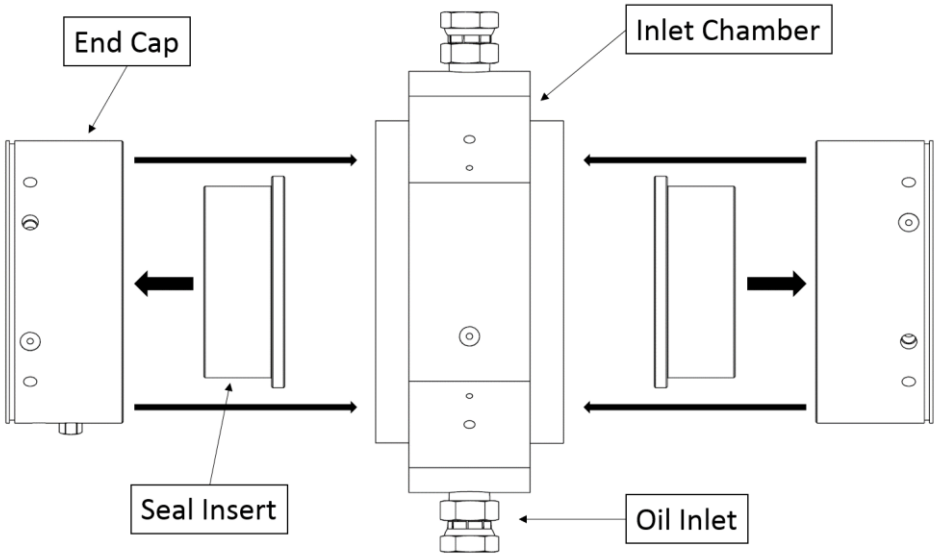

Figure 8. Stator assembly process.

Oil enters the stator radially through two diametrically-opposed inlets as shown in Fig. 9. It then passes through the pre-swirl insert to the plenum where it enters the seals and exits the stator axially. The back-to-back arrangement minimizes axial thrust on the stator. A single back-pressure labyrinth tooth in each end cap prevents cavitation of the lubricant and maintains a nominally atmospheric outlet pressure. Oil travels from the end cap outlet through flexible rubber hose to the discharge chambers before returning to the sump tank. Air buffer seals prevent the test lubricant from entering the ball bearings.

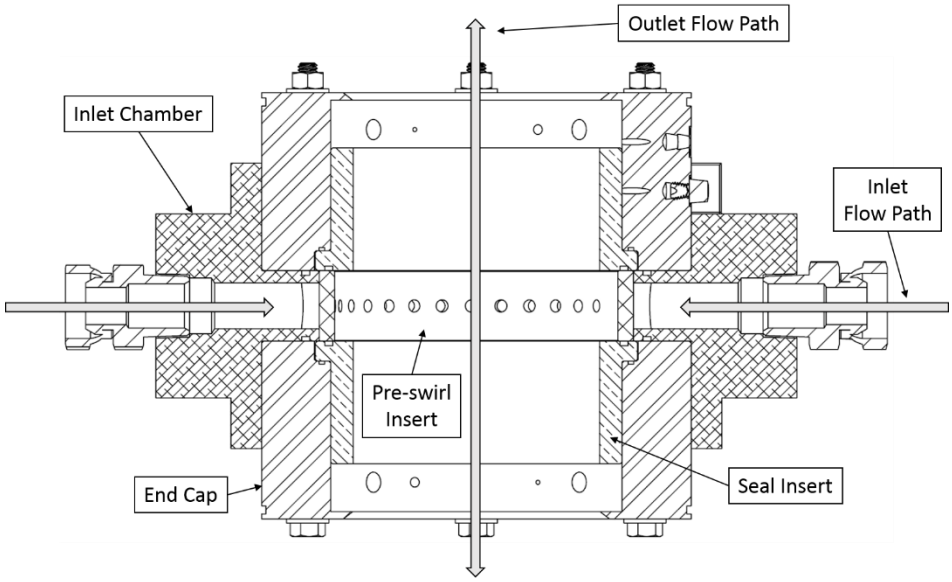

Figure 9. Assembled stator and lubricant flow path.

Three separate inlet chambers contain the three different pre-swirl inserts. They were designed for previous annular seal tests and reused for this project. Figure 10 shows the pre-swirl inserts. Radial injection provides zero to low pre-swirl conditions. With tangential injection, nozzle diameter, D_N, is varied from 4.978 mm (0.1960 in) to 4.039 (0.1590) to provide medium and high pre-swirl conditions, respectively.

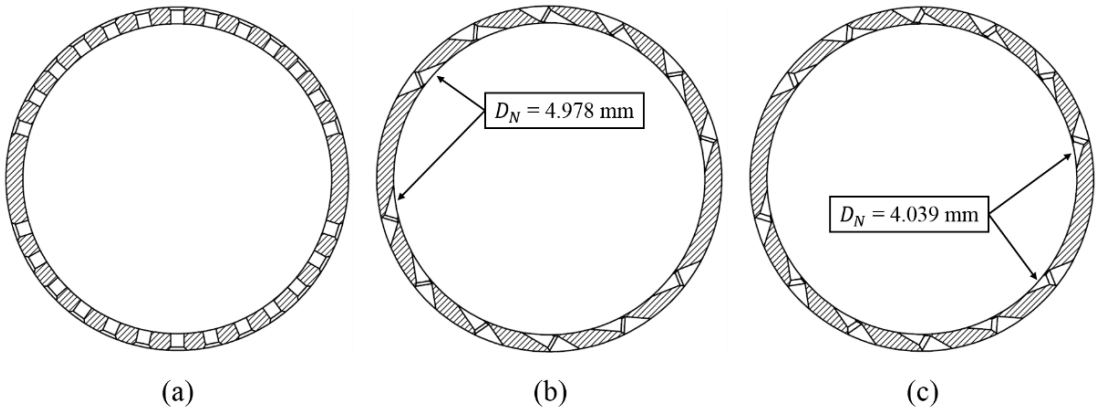

Figure 10. Pre-swirl inserts for (a) radial injection, (b) tangential injection for medium pre-swirl, and (c) tangential injection for high pre-swirl.

The stator assembly is connected to the pedestals by six pitch stabilizers which prevent axial, pitch, and yaw motion. They are adjustable to precisely align the stator with the rotor. Additionally, preliminary tests indicated the stator needed stiffeners to prevent instabilities. Vertical and diagonal stiffeners were constructed of die compression springs and fixed to the stator. The stiffener design arranges the compression springs such that the stiffeners act in both tension and compression. Figure 11 depicts the position of the stiffeners in relation to the shaker axes viewed from the non-drive end (NDE).

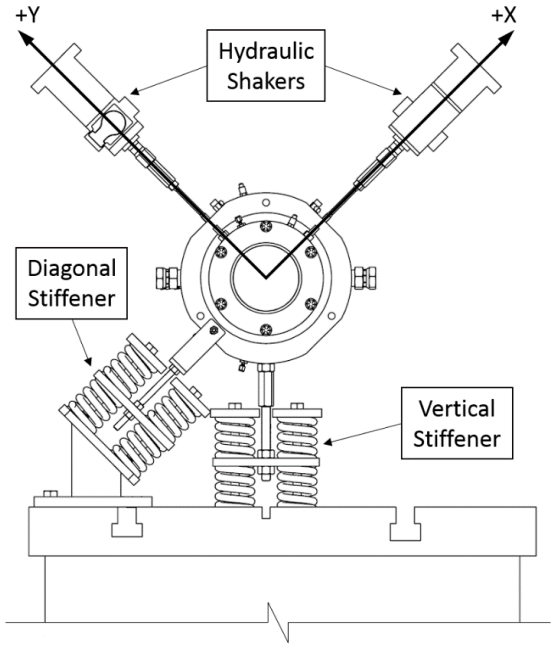

Figure 11. Shaker axes and stiffener positions.

3.2 Oil Supply System

The oil supply system delivers ISO VG 2 oil to the main test section at a target temperature of 46.1°C (115°F). Measured dynamic viscosity at 46.1°C is 1.79 cP. The main flow components are a 950 liter (250 gallon) main tank, a 380 liter (100 gallon) sump tank, and two Viking spur gear pumps. Flow from the main gear pump travels through an electro-pneumatic control valve that is manually controlled by the operator. After passing through the test section, lubricant returns to the sump tank. The sump pump delivers the fluid to either the main tank or directly to the main pump via two PID-controlled, electro-pneumatic valves used to regulate the mixing of the hot (sump tank) oil and cold (main tank) oil. Before starting the system, the oil is generally pre-heated using a 15.8 kW circulation heater and a small 30.28 LPM (8 GPM) pump. During

operation, the oil temperature can continue to rise due to heat generation in the gear pumps and in the seals. A heat exchanger and fan are used to cool the lubricant. With careful monitoring, inlet temperature can be regulated to ±1.1°C (2°F).

3.3 Hydraulic Shaker System

As previously shown in Fig. 6 and Fig. 11, the hydraulic shakers are rigidly mounted to the shaker frame and oriented orthogonally to the stator. A load cell and isolation stinger is connected in series between the shaker head and the stator. The stingers are designed according to [27] to isolate the stator from the shaker head dynamics. Each shaker is powered by a 207 bar (3000 psi), Zonic Corporation pump and controlled by a dual-loop master controller. The shaker heads "float" the stator and can provide excitations up to 1 kHz for dynamic measurements. Both shakers can exert forces up to 4450 N (1000 lb) in tension and compression.

3.4 Instrumentation and Data Acquisition

Figure 12 shows the instrumentation used to take static and dynamic measurements of the seals.

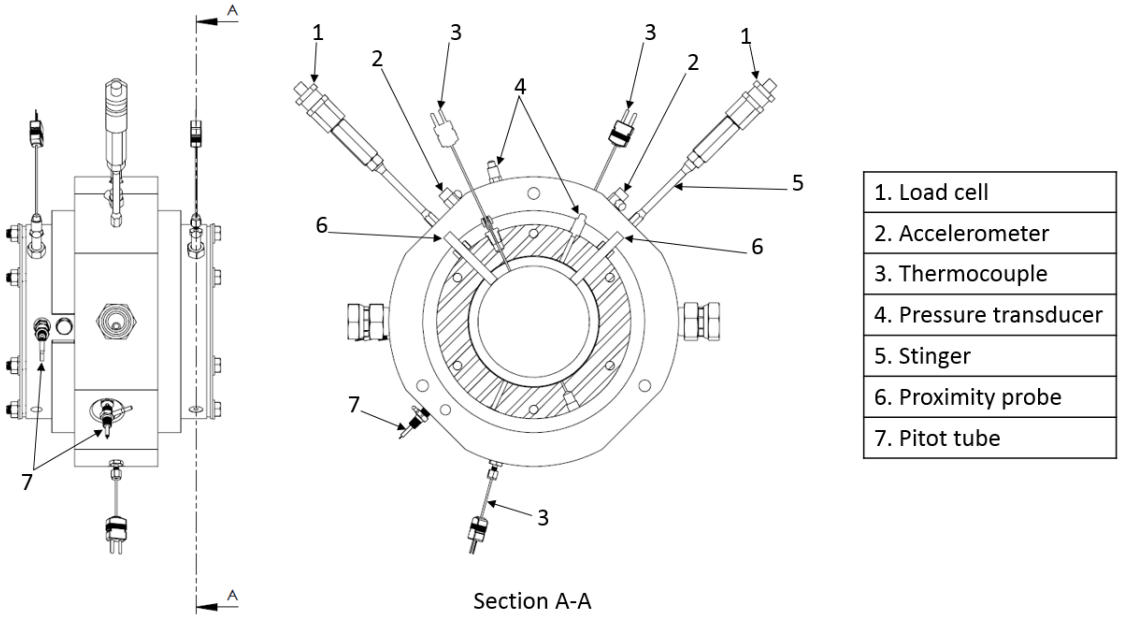

Figure 12. Assembled stator with instrumentation. Section A-A view from the NDE.

The Xcite Systems load cells (1) measure the static and dynamic loads applied to the stator assembly. PCB accelerometers (2) measure stator accelerations in both the X and Y directions. Two pairs of Lion Precision eddy-current proximity probes (6) measure the relative stator-rotor displacement in the X and Y directions in two different planes. One pair is located on the DE outlet while the other is on the NDE outlet so that pitch can be measured and removed. The probes have a 1 mm (40 mil) range and a 0.060 µm (2.4 µinch) resolution at 1 kHz. Three Kulite XTM-190 pressure transducers (4) with a 17

bar (250 psi) range measure inlet, DE outlet, and NDE outlet pressure. Type J Omega thermocouples (3) measure lubricant temperature at the inlet and outlets. A Flow Technology turbine flowmeter, located upstream of the oil inlet ports, measures $\dot{Q}$. A PHILTEC fiber-optic displacement sensor is used as a tachometer probe.

Two custom pitot tubes (7) from United Sensor measure the inlet and DE outlet swirl velocity. The outer tube OD = 1.65 mm (0.065 in) while the inner tube OD = 0.71 mm (0.028 in). Figure 13 shows the axial and radial location of the pitot tubes.

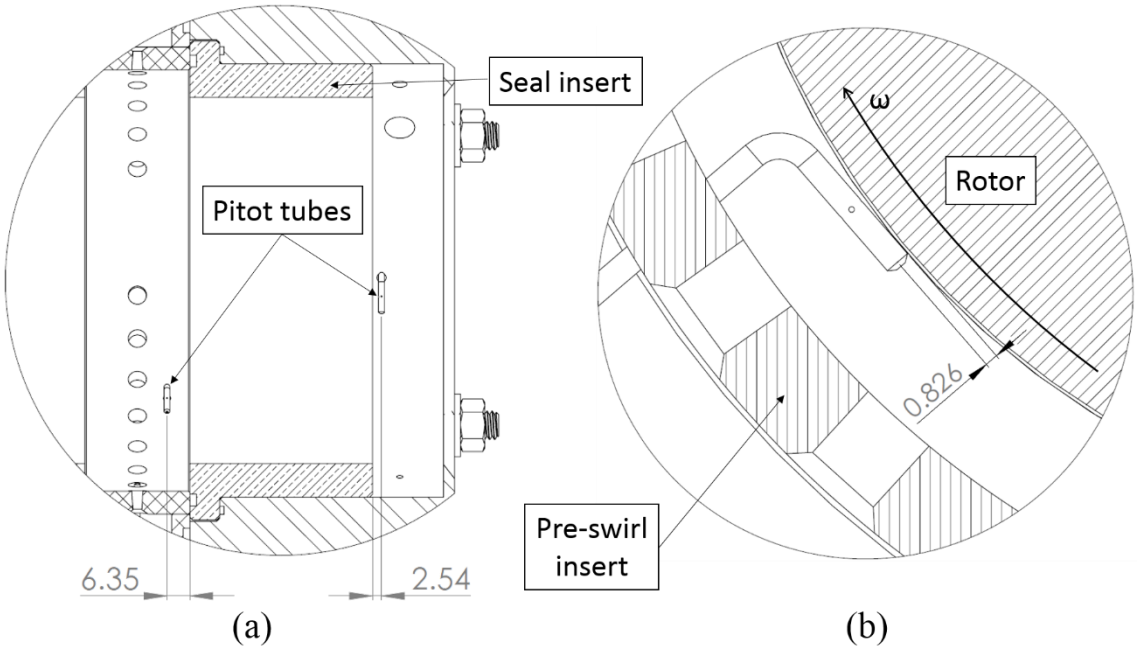

Figure 13. (a) Axial position and (b) radial position of the pitot tubes. All dimensions in mm.

The pitot tubes are positioned tangential to the rotor surface using precision gauge blocks. The centerlines of the pitot tubes are approximately 826 µm from the seal stator

surface as shown in Fig. 13b. Note that the pitot tubes are only positioned close to the inlet and outlet of the seal due to physical limitations. The location of true pre-swirl and outlet swirl would be within the seal annular clearance at the inlet and outlet. Nevertheless, the pitot tube measurements provide insight into circumferential fluid flow within the seal. Two Rosemount pressure transducers measure pitot tube differential pressure.

The data acquisition system consists of National Instruments PCI 6229 and PCI 4472 cards. A LabVIEW VI is used to control data acquisition.

4. TEST PROCEDURE

4.1 Cold Clearance

The test procedure begins with taking a "cold" clearance measurement before any oil has been run through the system. The operator precesses the stator about the rotor while maintaining contact. The result is a circular clearance measurement used to calculate C_r and determine the geometric center of the seal. This initial clearance measurement serves to establish relative stator-rotor position for the baselines.

4.2 Static and Dynamic Baselines

The addition of the vertical and diagonal stiffeners necessitates a static or deflection baseline measurement. While testing, both the fluid-film reaction forces, F_r, and the stiffeners oppose the applied static load, F_s. To isolate the two components, the operator slowly applies a static load to the stator through the Y shaker to $\varepsilon_0 > 0.8$. This is done with no oil in the system. The resultant deflection curve represents only the reaction of the stiffeners. This deflection baseline is subtracted from the measured static loads of test data to arrive at a corrected static load that represents only fluid-film reaction force.

Likewise, while testing, dynamic measurements represent both the fluid-film reaction forces as well as the stator and stiffeners. To isolate the dynamic stiffness of the stator and stiffeners, the operator applies dynamic force excitations to the stator with no lubricant in the system. These baselines are subtracted from the measured dynamic stiffness while testing with lubricant resulting solely in the fluid-film dynamic stiffness.

4.3 Hot Clearance

Next, the operator starts the rest of the system. Lubricant flows through the stator, and the rotor spins at the desired speed. Once the fluid within the stator reaches steady-state operating temperature (46.1°C), the system is quickly shut down, and the operator takes another clearance measurement. This "hot" clearance measurement reflects the radial growth in the seal due to thermal expansion. Growth for the bronze 660 seal inserts used is generally small (~5 μm).

4.4 Static Measurements

Following the hot clearance measurement, the operator restarts the lubricant flow and the electric motor. The operator controls the motor speed, lubricant flow rate ($\dot{Q}$), and applied static load (F_s) to reach the target rotor speed (ω), pressure drop (ΔP), and eccentricity ratio (ε_0). Once the system has reached steady state, the instrumentation measures ω, inlet and outlet pressures, $\dot{Q}$, X and Y position, F_s, and inlet and outlet temperature. Measured $\dot{Q}$ and F_s are for the whole stator system which includes two seal inserts. Therefore, measured values of $\dot{Q}$ and F_s are divided in half to provide the values for a single seal.

Figure 14a shows the test rig coordinate system superimposed on a NDE view of the stator. Position of the rotor is described in a stator-fixed reference frame as shown in Fig. 14b.

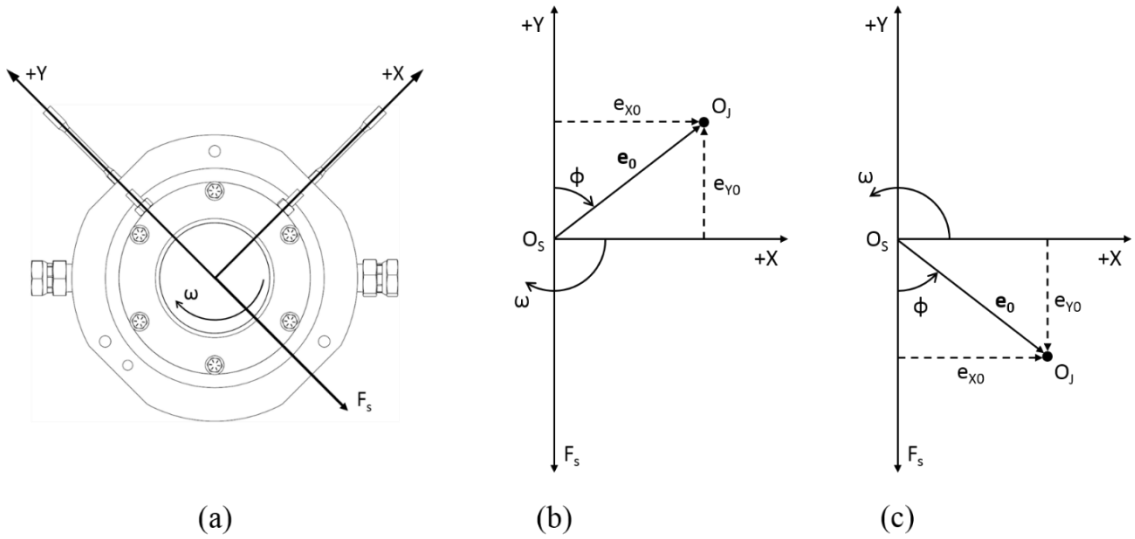

Figure 14. (a) NDE view of the rig coordinate system. (b) Definition of position in the rig coordinate system. (c) Presented coordinate system.

The stator geometric center, O_S, is located at (O_{XS}, O_{YS}). The journal (rotor) center, O_J, is located at (e_{X0}, e_{Y0}). For presented results, the coordinate system is modified to represent a traditional view with the static load acting in the $-Y$ direction and ω in the counter-clockwise direction as shown in Fig. 14c. The rotor-stator relative position is conveniently defined in non-dimensional form as

$$\varepsilon_0 = \sqrt{\varepsilon_{X0}^2 + \varepsilon_{Y0}^2} \tag{7}$$

where

$$\varepsilon_{X0} = \frac{e_{X0} - O_{XS}}{C_r}, \varepsilon_{Y0} = \frac{e_{Y0} - O_{YS}}{C_r} \tag{8}$$

Additionally, the attitude angle between $\boldsymbol{e_0}$ and the static load vector is

$$\phi = \tan^{-1}\frac{\varepsilon_{X0}}{\varepsilon_{Y0}} \tag{9}$$

4.5 Dynamic Measurements

The dynamic tests use a multiple-frequency excitation method detailed by Rouvas and Childs [28]. The hydraulic shakers perturb the stator with shake amplitudes approximately 10% of C_r about a static equilibrium position. The excitation is a pseudo-random waveform optimized to provide maximum excitation at a range of frequencies between ~10-350 Hz while keeping overall excitation levels low. Actual excitation frequencies occur at intervals of 9.765 Hz to avoid electrical noise. The test consists of two separate shakes; one in each orthogonal direction. Each shake consists of 320 excitations lasting 0.1024 seconds each for a total shake duration of 32.768 seconds. The sensors measure stator acceleration ($\ddot{X}_s$,$\ddot{Y}_s$), relative displacement (ΔX, ΔY), and applied dynamic forces (f_X, f_Y). The data acquisition system samples the measurements at 10 kHz.

5. DATA ANALYSIS

5.1 Dynamic Stiffness

Dynamic stiffness and rotordynamic coefficient calculations are adapted from Childs and Hale [29]. Translating the dynamic measurements into meaningful results begins with the equations of motion (EOM) for the stator system as

$$M_s \begin{Bmatrix} \ddot{X}_s \\ \ddot{Y}_s \end{Bmatrix} = \begin{Bmatrix} f_X \\ f_Y \end{Bmatrix} + \begin{Bmatrix} f_{rX} \\ f_{rY} \end{Bmatrix} \tag{10}$$

where M_s is the stator mass, and the fluid-film reaction-force components are f_{rX} and f_{rY}. Substituting the reaction force model of Eq. (2) into Eq. (10) and rearranging yields

$$\begin{Bmatrix} f_X \\ f_Y \end{Bmatrix} - M_s \begin{Bmatrix} \ddot{X}_s \\ \ddot{Y}_s \end{Bmatrix} = \begin{bmatrix} K_{XX} & K_{XY} \\ K_{YX} & K_{YY} \end{bmatrix} \begin{Bmatrix} \Delta X \\ \Delta Y \end{Bmatrix} + \begin{bmatrix} C_{XX} & C_{XY} \\ C_{YX} & C_{YY} \end{bmatrix} \begin{Bmatrix} \Delta \dot{X} \\ \Delta \dot{Y} \end{Bmatrix} + \begin{bmatrix} M_{XX} & M_{XY} \\ M_{YX} & M_{YY} \end{bmatrix} \begin{Bmatrix} \Delta \ddot{X} \\ \Delta \ddot{Y} \end{Bmatrix} \tag{11}$$

The measured dynamic data is separated into four sets of equal duration. An FFT converts the measured time domain data into frequency-domain data, resulting in excitation forces ($\boldsymbol{F_X}$, $\boldsymbol{F_Y}$), accelerations ($\boldsymbol{A_X}$, $\boldsymbol{A_Y}$), and relative displacements ($\boldsymbol{D_X}$, $\boldsymbol{D_Y}$). The system EOM is now written as

$$\begin{Bmatrix} \boldsymbol{F_X} - M_s \boldsymbol{A_X} \\ \boldsymbol{F_Y} - M_s \boldsymbol{A_Y} \end{Bmatrix} = \begin{bmatrix} \boldsymbol{H_{XX}} & \boldsymbol{H_{XY}} \\ \boldsymbol{H_{YX}} & \boldsymbol{H_{YY}} \end{bmatrix} \begin{Bmatrix} \boldsymbol{D_X} \\ \boldsymbol{D_Y} \end{Bmatrix} \tag{12}$$

where the dynamic stiffness is

$$\boldsymbol{H_{ij}} = \left(K_{ij} - \Omega^2 M_{ij}\right) + \boldsymbol{j}\left(\Omega C_{ij}\right) \tag{13}$$

where Ω is the excitation frequency. Note the imaginary operator $\boldsymbol{j} = \sqrt{-1}$. For two shakes in orthogonal directions the system EOM can be expressed as

$$\begin{bmatrix} \boldsymbol{F_{XX}} - M_s\boldsymbol{A_{XX}} & \boldsymbol{F_{XY}} - M_s\boldsymbol{A_{XY}} \\ \boldsymbol{F_{YX}} - M_s\boldsymbol{A_{YX}} & \boldsymbol{F_{YY}} - M_s\boldsymbol{A_{YY}} \end{bmatrix} = \begin{bmatrix} \boldsymbol{H_{XX}} & \boldsymbol{H_{XY}} \\ \boldsymbol{H_{YX}} & \boldsymbol{H_{YY}} \end{bmatrix} \begin{bmatrix} \boldsymbol{D_{XX}} & \boldsymbol{D_{XY}} \\ \boldsymbol{D_{YX}} & \boldsymbol{D_{YY}} \end{bmatrix} \tag{14}$$

With four equations and only four unknowns, the system dynamic stiffness $\boldsymbol{H_{ij}}$ is calculated. At this point in the analysis the baseline dynamic stiffness is subtracted from the calculated dynamic stiffness to isolate the dynamic stiffness due to the annular seal alone. Additionally, the dynamic stiffness is divided in half to represent the reaction of a single seal instead of the two seals that compose the stator assembly. Recalling that the time domain data is divided into four sets, the resulting calculated dynamic stiffness are averaged together, and the repeatability is calculated. Repeatability calculations are shown in Appendix C.

5.2 Curve Fits

Next, the investigator calculates rotordynamic coefficients by applying a least-squares regression curve fit to the dynamic stiffness. Dynamic stiffness is separated into real and imaginary parts:

$$\begin{aligned} \mathrm{Re}\left(\boldsymbol{H_{ij}}\right) &= K_{ij} - \Omega^2 M_{ij} = K_{ij} - \Lambda M_{ij} \\ \mathrm{Im}\left(\boldsymbol{H_{ij}}\right) &= \Omega C_{ij} \end{aligned} \tag{15}$$

The curve fit assumes a linear relationship between the input, x_i, and the output, $y(x_i)$, such that

$$y(x_i) = a + bx_i \tag{16}$$

Given a set of input measurements (x_i) and calculated outputs [$y(x_i)$], the intercept is

$$a = \frac{\sum y_i \sum x_i^2 - \sum x_i \sum x_i y_i}{n \sum x_i^2 - (\sum x_i)^2} \tag{17}$$

and the slope is

$$b = \frac{n \sum x_i y_i - \sum x_i \sum y_i}{n \sum x_i^2 - (\sum x_i)^2} \tag{18}$$

This regression method, as described by Beckwith et al. [30] is applied to Eq. (15). The curve fit is used for frequencies up to 200 Hz which is 1.5x the maximum running speed (8 krpm = 133.33 Hz).

5.3 Pre-swirl and Outlet Swirl Ratio

As described in Section 3.4, the pitot tubes measure the difference between dynamic and static pressure at the inlet and outlet of the seals. From these measurements, the fluid circumferential velocity is

$$u = \sqrt{\frac{2\Delta P_u}{\rho}} \tag{19}$$

where ΔP_u is the pitot tube differential pressure measurement, and ρ is the fluid density. Swirl is conveniently defined in terms of the ratio of circumferential fluid velocity to the rotor surface speed. The pre-swirl ratio is

$$PSR = \frac{u(Z = 0)}{\omega R} \tag{20}$$

where $u(Z = 0)$ is the measured circumferential fluid velocity near the seal inlet, and R is the rotor radius. Outlet swirl ratio is

$$OSR = \frac{u(Z = L)}{\omega R} \tag{21}$$

where $u(Z = L)$ is the circumferential fluid velocity measured near the seal outlet.

5.4 Reynolds Number

The Reynolds number is calculated to determine the flow regime. As mentioned in Section 2, the target flow regime is turbulent. The maximum clearance between the stator and rotor is used for the calculation. The axial Reynolds number is defined as

$$Re_Z = \rho 2(C_r + B)w/\mu \tag{22}$$

where μ is lubricant viscosity. The average axial flow velocity is

$$w = \dot{Q}/A \tag{23}$$

where A is the annular clearance area

$$A = 2\pi R(B + C_r) \tag{24}$$

Circumferential Reynolds number is defined as

$$Re_\theta = \rho R\omega(C_r + B)/\mu \tag{25}$$

The total vector Reynolds number is defined as

$$Re = \sqrt{Re_z^2 + Re_\theta^2} \tag{26}$$

Additionally, the ratio Re_θ/Re_Z provides insight into the behavior of the fluid flow within the annulus.

6. STATIC RESULTS

Even with the vertical and diagonal stiffeners attached, some test points at high ω and high ε_0 could not be safely obtained. At these points the stator would be "sucked" into the side of the rotor. These high-risk test points were excluded due to the high chance of rubbing. However, this does not detract from the trends and conclusions observed in the overall results. Additionally, unless otherwise noted, presented results are from the radial injection (low pre-swirl) assembly.

6.1 Clearance Measurements

The SS/GR seal was designed to have a nominal clearance of C_r = 203.2 μm (8 mils). However, measured values are lower. Table 2 shows the measured, average radial hot clearance. The measured hot C_r is used for the calculation of ε_0.

Table 2. Measured average radial hot clearances.

Assembly Configuration	Assembly 1 Low Pre-swirl	Assembly 2 Medium Pre-swirl	Assembly 3 High Pre-swirl
C_r [μm]	183.81	185.62	187.12

6.2 Leakage

Figure 15 presents leakage values for the SS/GR seal. $\dot{Q}$ increases slightly with increasing ε_0. A strong function of ΔP, $\dot{Q}$ increases by approximately 10 LPM for every 2.07 bar pressure increase. Figure 15b shows reduction in $\dot{Q}$ with increasing ω. Measured $\dot{Q}$ ranges from 7.8 LPM at ω = 8 krpm, ΔP = 2.07, and ε_0 = 0.00 to 51.1 LPM at ω = 2 krpm, ΔP = 8.27, and ε_0 = 0.80.

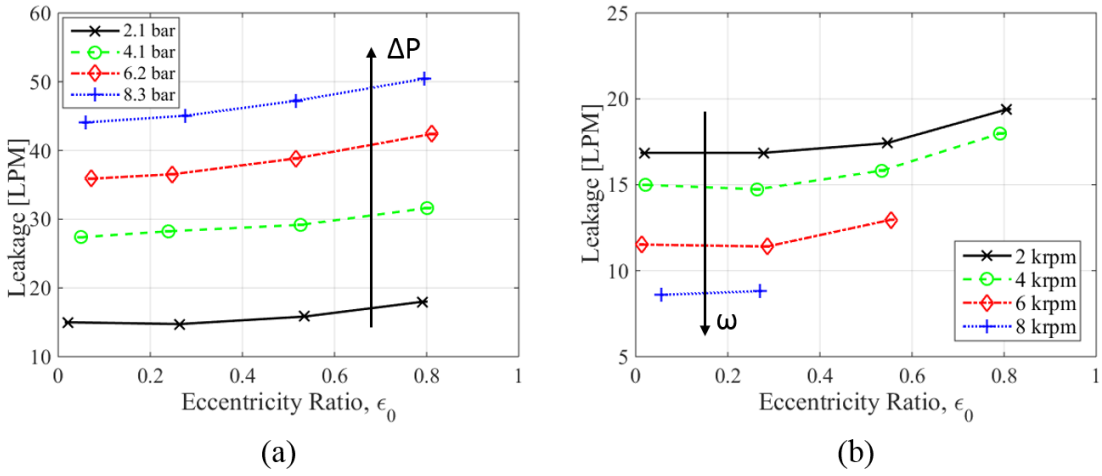

Figure 15. $\dot{Q}$ versus ε_0 for (a) ω = 4 krpm over a ΔP range, and (b) ΔP = 2.07 bar for a range of ω values.

Figure 16 shows the $\dot{Q}$ for both the SS/GR seal and the SS/SR seal as a function of ε_0. At high ΔP, the SS/GR seal significantly reduces $\dot{Q}$ compared to the SS/SR seal. Additionally, there is greater reduction in $\dot{Q}$ from the smooth seal to the groove seal at lower ω. The largest reduction is at ω = 2 krpm and ΔP = 8.27 bar where SS/GR seal $\dot{Q}$ is 70% of the SS/SR seal $\dot{Q}$, a reduction of approximately 19 LPM. Figure 16b shows

that at low ΔP and high ω the grooves do not significantly reduce $\dot{Q}$. At these high speeds SS/GR seal $\dot{Q}$ is only 80-90% that of the SS/SR seal $\dot{Q}$. Therefore, machining grooves into the rotor to reduce $\dot{Q}$ is only advantageous when operating at higher ΔP and lower ω values.

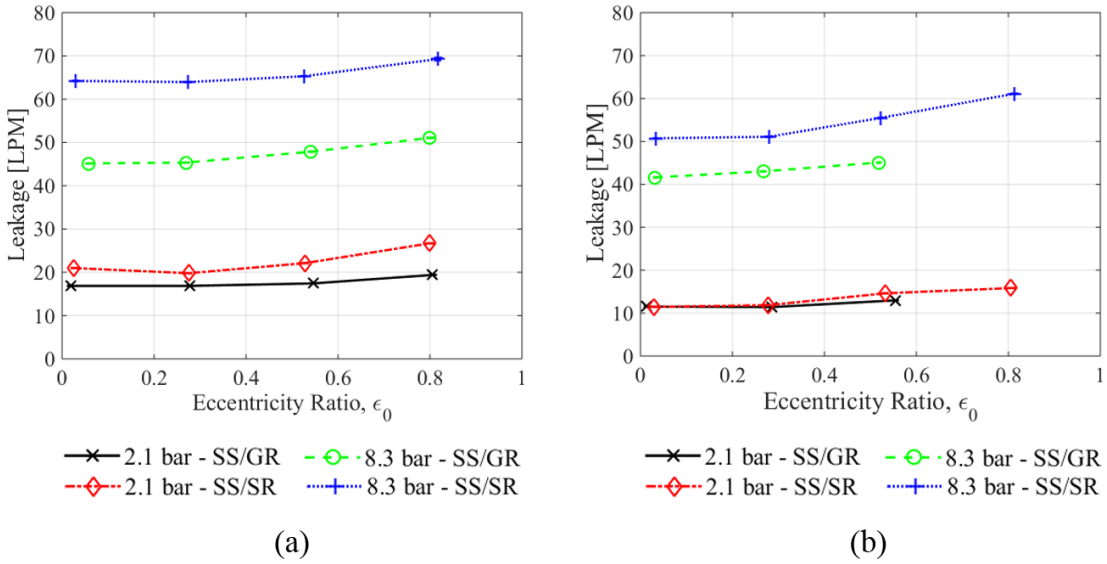

Figure 16. Comparison of $\dot{Q}$ for the SS/GR seal and SS/SR seal. $\dot{Q}$ versus ε_0 for (a) ω = 2 krpm and (b) ω = 6 krpm.

6.3 Seal Loci and Fluid-film Reaction Force

As mentioned in Section 3.1, the stiffeners prevent stator instabilities and aid in holding the stator in position at desired eccentricities. Unfortunately, this had the adverse effect of complicating the measurement of the static fluid-film reaction force, F_r, as described in Section 4.2. Even with the deflection baseline procedure, the calculated F_r does not always agree with measured direct stiffness values. At times F_r shows positive

centering force while there are negative direct stiffness values for a given set of operating conditions. The author believes that the difficulty in accurately measuring F_r arises due to the large magnitude of the stiffener forces and the small magnitude of the fluid-film reaction force, F_r. Consequently, F_r values are only reported in Appendix A.

It is worth noting that the SS/GR seal required stiffeners while testing but the SS/SR seal did not. For the smooth seal, the fluid-film reaction force, F_r, was always positive and centering.

While the fluid-film reaction force, F_r, was calculated using the deflection baseline method described in Section 4.2 there was no analogous approach to eliminating the influence of the stiffeners from seal loci. Consequently, there is no meaningful insight to be gained from seal loci and attitude-angle measurements. Therefore, these measurements are only reported in Appendix A.

6.4 Pre-swirl Ratio

Imposed pre-swirl ratio was a function of leakage rate and rotor speed. The ranges of imposed PSR for each ω are summarized in Table 3. The pre-swirl inserts were more effective at producing a wider range of imposed PSR at the low ω. This is readily apparent if one recalls that ω is in the denominator of Eq. (20).

Table 3. Minimum and maximum imposed PSR for each running speed.

Running Speed, ω [krpm]	Minimum PSR [-]	Maximum PSR [-]
2	0.00	0.88
4	0.00	0.56
6	0.13	0.42
8	0.18	0.40

6.5 Outlet Swirl Ratio

Figure 17 shows the OSR increasing with increasing ε_0. Additionally, OSR increases with increasing ΔP at ω = 2 krpm, but the trend is unclear for other speeds. There is no clear relation between ω and OSR.

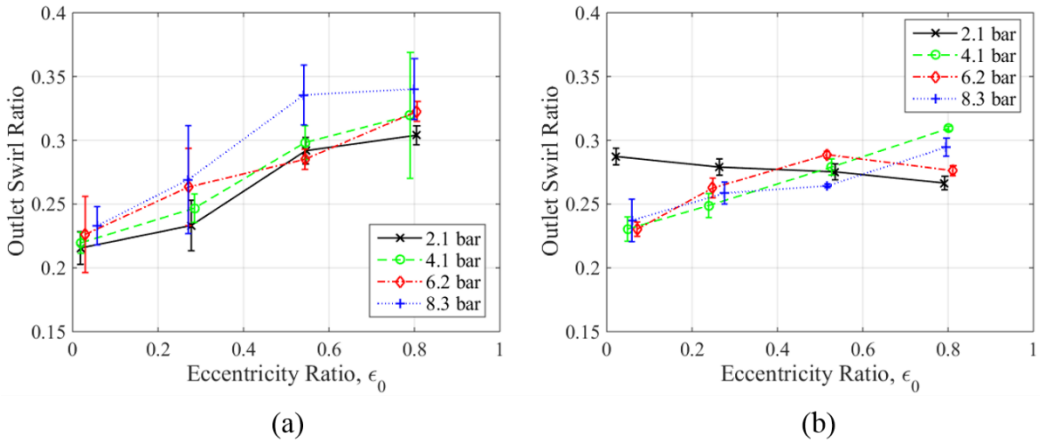

Figure 17. SS/GR seal OSR versus ε_0 for a range of ΔP at (a) ω = 2 krpm and (b) ω = 4 krpm.

Figure 18 shows the relationship between PSR and OSR. At $\omega \leq 4$ krpm, OSR tends to increase as PSR increases. There is no clear trend at $\omega \geq 6$ krpm.

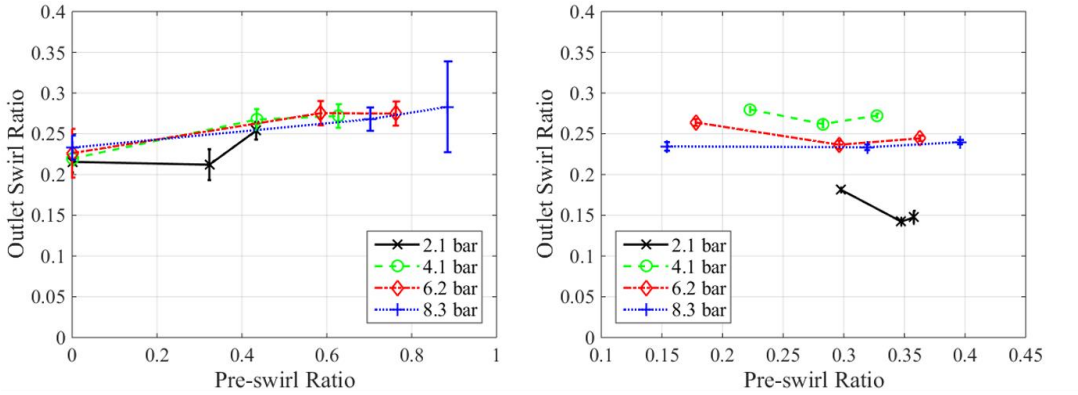

Figure 18. SS/GR seal OSR versus PSR at ε_0 = 0.00 for a range of ΔP at (a) $\omega = 2$ krpm and (b) $\omega = 6$ krpm.

One expects the additional surface area on the grooved rotor to increase average $u(Z)$ and, therefore, OSR relative to the smooth rotor. Measured results, however, indicate that OSR tends to be lower for the SS/GR seal than the SS/SR seal. However, the differences in OSR between the two seals tend to be small.

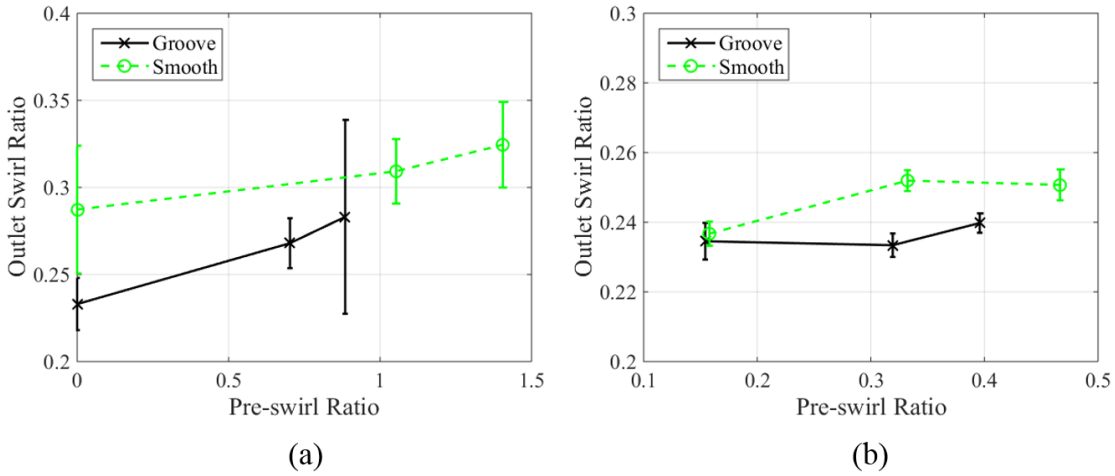

Figure 19. Comparison of OSR between SS/GR seal and SS/SR seal. OSR versus PSR for ε_0 = 0.00 at (a) $\omega = 2$ krpm, $\Delta P = 8.27$ bar and (b) $\omega = 6$ krpm, $\Delta P = 8.27$ bar.

Note particularly, measured OSR was less than 0.5 for both the SS/SR seal and the SS/GR seal. According to the analysis of Black et al. [12], one would expect outlet swirl to be greater than $0.5R\omega$ for the SS/GR seal especially when imposed PSR is greater than 0.5. The axial and radial location of the outlet swirl pitot tube shown previously in Fig. 13 and the sudden radial expansion of the fluid as it exits the seal may be the cause for this disagreement.

6.6 Reynolds Number

The maximum calculated Reynolds number is $Re = 3.34 \times 10^4$ while the minimum was $Re = 7.88 \times 10^3$. Clearly, flow is turbulent for all test cases. Figure 20 shows an example of the Re components.

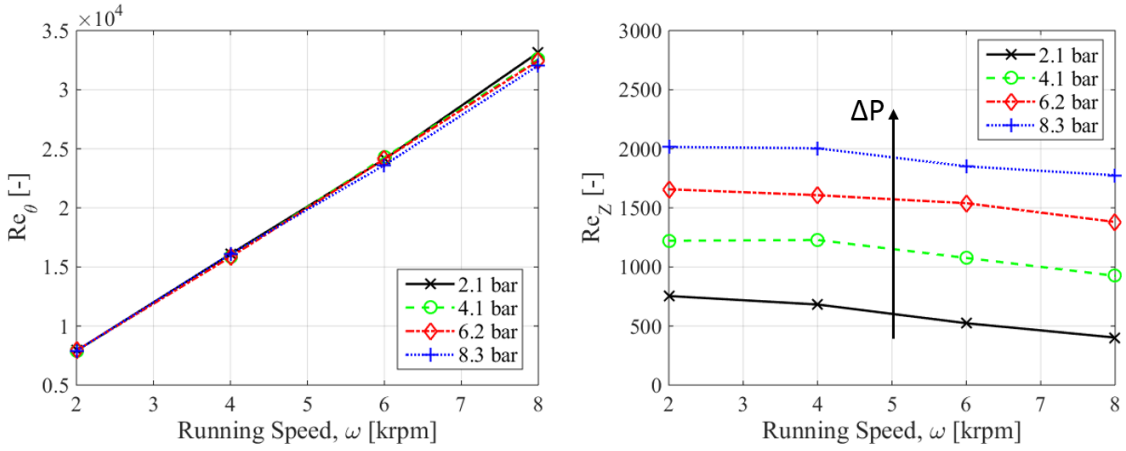

Figure 20. SS/GR seal (a) circumferential and (b) axial Re versus ω for the centered position and varying ΔP values.

As expected, Re_θ increases with ω but remains relatively constant with ΔP, whereas Re_Z increases with ΔP but decreases with ω. Note the large magnitude of Re_θ relative to the magnitude of Re_Z. Figure 21 shows the ratio Re_θ/Re_Z as a function of ω.

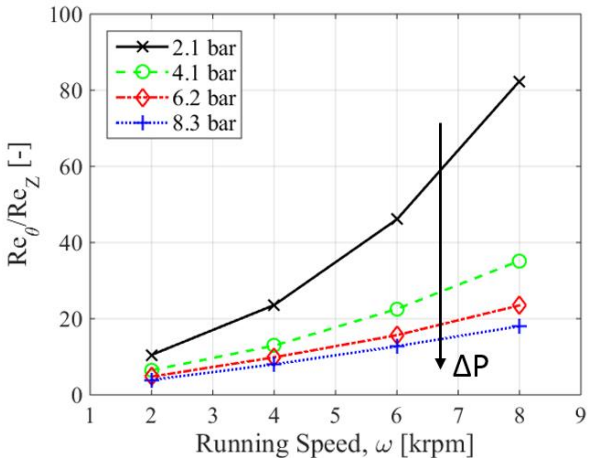

Figure 21. SS/GR seal Re_θ/Re_Z versus ω for the centered position and varying ΔP values.

The maximum Re_θ/Re_Z for the test data is 91.3 while the minimum is 3.5. Clearly, circumferential flow dominates within the seal annulus.

7.1 Dynamic Stiffness

An example of the real component of the calculated dynamic stiffness after the baseline has been subtracted is presented in Fig. 22.

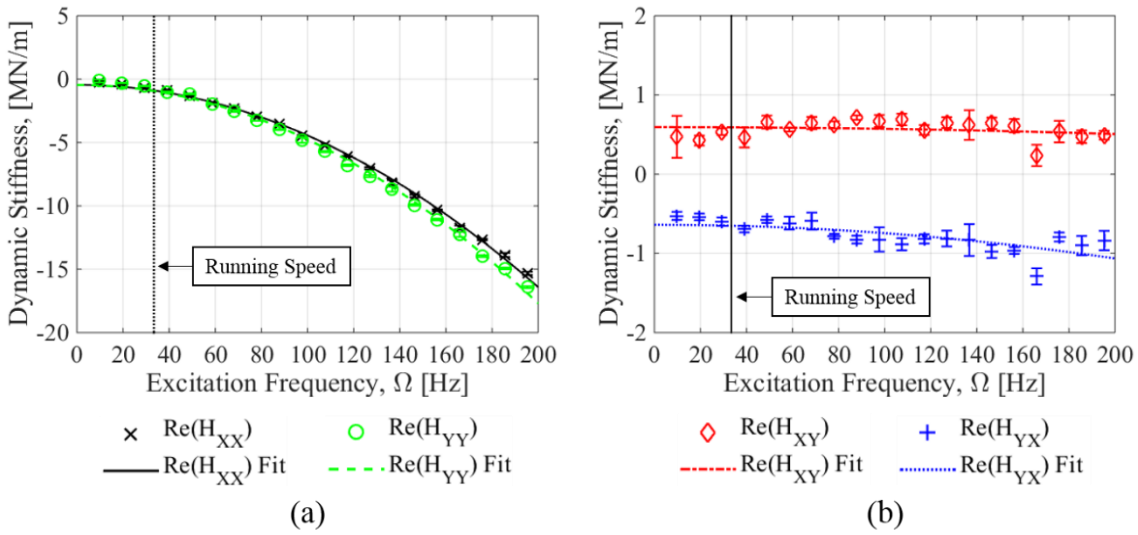

Figure 22. Real component of the SS/GR seal (a) direct and (b) cross-coupled dynamic stiffness versus Ω for ω = 2 krpm, ΔP = 2.07 bar, ε_0 = 0.00.

Figure 22a shows good agreement with the model in Eq. (15). Figure 22b shows little variation in dynamic stiffness with Ω. Figure 23 shows the imaginary component of $\boldsymbol{H_{ij}}$.

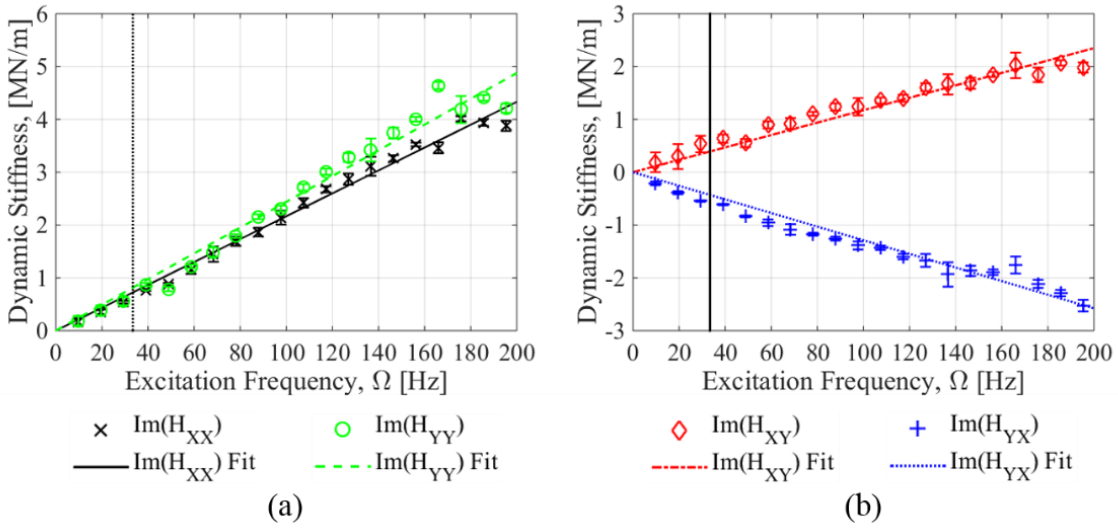

Figure 23. Imaginary component of the SS/GR seal (a) direct and (b) cross-coupled dynamic stiffness versus Ω for ω = 2 krpm, ΔP = 2.07 bar, ε_0 = 0.00

Clearly, the data agrees well with the model in Eq. (15). These dynamic stiffness are representative of the remainder of the data with the exception of a few data points with erratic dynamic stiffness values at high frequencies ($\Omega > 140$).

7.2 Rotordynamic Coefficients

7.2.1 Stiffness Coefficients

For most of the test points, direct stiffness was negative in one or both of the coordinate axes. Generally direct stiffness decreases (becomes more negative) with increasing ε_0 and increasing ω as shown in Fig. 24.

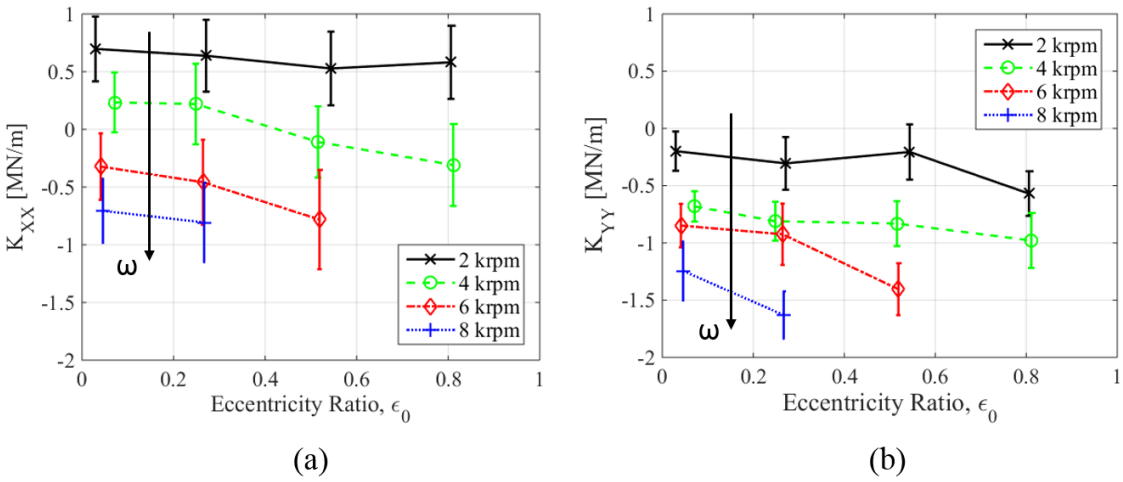

Figure 24. SS/GR seal (a) K_{XX} and (b) K_{YY} versus ε_0 at ΔP = 6.21 bar and a range of ω values.

Note that $K_{XX} \neq K_{YY}$ as suggested by Eq. (1) for $\varepsilon_0 \cong 0$. Negative stiffness would significantly affect pump rotordynamics and lower the system natural frequency.

Figure 25 shows cross-coupled stiffness as a function of ε_0. Note that the *y*-axis in Fig. 25b is reversed. The magnitudes of the cross-coupled stiffness are equal and opposite ($K_{XY} = -K_{YX}$) as predicted by Eq. (1), and the values tend to decrease as ε_0 increases. Cross-coupled stiffness increases strongly with increasing ω. The SS/SR seal stiffness follows the same trends with respect to ω.

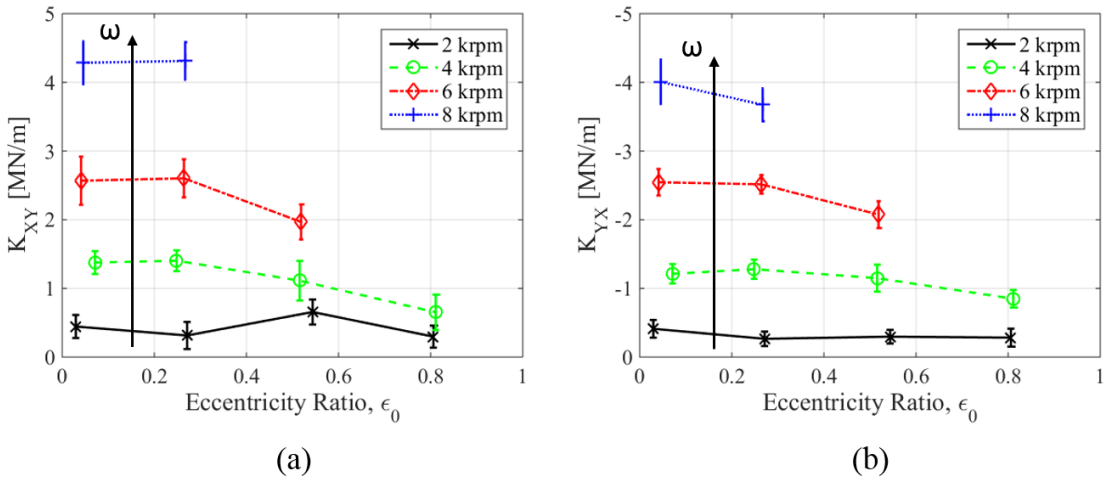

Figure 25. SS/GR seal (a) K_{XY} and (b) K_{YX} versus ε_0 at ΔP = 6.21 bar and a range of ω values.

Figure 26 compares SS/GR seal stiffness with SS/SR seal stiffness as a function of ε_0. Clearly, direct stiffness is greater for the SS/SR seal. The smooth seals also show a greater dependence on ε_0 with relatively large magnitudes at ε_0 = 0.8. Cross-coupled stiffness is comparable at low ε_0 but diverges as $\varepsilon_0 \rightarrow 0.8$ for the SS/SR seal. The opposite is the case for the SS/GR seal. In general, cross-coupled stiffness magnitude is greater for the SS/SR seal than for the SS/GR seal.

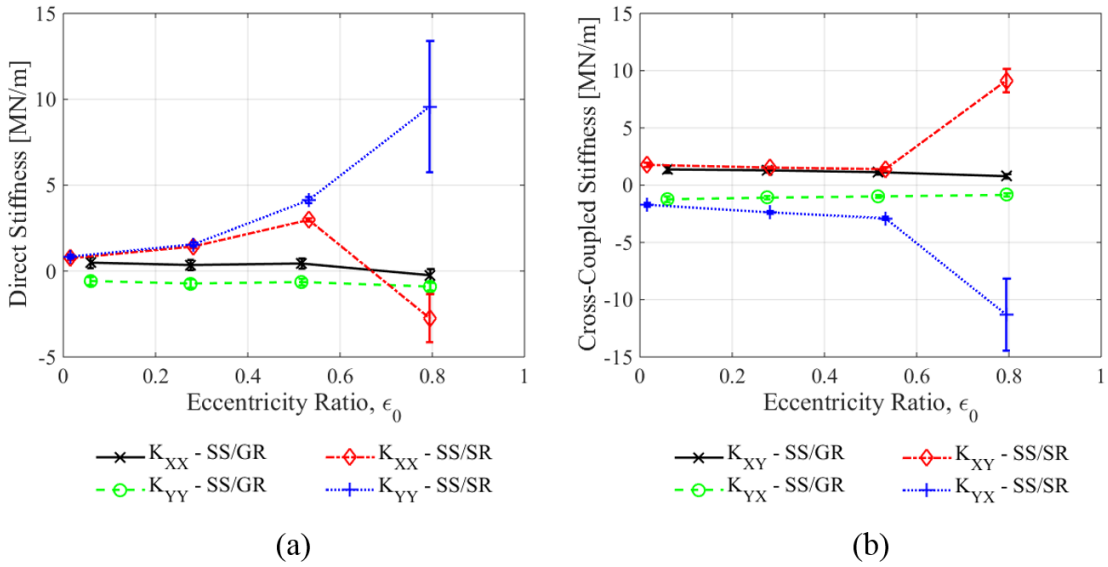

Figure 26. Comparison between SS/GR and SS/SR seals. (a) Direct and (b) cross-coupled stiffness versus $\boldsymbol{\epsilon_0}$ at $\boldsymbol{\omega}$ = 4 krpm, $\boldsymbol{\Delta P}$ = 8.27 bar.

With respect to ΔP, the SS/GR seal shows weak dependence. Figure 27 compares the SS/GR seal stiffness to the SS/SR seal stiffness with varying ΔP. While the SS/GR seal direct stiffness values generally increase slightly or remain relatively constant with increasing ΔP, the SS/SR seal stiffness increases dramatically. The magnitude of cross-coupled stiffness increases comparably with increasing ΔP for both seals.

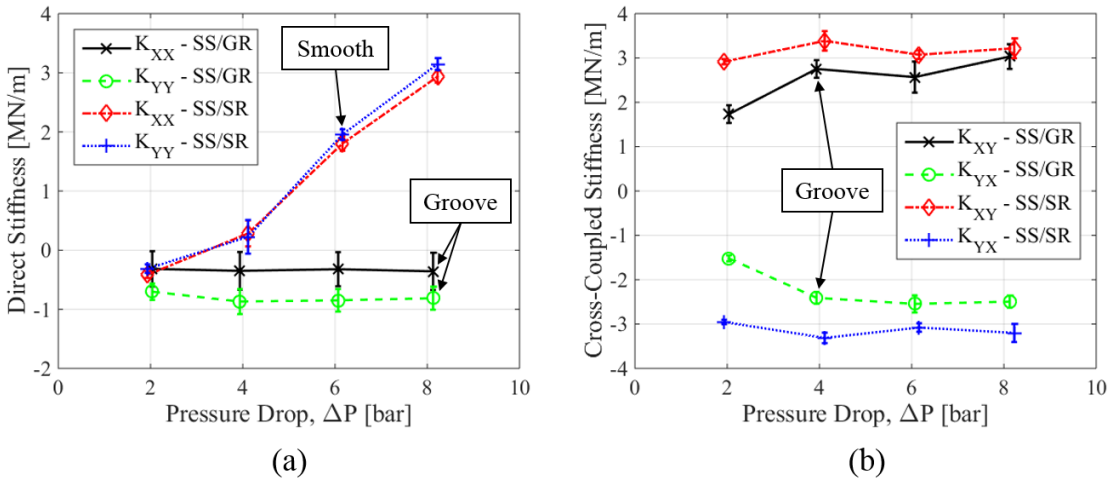

Figure 27. Comparison between SS/GR and SS/SR seals. (a) Direct and (b) cross-coupled stiffness versus ΔP at ω = 6 krpm, ε_0 = 0.00.

Figure 28 shows the stiffness coefficients versus increasing PSR. Direct stiffness generally decreases with increasing PSR for the SS/GR seal, while the trend is unclear for the SS/SR seal. As expected, PSR is a destabilizing factor for both seals which show cross-coupled stiffness increasing in magnitude with PSR.

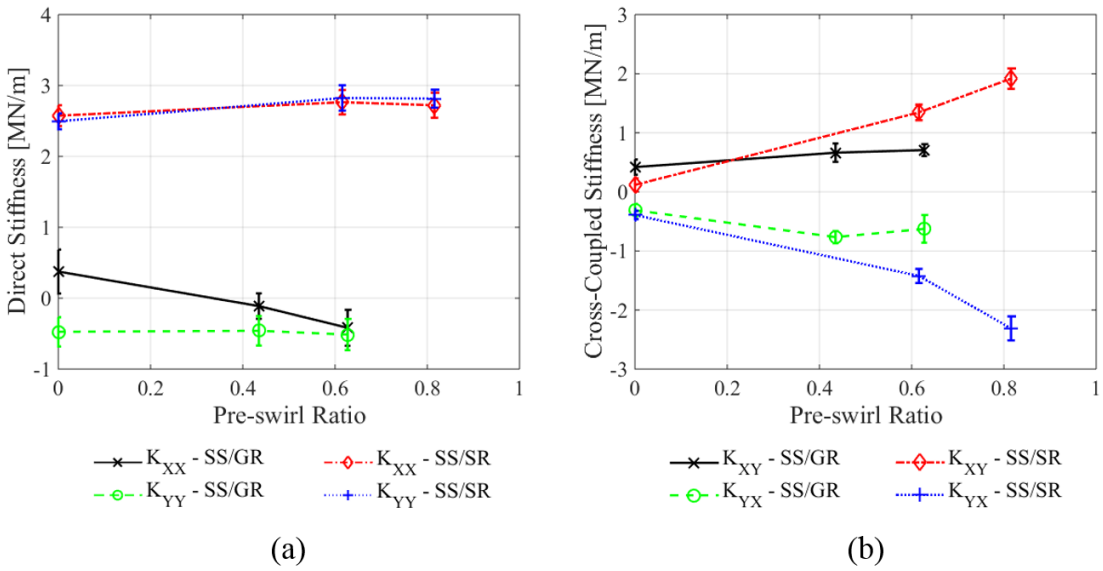

Figure 28. Comparison between SS/GR and SS/SR seals. (a) Direct and (b) cross-coupled stiffness versus PSR at ω = 2 krpm, ΔP = 4.14 bar, and ε_0 = 0.00.

In summary, low ω, high ΔP, low PSR, and centered operation provide the most favorable stiffness coefficients for the SS/GR seal. These conditions maximize K_{XX} and K_{YY} while minimizing $|K_{XY}|$ and $|K_{YX}|$. Unfortunately, negative direct stiffness is present for the vast majority of operating conditions tested.

7.2.2 Damping Coefficients

Figure 29 shows direct damping versus ε_0 for the SS/GR seal. Direct damping tends to decrease with increasing ε_0 but increase with increasing ΔP.

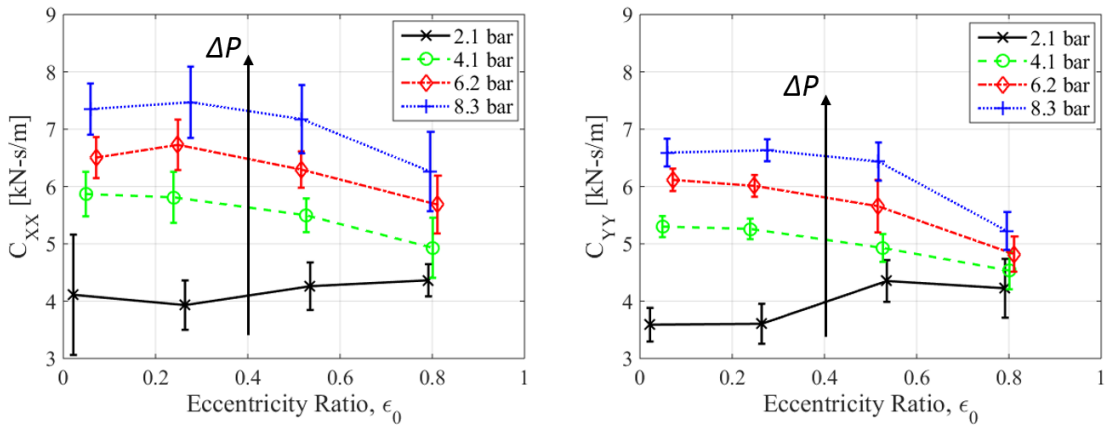

Figure 29. (a) C_{XX} and (b) C_{YY} versus ε_0 at ω = 4 krpm and a range of ΔP for the SS/GR seal.

Figure 30 shows cross-coupled damping increasing in magnitude with increasing ε_0 and ΔP. Note the reversed *y*-axis in Fig. 30b. With regards to ΔP, the SS/GR seal follows similar trends as the SS/SR seal.

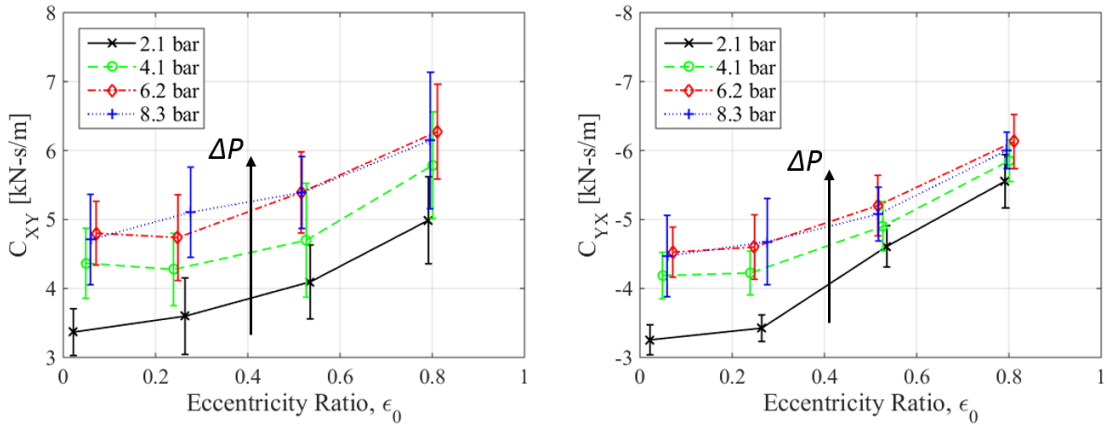

Figure 30. (a) C_{XY} and (b) C_{YX} versus ε_0 at ω = 4 krpm and a range of ΔP for the SS/GR seal.

Figure 31 shows that the SS/GR seal damping coefficients are much less dependent on ε_0 compared to the SS/SR seal. At low ε_0 the direct damping of the groove seal is approximately half that of the smooth seal while cross-coupled damping is of similar value. Most notable is the dramatic difference at ε_0 = 0.80.

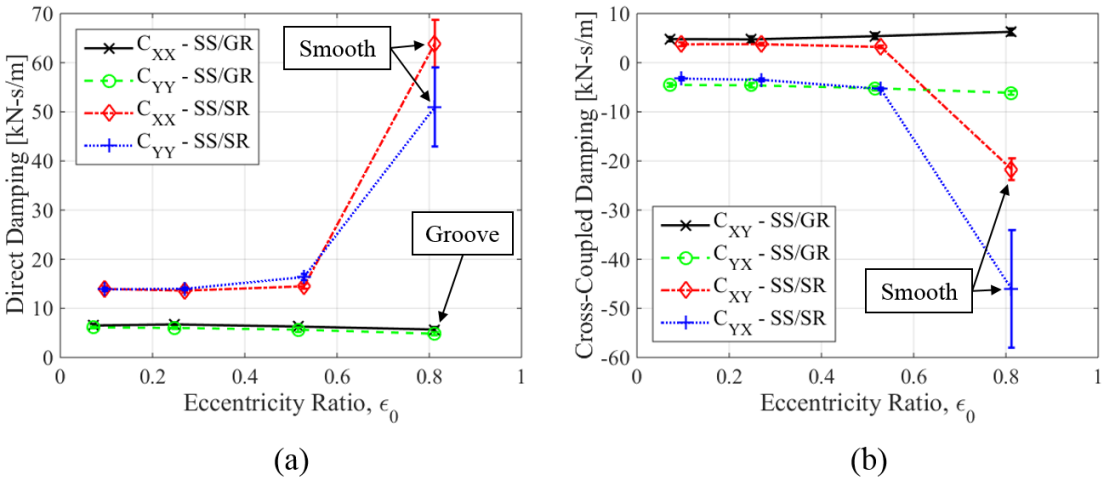

Figure 31. Comparison between SS/GR and SS/SR seals. (a) Direct and (b) cross-coupled damping versus ε_0 at ω = 4 krpm, ΔP = 6.21 bar.

Figure 32 shows damping versus ω for both seals. Generally, for both seals, direct damping and the magnitude of cross-coupled damping increase with ω.

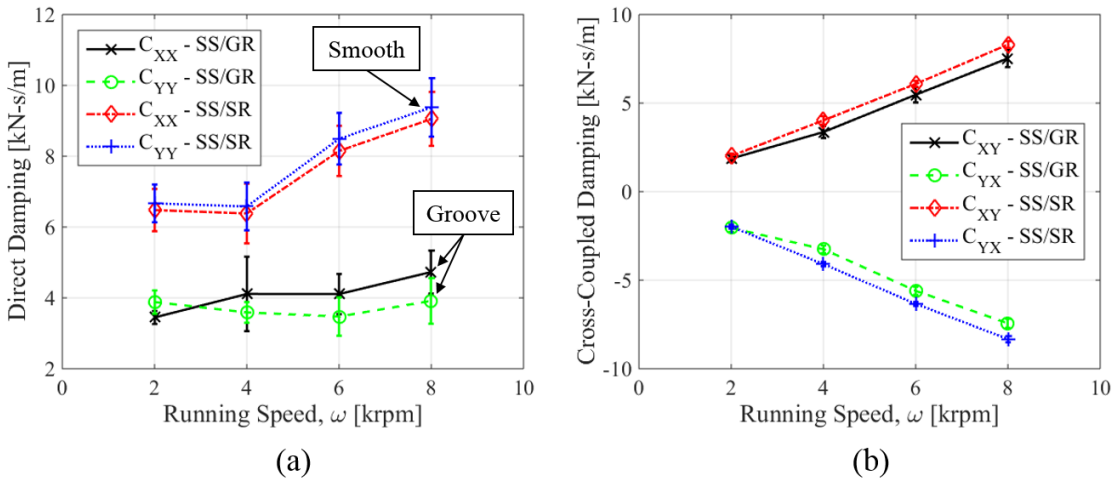

Figure 32. Comparison between SS/GR and SS/SR seals. (a) Direct and (b) cross-coupled damping versus ω at ΔP = 2.07 bar, ε_0 = 0.00.

Pre-swirl ratio has a small effect on the damping coefficients of both seals. Figure 33a shows direct damping remaining relatively constant with increasing PSR while Fig. 33b shows cross-coupled damping increasing modestly with PSR.

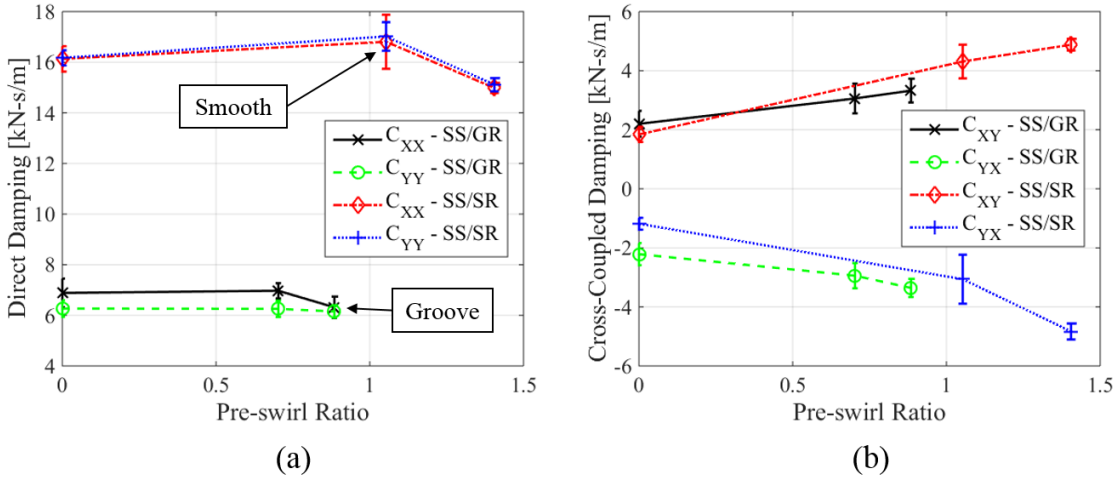

Figure 33. Comparison between SS/GR and SS/SR seals. (a) Direct and (b) cross-coupled damping versus PSR at ω = 2 krpm, ΔP = 8.27 bar, ε_0 = 0.00.

7.2.3 Virtual Mass Coefficients

Figure 34 shows M_{XX} and M_{YY} increasing with increasing ε_0 and increasing ΔP at ω = 4 krpm. Values of M_{XY} and M_{YX} are generally small and show no clear relation to ε_0 and ΔP.

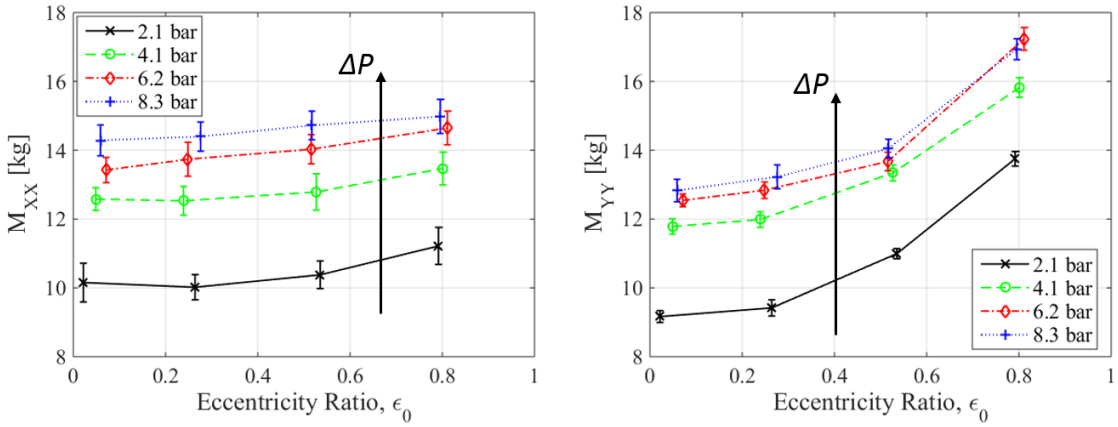

Figure 34. (a) M_{XX} and (b) M_{YY} versus ε_0 at ω = 4 krpm and a range of ΔP for the SS/GR seal.

Figure 35 shows a comparison of the two seals at ω = 4 krpm and ΔP = 8.27 bar. Compared to the SS/SR seal, direct virtual mass of the groove seal is smaller and relatively independent of ε_0. Note the particularly large differences in both the direct and cross-coupled virtual mass terms at ε_0 = 0.80.

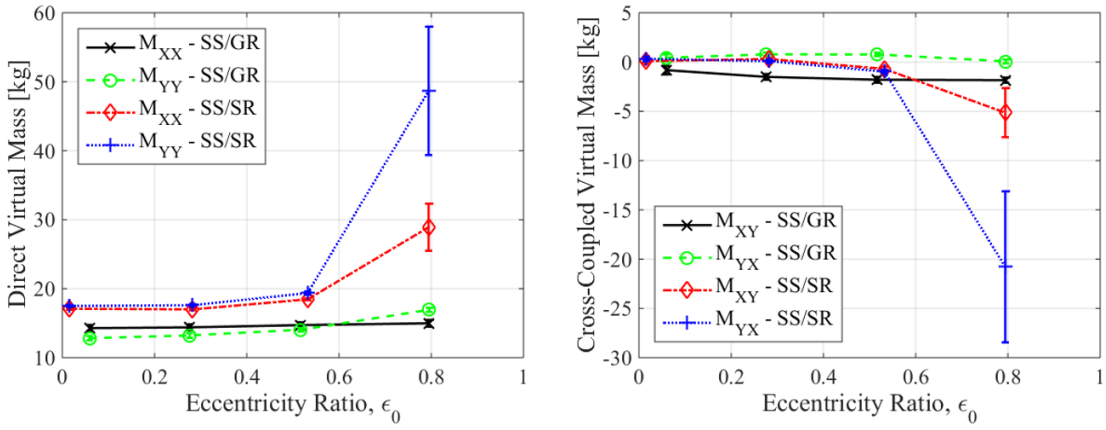

Figure 35. Comparison between SS/GR and SS/SR seals. (a) Direct and (b) cross-coupled virtual mass versus ϵ_0 at ω = 4 krpm, ΔP = 8.27 bar.

Figure 36a shows M_{XX} and M_{YY} decreasing with respect to increasing ω for both seals. Figure 36b shows M_{XY} and M_{YX} for both seals. For the smooth seal cross-coupled virtual mass, $M_{XY} = -M_{YX}$, increases in magnitude with ω while there is no clear trend for the groove seal. Cross-coupled virtual mass terms of opposite sign are a destabilizing factor. Consequently, the effect of M_{XY} and M_{YX} is considered in the calculation of WFR.

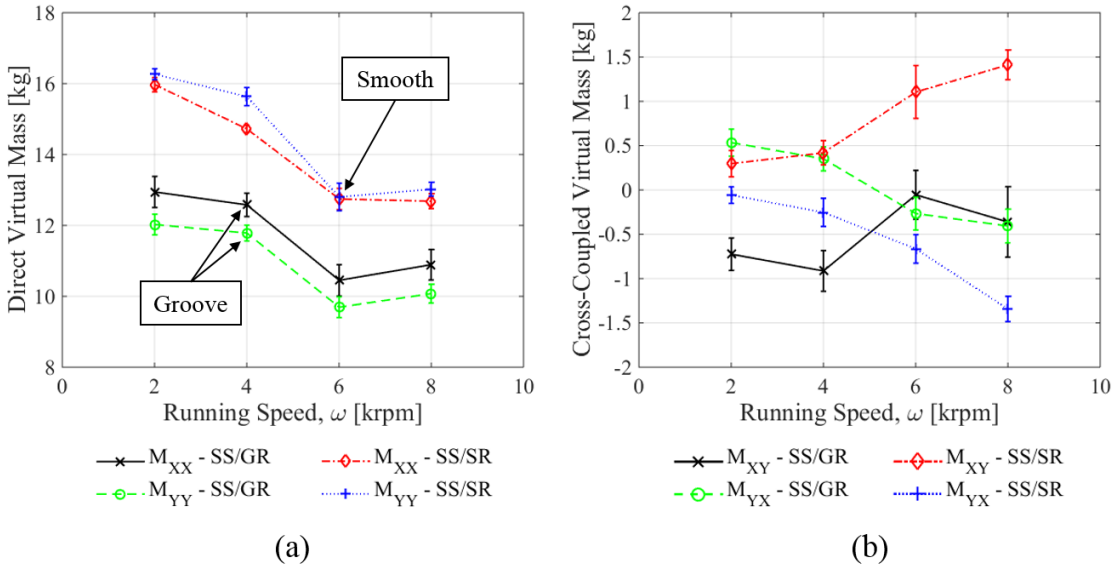

Figure 36. Comparison between SS/GR and SS/SR seals. (a) Direct and (b) cross-coupled virtual mass versus ω at ΔP = 4.14 bar, ε_0 = 0.00.

Changes in the direct and cross-coupled virtual mass terms with respect to PSR are all small. Figure 37 shows only M_{XX} and M_{YY} versus PSR. For the SS/SR seal, M_{XX} and M_{YY} generally increase with PSR. With the exception of the ω = 2 krpm data points, M_{XX} and M_{YY} of the groove seal follows this same trend.

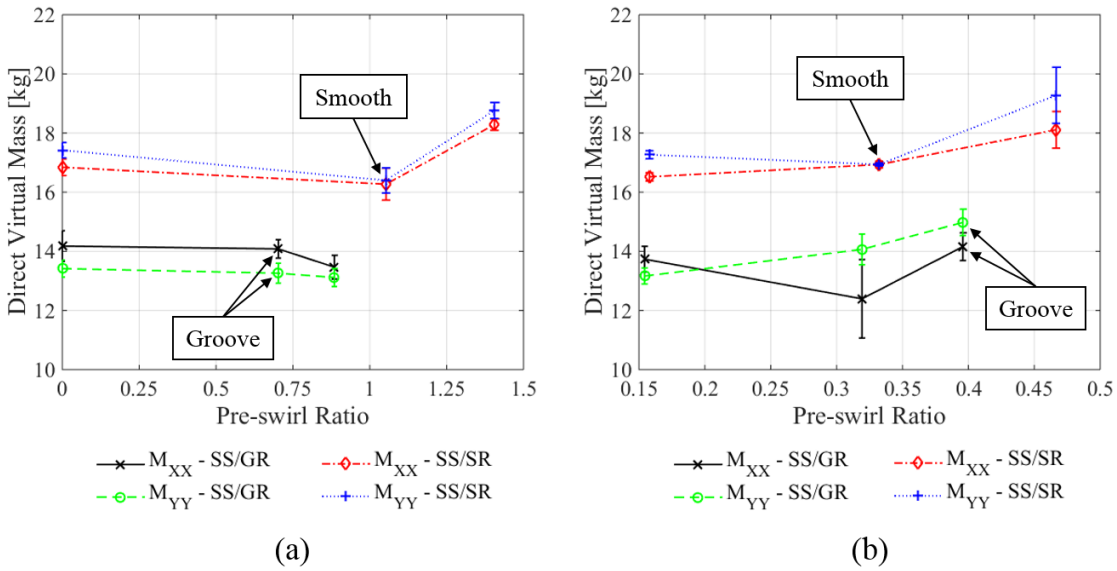

Figure 37. Comparison between SS/GR and SS/SR seals. Direct virtual mass versus PSR at (a) ω = 2 krpm, ΔP = 8.27 bar, ε_0 = 0.00 and (b) ω = 6 krpm, ΔP = 8.27 bar, ε_0 = 0.00.

7.3 Whirl Frequency Ratio

To account for the destabilizing nature of the cross-coupled virtual mass, the author uses the definition of WFR given by San Andrés [11] and detailed in Appendix B. Calculations for WFR using both San Andrés' definition and Lund's definition [10] are given in Appendix A.

Figure 38 shows the whirl frequency ratio for the SS/GR seal at various operating conditions. For the WFR values shown in Fig. 38, the pre-swirl values range from 0 to 0.34. Figure 38a shows WFR decreasing with increasing ε_0. This trend is representative of the rest of the data. Additionally, WFR generally decreases with increasing ΔP, although the effect is more pronounced at lower speeds. As shown in Fig. 38b, WFR

generally increases with increasing ω. Generally, WFR ≥ 0.5 indicating that the SS/GR seal possesses stability characteristics worse than a plain journal bearing (WFR ≈ 0.5).

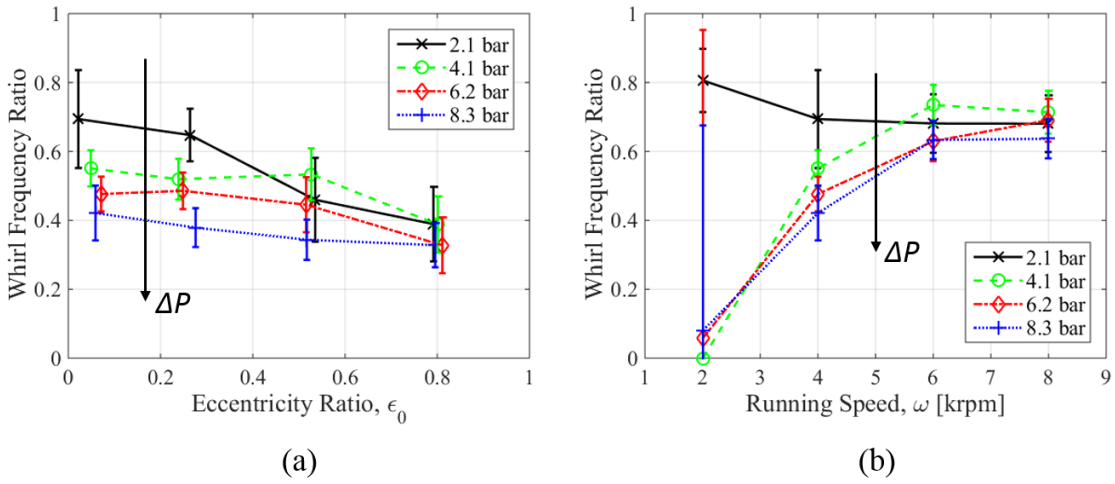

Figure 38. (a) SS/GR seal WFR versus ε_0 at ω = 4 krpm. (b) SS/GR seal WFR versus ω at ε_0 = 0.00. For the values shown, PSR ranges from 0 to 0.34.

Note the large uncertainty bars for the low WFR values in Fig. 38b. These large error bars arise because of the small WFR value coupled with the method of uncertainty propagation as described in Appendix C. Nevertheless, the points are included in the plots because they agree with the trends present in the rest of the data.

Figure 39 shows the effect of PSR on the WFR. At $\omega \leq 4$ krpm, WFR increases with increasing PSR as shown in Fig. 39a, once again demonstrating the destabilizing effect of increasing PSR. At $\omega \geq 6$ krpm, WFR remains relatively constant as shown in Fig. 39b. Notice the differing *x*-axis and *y*-axis scales between Fig. 39a and Fig. 39b.

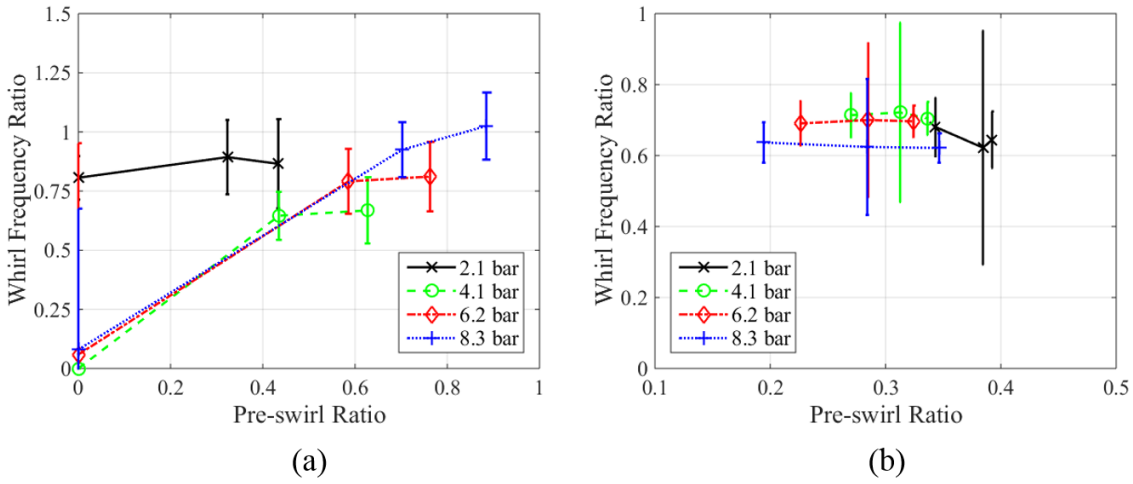

Figure 39. SS/GR seal WFR versus PSR for the centered position at (a) ω = 2 krpm and (b) ω = 8 krpm.

Note that calculated WFR can reach values up to 1.2 indicating that the system would go unstable at $0.83\omega_{n1}$. Additionally, note that WFR is generally greater than the measured PSR. Clearly, from a rotordynamics stability perspective, the seals perform poorly.

7.4 Effective Damping

Figure 40 compares C_{eff} of the SS/GR seal to the SS/SR seal. For the C_{eff} values shown in Fig. 40, the pre-swirl values range from 0 to 0.36. Figure 40a shows C_{eff} as a function of ΔP while Fig. 40b shows C_{eff} as a function of ω. From the definition of C_{eff} in Eq. (6), values are reported for the centered position. Grooved seal C_{eff} is lower than smooth seal C_{eff} once again indicating that the smooth seal rotordynamic characteristics are preferable. Both the SS/GR seal and SS/SR seal C_{eff} follow the same trends with regards to ΔP and ω, namely C_{eff} increases with increasing ΔP and decreases with increasing ω.

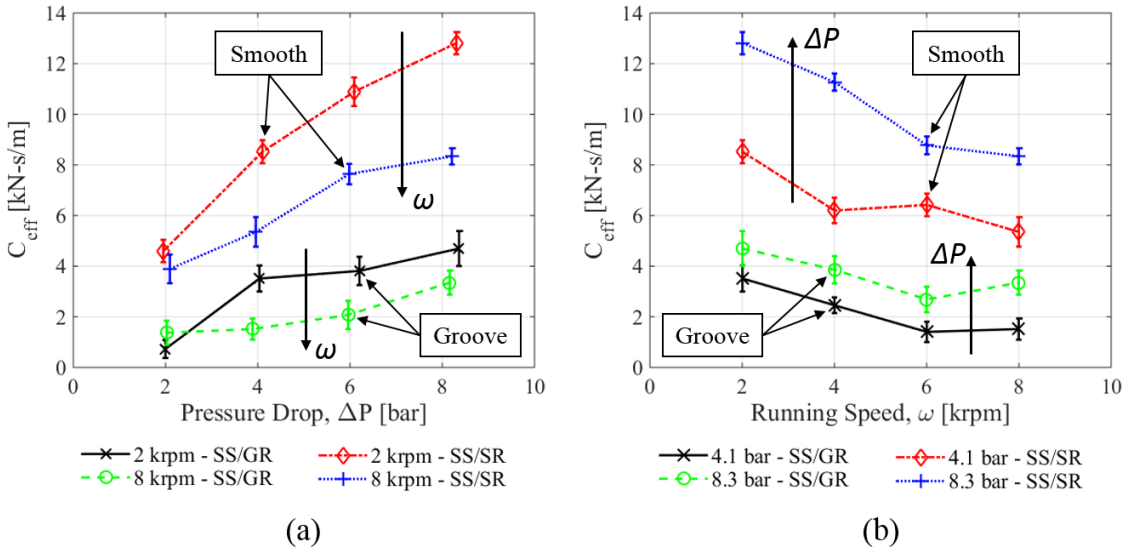

Figure 40. Comparison of SS/GR seal and SS/SR seal. (a) C_{eff} versus ΔP and (b) C_{eff} versus ω. For the values shown, PSR ranges from 0 to 0.36.

Figure 41 shows C_{eff} versus PSR. C_{eff} decreases with increasing PSR at $\omega \leq 4$ krpm for the SS/GR seal but remains relatively constant for $\omega \geq 6$ krpm. For the SS/SR seal, C_{eff} decreases with increasing PSR at all speeds. The effect of PSR on C_{eff} demonstrates once more the destabilizing nature inlet swirl.

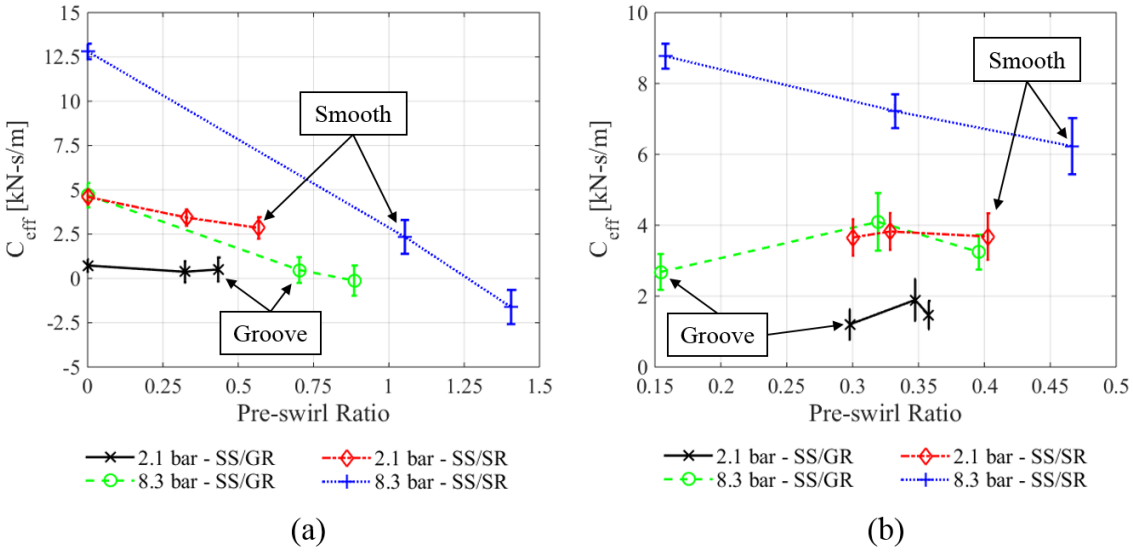

Figure 41. Comparison of SS/GR seal and SS/SR seal. C_{eff} versus PSR at (a) ω = 2 krpm and (b) ω = 6 krpm.

8. SUMMARY AND CONCLUSIONS

Available literature regarding smooth stator/circumferentially grooved rotor liquid annular seals is scarce. The author was unable to find measured tests results for a smooth stator/grooved rotor (SS/GR) seal. Furthermore, test results within the literature for liquid annular seals at higher eccentricity ratios ($\varepsilon_0 > 0.5$) are limited. Additionally, very few investigators test seals with imposed and measured pre-swirl, and, to the author's knowledge, there exist no measured outlet swirl results. Consequently, this project aims to address these deficiencies and quantify the effect of varying pre-swirl and wide-ranging static eccentricity on the static and dynamic characteristics of the SS/GR seal.

The seal has 15 square grooves, a nominal radial clearance of C_r = 203.2 μm (8 mil), and a length-to-diameter ratio of L/D = 0.5. The author conducts tests at speeds of ω = 2, 4, 6, 8 krpm, axial pressure drops of ΔP = 2.07, 4.14, 6.21, 8.27 bar (30, 60, 90, 120 psi), and eccentricity ratios of ε_0 = 0.00, 0.27, 0.53, and 0.80. Pre-swirl is imposed and varied between low, medium, and high velocities using three distinct radial- and tangential-injection stator inserts. The lubricant is ISO VG 2 oil at 46.1°C (115°F). Flow is turbulent for all test points. Grooved-seal results are compared to results of a smooth stator/smooth rotor (SS/SR) seal of equal L, D, and nominal C_r at the same operating conditions

Static measurements include leakage rate ($\dot{Q}$), applied static load (F_s), static eccentricity ratio (ε_0), pre-swirl ratio (PSR), and outlet swirl ratio (OSR). Grooves

significantly reduce $\dot{Q}$ at higher ΔP and lower ω. At ω = 2 krpm and ΔP = 8.27 bar, the SS/GR seal $\dot{Q}$ is 0.70 times the SS/SR seal $\dot{Q}$ for a total reduction of 19 LPM. However, at high ω and low ΔP grooved seal $\dot{Q}$ is 0.8 to 0.9 times that of the smooth seal. At these operating conditions $\dot{Q}$ reductions are on the order of 2 LPM. Consequently, machining grooves onto the rotor for $\dot{Q}$ reduction is only productive at higher ΔP and lower ω.

Measured OSR is generally lower for the SS/GR seal than for the SS/SR seal. Measured OSR is also generally less than 0.5 contrary to the predictions of Black et al. [12]. This disagreement may be due to the position of the outlet pitot tube.

Dynamic measurements include rotor-stator relative displacement, stator acceleration, and applied dynamic excitations. The author calculates the rotordynamic coefficients using a least-squares fit of the dynamic stiffness data. Most noteworthy of the dynamic results is the negative direct stiffness of the SS/GR seal. Negative direct stiffness would have a detrimental effect to pump rotordynamics, lowering both the natural frequency and the onset speed of instability. Direct stiffness becomes more negative with increasing ε_0, ω, and PSR. Increasing PSR is also a destabilizing force as it increases the difference between K_{XY} and K_{YX}. The author recommends efforts to minimize pre-swirl, for example, by adding swirl brakes. The magnitude of cross-coupled stiffness is generally slightly larger for the smooth seal than for the groove seal.

Calculated WFR is generally high ($\geq$0.5) for the SS/GR seal with values reaching 1.2. WFR increases with PSR at $\omega \leq$ 4 krpm but remains relatively constant at $\omega \geq$ 6 krpm. WFR is generally greater than measured PSR. Direct damping coefficients of the SS/GR seal are typically half the value of the SS/SR seal coefficients. This leads

to lower C_{eff} values for the SS/GR seal than the SS/SR seal indicating that the SS/GR seal has worse rotordynamic characteristics.

Recalling the work of Marquette et al. [20], [21], the magnitudes of the stiffness and damping coefficients of their grooved stator/smooth rotor (GS/SR) seals shown in Table 1 are comparable to the values of the SS/GR seal in this study, despite testing at much higher running speeds ($\omega = 10.2, 17.4, 24.6$ krpm) and pressure drops ($\Delta P = 41.4, 55.2, 68.9$ bar). Similar to this present study, Marquette et al. found that direct stiffness coefficients of their grooved seals decreased with increasing ω and were weak functions of ε_0. Additionally, both types of grooved seals (GS/SR and SS/GR) had C_{eff} values lower than the analogous smooth-seal C_{eff} values. The low direct damping values in both types of grooved seal lead to poor rotordynamic performance characteristics relative to smooth seals.

Overall, increases in PSR have a detrimental effect on SS/GR seal rotordynamic performance. Additionally, operation at high ε_0 for the SS/GR seal had negative effects on $\dot{Q}$ and direct stiffness. Future work should include the development of a SS/GR seal computer code to compare predictions with measured results. Additionally, the author recommends conducting a CFD analysis on the OSR to determine if the location of the pitot tube is the cause for the disagreement with Black et al. [12]. This will provide insight into possible stator redesigns.

REFERENCES

[1] Childs, D.W., 2013, *Turbomachinery Rotordynamics with Case Studies*, Wellborn, Texas: Minter Spring Publishing.

[2] Childs, D.W., 1983, "Finite-Length Solutions for Rotordynamic Coefficients of Turbulent Annular Seals," *ASME Journal of Lubrication*, **105**, pp. 437-444.

[3] Black, H.F., 1979, "Effects of Fluid-Filled Clearance Spaces on Centrifugal Pump and Submerged Motor Vibrations," in *Eighth Turbomachinery Symposium*, College Station, Texas, Texas A&M University, pp. 29-34.

[4] Black, H.F., 1969, "Effects of Hydraulic Forces in Annular Pressure Seals on the Vibrations of Centrifugal Pump Rotos," *Journal of Mechanic Engineering Science*, **11**, pp. 206-213.

[5] Pinkus, O., and Sternlicht, B., 1961, *Theory of Hydrodynamic Lubrication*, New York: McGraw-Hill.

[6] Lomakin, A., 1958, "Calculation of Critical Number of Revolutions and the Conditions Necessary for Dynamic Stability of Rotors in High-Pressure Hydraulic Machines When Taking Into Account Forces Originating in Sealings," *Journal for Power and Mechanical Engineering (In Russian),* **14**.

[7] San Andrés, L., "Notes 5 - Dynamics of a Rigid Rotor-Fluid Film Bearing System," 2009. [Online]. Available: http://rotorlab.tamu.edu/tribgroup/default.htm. [Accessed January 2016].

[8] Nelson, C., and Nguyen, D., 1988, "Analysis of Eccentric Annular Incompressible Seals: Part 1 - A New Solution Using Fast Fourier Transforms for Determining Hydrodynamic Force," *Journal of Tribology*, **110**, pp. 354-359.

[9] Nelson, C., and Nguyen, D., 1988, "Analysis of Eccentric Annular Incompressible Seals: Part 2 - Effects of Eccentricity on Rotordynamic Coefficients," *Journal of Tribology*, **110**, pp. 361-366.

[10] Lund, J., 1966, *Self-excited, Stationary Whirl Orbits of a Journal in a Sleeve Bearing*, Rensselaer Polytechnic Institute.

[11] San Andrés, L., 1991, "Effect of Eccentricity on the Force Response of a Hybrid Bearing," *Tribology Transactions*, **34**, pp. 537-544.

[12] Black H.F., Allaire, P., and Barret, L., 1981, "Inlet Flow Swirl in Short Turbulent Annular Seal Dynamics," in *Ninth International Conference on Fluid Sealing*, Noordwijkerhout, Netherlands, pp. 141-152.

[13] Benckert, H., and Wachter, J., 1980 "Flow Induced Spring Constants of Labyrinth Seals for Applications in Rotor Dynamics," in *Proceedings of the 1st Workshop on Rotordynamic Instability Problems in High-Performance Turbomachinery*, College Station, Texas, Texas A&M University, pp 189-212.

[14] Iwatsubo, T., Sheng, B., and Matsumoto, T., 1989, "An Experimental Study on the Static and Dynamic Characteristics of Pump Annular Seals," in *Rotordynamic Instability Problems in High Performance Turbomachinery*, NASA, Lewis Research Center, pp. 229-251.

[15] Iwatsubo, T., Sheng, B., and Ono, M., 1990, "Experiment of Static and Dynamic Characteristics of Spiral Grooved Seals," in *Proceedings of the 6th Workshop on Rotordynamic Instability*, pp. 223-233.

[16] Nordmann, R., Dietzen, F., Janson, W., Frei, A., and Florjancic, S., 1987 "Rotordynamic Coefficients and Leakage Flow of Parallel Grooved Seals and Smooth Seals," in *Rotordynamic Instability Problems in High-Performance Turbomachinery*, NASA, Lewis Research Center, pp. 129-153.

[17] Iwatsubo, T., Yang, B., and Ibaraki, R., 1987, "Static and Dynamic Characteristics of Parallel-Grooved Seals," in *Rotordynamic Instability Problems in High-Performance Turbomachinery*, NASA, Lewis Research Center, pp. 99-126.

[18] Iwatsubo, T., and Sheng, B., 1990, "Evaluation of Dynamic Characteristics Parallel Grooved Annular Seals by Theory and Experiment," in *IFToMM Third International Conference on Rotorydynamics*, Lyon, France, pp. 313-318.

[19] Marquette, O.R., and Childs, D.W., 1996, "An Extended Three-Control-Volume Theory for Circumferentially-Grooved Liquid Seals," *Journal of Tribology*, **118**, pp. 276-285.

[20] Marquette, O.R., Childs, D.W., and Philips, S.G., 1997, "Theory Versus Experiments for Leakage and Rotordynamic Coefficients of Circumferentially-Grooved Liquid Annular Seals With L/D of 0.45," in *Proceedings of the 1997 ASME Fluids Engineering Division Summer Meeting*, Vancouver, Canada, pp. 1-16.

[21] Marquette, O.R., Childs, D.W., and San Andrés, L., 1997, "Eccentricity Effects on the Rotordynamic Coefficients of Plain Annular Seals: Theory Versus Experiment," *Journal of Tribology*, **119**, pp. 443-447.

[22] Kanki, H., and Kawakami, T., 1984, "Experimental Study on the Dynamic Characteristics of Pump Annular Seals," in *Proceedings of the Third IMechE International Conference on Vibrations in Rotating Machinery*, York, England, pp. 159-166.

[23] Falco, M., Mimmi, G., and Marenco, G., 1986, "Effects of Seals on Rotor Dynamics," in *Proceedings of the International Conference on Rotordynamics*, Tokyo, Japan.

[24] Salas III, J., 2016, *Influence of Pressure-Dams in Liquid Annular Seals in the Laminar Flow Regime, Measured Results for Static and Rotordynamic Characteristics*, Texas A&M University, College Station, Texas.

[25] Kaul, A., 1999, *Design and Development of a Test Setup for the Experimental Determination of the Rotordynamic and Leakage Characteristics of Annular Bushing Oil Seals,* College Station, Texas: Texas A&M University.

[26] Glienicke, J., 1966-67, "Experimental Investigation of the Stiffness and Damping Coefficients of Turbine Bearings and Their Application to Instability Prediction," in *Proceedings of IMechE 1966-67,* **181**, pp. 116-129.

[27] Mitchell, L.D., and Elliott, K.B., 1984, "How to Design Stingers for Vibration Testing of Structures," *Sound and Vibration,* **18**, pp. 14-18.

[28] Rouvas, C., and Childs, D.W., 1993, "A Parameter Identification Method for the Rotordynamic Coefficients of a High Reynolds Number Hydrostatic Bearing," *Jounal of Vibration and Acoustics,* **115**, pp. 264-270.

[29] Childs, D.W., and Hale, K., 1994, "A Test Apparatus and Facility to Identify the Rotordynamic Coefficients of High-Speed Hydrostatic Bearings," *Journal of Tribology,* **116**, pp. 337-343.

[30] Beckwith, T., Marangoni, R., and Lienhard V, J. , 2007, *Mechanical Measurements*, Upper Saddle River, NJ: Pearson Education, Inc.

APPENDIX A: TABULATED RESULTS

Assembly 1 – Radial Injection

Table A.1. Static results of the SS/GR seal with radial injection.

Test Point	Target ω	Target ΔP	Target ε_0	Measured ω	Measured ΔP	Measured ε_0	ϕ	$\dot{Q}$	F_r
	[rpm]	[bar]	[-]	[rpm]	[bar]	[-]	[deg]	[LPM]	[N]
1	2000	2.068	0.00	2003.9	1.994	0.018	-130.5	16.86	2.1
2	2000	2.068	0.27	2005.3	1.996	0.278	54.8	16.86	28.8
3	2000	2.068	0.53	2004.5	1.984	0.545	-0.3	17.43	-11.1
4	2000	2.068	0.80	2004.5	2.052	0.805	1.3	19.38	-25.7
5	2000	4.137	0.00	2004.8	4.031	0.019	34.6	27.35	-0.2
6	2000	4.137	0.27	2004.7	4.111	0.285	1.6	28.14	-3.7
7	2000	4.137	0.53	2004.8	4.008	0.544	4.1	29.22	-2.0
8	2000	4.137	0.80	2004.8	4.118	0.790	3.4	32.34	-6.8
9	2000	6.205	0.00	2005.2	6.194	0.029	122.7	36.98	1.4
10	2000	6.205	0.27	2004.7	6.213	0.271	9.3	37.37	8.8
11	2000	6.205	0.53	2005.4	6.245	0.544	4.4	39.76	11.8
12	2000	6.205	0.80	2005.5	6.183	0.806	3.8	42.69	13.0
13	2000	8.274	0.00	2005.5	8.350	0.057	121.7	45.15	0.9
14	2000	8.274	0.27	2005.1	8.263	0.271	14.8	45.37	16.1
15	2000	8.274	0.53	2005.1	8.328	0.541	6.7	47.87	22.7
16	2000	8.274	0.80	2005.0	8.243	0.800	6.0	51.06	27.9
17	4000	2.068	0.00	4001.6	2.042	0.022	149.4	14.99	8.3
18	4000	2.068	0.27	4001.2	2.041	0.264	4.1	14.74	0.2
19	4000	2.068	0.53	4002.8	2.000	0.535	1.5	15.83	-24.5
20	4000	2.068	0.80	4002.3	2.026	0.792	2.4	17.99	-76.0
21	4000	4.137	0.00	4000.8	4.082	0.049	78.2	27.37	18.6
22	4000	4.137	0.27	4002.7	4.200	0.239	17.5	28.24	2.8
23	4000	4.137	0.53	4002.6	4.045	0.527	8.1	29.18	-12.1
24	4000	4.137	0.80	4003.1	4.025	0.801	4.4	31.62	-55.0
25	4000	6.205	0.00	4002.8	6.109	0.071	128.7	35.89	22.1
26	4000	6.205	0.27	4002.4	6.098	0.248	13.0	36.54	-4.1
27	4000	6.205	0.53	4003.2	6.132	0.516	10.5	38.84	-22.3
28	4000	6.205	0.80	4003.7	6.125	0.811	5.6	42.40	-44.9
29	4000	8.274	0.00	4002.8	8.313	0.059	66.8	44.07	18.0
30	4000	8.274	0.27	4003.1	8.350	0.276	18.4	45.05	9.8
31	4000	8.274	0.53	4003.0	8.356	0.517	15.2	47.23	2.9
32	4000	8.274	0.80	4003.6	8.124	0.795	7.3	50.44	-34.3

Table A.1. Continued.

Test Point	Target ω	Target ΔP	Target ε_0	Measured ω	Measured ΔP	Measured ε_0	ϕ	$\dot{Q}$	F_r
	[rpm]	[bar]	[-]	[rpm]	[bar]	[-]	[deg]	[LPM]	[N]
33	6000	2.068	0.00	6001.2	2.038	0.012	-82.1	11.52	14.2
34	6000	2.068	0.27	6000.1	1.983	0.286	-1.4	11.41	-12.5
35	6000	2.068	0.53	5999.8	2.004	0.554	0.1	12.97	-59.8
36	6000	2.068	0.80	-	-	-	-	-	-
37	6000	4.137	0.00	6003.7	3.932	0.026	-168.6	23.54	20.9
38	6000	4.137	0.27	6004.8	3.893	0.266	8.1	23.76	29.7
39	6000	4.137	0.53	5999.5	3.952	0.533	5.5	25.92	-14.2
40	6000	4.137	0.80	-	-	-	-	-	-
41	6000	6.205	0.00	5999.6	6.059	0.041	-111.7	33.87	19.5
42	6000	6.205	0.27	6003.5	6.081	0.264	1.8	34.72	3.1
43	6000	6.205	0.53	6005.5	6.029	0.519	4.0	36.13	-28.8
44	6000	6.205	0.80	-	-	-	-	-	-
45	6000	8.274	0.00	5999.8	8.114	0.032	-174.4	41.61	18.4
46	6000	8.274	0.27	6003.3	8.161	0.268	5.0	43.03	7.8
47	6000	8.274	0.53	6005.1	8.113	0.517	5.3	45.07	-25.2
48	6000	8.274	0.80	-	-	-	-	-	-
49	8000	2.068	0.00	7993.7	2.025	0.056	115.9	8.60	15.8
50	8000	2.068	0.27	8000.2	2.002	0.270	23.0	8.81	-16.9
51	8000	2.068	0.53	-	-	-	-	-	-
52	8000	2.068	0.80	-	-	-	-	-	-
53	8000	4.137	0.00	7995.6	3.884	0.041	108.9	20.11	4.7
54	8000	4.137	0.27	7997.9	3.818	0.269	25.3	19.66	-0.3
55	8000	4.137	0.53	-	-	-	-	-	-
56	8000	4.137	0.80	-	-	-	-	-	-
57	8000	6.205	0.00	7992.7	5.954	0.046	84.0	30.13	-0.8
58	8000	6.205	0.27	7991.1	6.042	0.267	30.1	31.65	28.1
59	8000	6.205	0.53	-	-	-	-	-	-
60	8000	6.205	0.80	-	-	-	-	-	-
61	8000	8.274	0.00	7995.1	8.151	0.074	116.9	39.22	12.2
62	8000	8.274	0.27	7997.6	8.109	0.247	33.2	39.86	22.1
63	8000	8.274	0.53	-	-	-	-	-	-
64	8000	8.274	0.80	-	-	-	-	-	-

Table A.2. Additional static results of the SS/GR seal with radial injection.

Test Point	PSR	OSR	Inlet Temperature	Average Outlet Temperature	Re_Z	Re_θ	Re
	[-]	[-]	[°C]	[°C]	[-]	[-]	[-]
1	0.000	0.215	46.1	46.9	7.54E+02	7.92E+03	7.96E+03
2	0.000	0.233	46.5	47.2	7.58E+02	7.98E+03	8.01E+03
3	0.000	0.292	45.9	46.9	7.77E+02	7.91E+03	7.95E+03
4	0.000	0.304	46.5	45.9	8.61E+02	7.87E+03	7.92E+03
5	0.000	0.220	46.0	46.9	1.22E+03	7.92E+03	8.01E+03
6	0.000	0.247	46.9	47.1	1.27E+03	7.99E+03	8.09E+03
7	0.000	0.298	46.4	46.1	1.30E+03	7.89E+03	8.00E+03
8	0.000	0.320	46.5	47.5	1.46E+03	8.00E+03	8.13E+03
9	0.000	0.226	46.2	47.2	1.66E+03	7.95E+03	8.12E+03
10	0.000	0.263	46.1	46.2	1.66E+03	7.87E+03	8.05E+03
11	0.000	0.285	46.7	47.6	1.80E+03	8.02E+03	8.22E+03
12	0.000	0.323	46.5	47.5	1.92E+03	7.99E+03	8.22E+03
13	0.000	0.233	46.0	47.0	2.02E+03	7.92E+03	8.17E+03
14	0.000	0.269	45.7	46.4	2.01E+03	7.86E+03	8.12E+03
15	0.000	0.336	46.7	47.6	2.17E+03	8.02E+03	8.31E+03
16	0.000	0.340	46.0	46.9	2.28E+03	7.91E+03	8.24E+03
17	0.217	0.287	46.9	48.1	6.82E+02	1.61E+04	1.61E+04
18	0.225	0.279	46.4	47.0	6.60E+02	1.59E+04	1.59E+04
19	0.212	0.275	46.5	47.5	7.14E+02	1.60E+04	1.60E+04
20	0.197	0.266	46.0	47.6	8.08E+02	1.59E+04	1.59E+04
21	0.146	0.230	46.3	47.2	1.23E+03	1.59E+04	1.59E+04
22	0.129	0.249	46.6	47.0	1.27E+03	1.59E+04	1.59E+04
23	0.118	0.279	46.3	47.8	1.32E+03	1.60E+04	1.60E+04
24	0.111	0.309	46.8	48.0	1.44E+03	1.61E+04	1.61E+04
25	0.123	0.230	46.4	46.9	1.61E+03	1.58E+04	1.59E+04
26	0.092	0.263	46.0	46.8	1.63E+03	1.58E+04	1.59E+04
27	0.080	0.289	46.5	47.8	1.75E+03	1.60E+04	1.61E+04
28	0.034	0.276	46.9	48.2	1.93E+03	1.61E+04	1.63E+04
29	0.072	0.237	46.9	48.1	2.00E+03	1.61E+04	1.62E+04
30	0.059	0.259	46.8	47.9	2.04E+03	1.61E+04	1.62E+04
31	0.000	0.264	46.1	47.1	2.11E+03	1.58E+04	1.60E+04
32	0.102	0.295	46.1	46.9	2.25E+03	1.58E+04	1.60E+04

Table A.2. Continued.

Test Point	PSR	OSR	Inlet Temperature	Average Outlet Temperature	Re_Z	Re_θ	Re
	[-]	[-]	[°C]	[°C]	[-]	[-]	[-]
33	0.298	0.181	46.5	48.3	5.23E+02	2.41E+04	2.41E+04
34	0.294	0.332	46.9	49.0	5.23E+02	2.44E+04	2.44E+04
35	0.276	0.293	46.8	49.1	5.95E+02	2.44E+04	2.44E+04
36	-	-	-	-	-	-	-
37	0.223	0.280	46.9	48.6	1.08E+03	2.43E+04	2.43E+04
38	0.218	0.275	45.8	46.4	1.05E+03	2.36E+04	2.36E+04
39	0.202	0.272	45.9	46.6	1.15E+03	2.36E+04	2.36E+04
40	-	-	-	-	-	-	-
41	0.178	0.264	46.7	48.2	1.54E+03	2.41E+04	2.42E+04
42	0.166	0.263	46.2	47.5	1.56E+03	2.39E+04	2.39E+04
43	0.155	0.273	46.1	46.8	1.61E+03	2.37E+04	2.38E+04
44	-	-	-	-	-	-	-
45	0.154	0.235	46.2	46.4	1.85E+03	2.36E+04	2.37E+04
46	0.138	0.270	46.3	48.1	1.95E+03	2.40E+04	2.41E+04
47	0.127	0.292	46.6	47.9	2.04E+03	2.41E+04	2.41E+04
48	-	-	-	-	-	-	-
49	0.343	0.097	46.6	51.3	4.02E+02	3.31E+04	3.31E+04
50	0.335	0.125	46.1	50.3	4.07E+02	3.27E+04	3.27E+04
51	-	-	-	-	-	-	-
52	-	-	-	-	-	-	-
53	0.270	0.359	46.7	49.5	9.25E+02	3.26E+04	3.26E+04
54	0.265	0.306	46.3	48.6	8.93E+02	3.22E+04	3.22E+04
55	-	-	-	-	-	-	-
56	-	-	-	-	-	-	-
57	0.226	0.290	46.6	49.2	1.38E+03	3.24E+04	3.24E+04
58	0.215	0.290	45.9	48.9	1.44E+03	3.21E+04	3.22E+04
59	-	-	-	-	-	-	-
60	-	-	-	-	-	-	-
61	0.194	0.279	46.4	48.0	1.78E+03	3.20E+04	3.21E+04
62	0.183	0.273	46.5	49.0	1.82E+03	3.24E+04	3.24E+04
63	-	-	-	-	-	-	-
64	-	-	-	-	-	-	-

Table A.3. Stiffness coefficients and uncertainties for the SS/GR seal with radial injection.

Test Point	K_{XX} [MN/m]	K_{XY} [MN/m]	K_{YX} [MN/m]	K_{YY} [MN/m]	$u_{K_{XX}}$ [MN/m]	$u_{K_{XY}}$ [MN/m]	$u_{K_{YX}}$ [MN/m]	$u_{K_{YY}}$ [MN/m]
1	-0.45	0.59	-0.64	-0.46	0.14	0.08	0.10	0.20
2	-0.45	0.56	-0.52	-0.52	0.20	0.06	0.15	0.21
3	0.23	0.52	-0.42	-0.56	0.28	0.15	0.13	0.18
4	0.25	0.45	-0.35	-0.73	0.25	0.11	0.14	0.22
5	0.38	0.42	-0.31	-0.47	0.31	0.13	0.11	0.21
6	0.39	0.44	-0.32	-0.48	0.25	0.18	0.14	0.24
7	0.45	0.43	-0.47	-0.47	0.28	0.16	0.09	0.25
8	0.37	0.17	-0.32	-0.65	0.31	0.18	0.10	0.23
9	0.70	0.45	-0.41	-0.20	0.28	0.17	0.13	0.17
10	0.64	0.31	-0.27	-0.31	0.31	0.20	0.10	0.23
11	0.53	0.66	-0.30	-0.21	0.32	0.18	0.10	0.24
12	0.58	0.30	-0.28	-0.57	0.32	0.16	0.13	0.19
13	0.73	0.44	-0.35	-0.05	0.37	0.19	0.17	0.21
14	0.80	0.33	-0.32	-0.15	0.34	0.13	0.14	0.24
15	0.74	0.18	-0.20	-0.20	0.33	0.15	0.11	0.21
16	0.81	0.13	-0.18	-0.46	0.34	0.17	0.16	0.23
17	0.38	1.23	-1.17	-0.59	0.40	0.23	0.07	0.12
18	0.18	1.09	-1.05	-0.63	0.26	0.15	0.06	0.17
19	-0.36	0.76	-0.93	-0.96	0.29	0.35	0.10	0.11
20	-0.68	0.70	-0.71	-1.21	0.39	0.29	0.18	0.15
21	0.16	1.33	-1.29	-0.71	0.23	0.16	0.10	0.16
22	0.09	1.22	-1.21	-0.65	0.30	0.18	0.11	0.16
23	-0.33	1.14	-1.15	-0.71	0.38	0.25	0.16	0.17
24	-0.49	0.67	-0.89	-1.06	0.35	0.24	0.10	0.21
25	0.23	1.38	-1.21	-0.68	0.26	0.17	0.14	0.13
26	0.22	1.40	-1.28	-0.81	0.35	0.15	0.14	0.17
27	-0.11	1.11	-1.15	-0.83	0.31	0.29	0.20	0.20
28	-0.31	0.65	-0.85	-0.98	0.35	0.26	0.13	0.24
29	0.49	1.38	-1.23	-0.58	0.32	0.31	0.24	0.23
30	0.35	1.30	-1.09	-0.73	0.30	0.20	0.13	0.25
31	0.44	1.13	-0.98	-0.64	0.30	0.21	0.12	0.19
32	-0.25	0.78	-0.85	-0.90	0.36	0.19	0.14	0.22

Table A.3. Continued.

Test Point	K_{XX} [MN/m]	K_{XY} [MN/m]	K_{YX} [MN/m]	K_{YY} [MN/m]	$u_{K_{XX}}$ [MN/m]	$u_{K_{XY}}$ [MN/m]	$u_{K_{YX}}$ [MN/m]	$u_{K_{YY}}$ [MN/m]
33	-0.32	1.73	-1.52	-0.70	0.30	0.20	0.07	0.14
34	-0.41	1.70	-1.48	-0.95	0.24	0.16	0.10	0.11
35	-0.64	1.33	-1.43	-1.63	0.32	0.30	0.11	0.14
36	-	-	-	-	-	-	-	-
37	-0.35	2.75	-2.41	-0.87	0.32	0.20	0.13	0.21
38	-0.37	2.43	-2.21	-0.85	0.32	0.23	0.14	0.16
39	-0.73	1.74	-2.07	-1.92	0.31	0.36	0.24	0.14
40	-	-	-	-	-	-	-	-
41	-0.32	2.57	-2.55	-0.85	0.29	0.35	0.19	0.19
42	-0.46	2.60	-2.52	-0.92	0.37	0.28	0.14	0.27
43	-0.78	1.97	-2.07	-1.40	0.43	0.26	0.20	0.23
44	-	-	-	-	-	-	-	-
45	-0.36	3.03	-2.49	-0.81	0.31	0.28	0.14	0.19
46	-0.48	2.56	-2.44	-0.77	0.31	0.29	0.14	0.27
47	-0.49	1.93	-2.04	-1.43	0.32	0.22	0.19	0.20
48	-	-	-	-	-	-	-	-
49	-0.90	2.58	-2.36	-1.46	0.31	0.27	0.11	0.09
50	-1.14	2.80	-2.24	-1.69	0.23	0.23	0.11	0.11
51	-	-	-	-	-	-	-	-
52	-	-	-	-	-	-	-	-
53	-0.56	3.44	-3.07	-1.18	0.30	0.28	0.13	0.19
54	-0.80	3.25	-2.87	-1.67	0.32	0.21	0.19	0.11
55	-	-	-	-	-	-	-	-
56	-	-	-	-	-	-	-	-
57	-0.71	4.29	-4.01	-1.24	0.28	0.31	0.32	0.26
58	-0.81	4.31	-3.67	-1.63	0.34	0.27	0.24	0.21
59	-	-	-	-	-	-	-	-
60	-	-	-	-	-	-	-	-
61	-0.78	4.35	-3.89	-1.47	0.30	0.49	0.20	0.19
62	-0.99	4.25	-3.81	-1.67	0.35	0.36	0.22	0.22
63	-	-	-	-	-	-	-	-
64	-	-	-	-	-	-	-	-

Table A.4. Damping coefficients and uncertainties for the SS/GR seal with radial injection.

Test Point	C_{XX} [kN-s/m]	C_{XY} [kN-s/m]	C_{YX} [kN-s/m]	C_{YY} [kN-s/m]	$u_{C_{XX}}$ [kN-s/m]	$u_{C_{XY}}$ [kN-s/m]	$u_{C_{YX}}$ [kN-s/m]	$u_{C_{YY}}$ [kN-s/m]
1	3.45	1.87	-2.05	3.88	0.18	0.20	0.22	0.33
2	3.41	2.01	-2.20	3.84	0.44	0.18	0.53	0.28
3	4.07	2.27	-2.13	3.74	0.48	0.40	0.27	0.31
4	3.72	2.72	-2.76	3.62	0.51	0.49	0.26	0.32
5	5.47	2.20	-2.15	5.03	0.56	0.41	0.39	0.32
6	5.31	2.26	-2.19	4.94	0.56	0.38	0.27	0.25
7	5.14	2.33	-2.22	4.88	0.49	0.43	0.33	0.26
8	4.92	2.68	-2.70	4.54	0.50	0.45	0.33	0.31
9	6.10	2.34	-2.31	5.60	0.39	0.40	0.28	0.31
10	6.18	2.24	-2.22	5.63	0.55	0.55	0.31	0.39
11	6.11	2.24	-2.33	5.24	0.62	0.30	0.35	0.32
12	5.60	2.74	-2.77	4.61	0.61	0.48	0.26	0.29
13	6.88	2.20	-2.21	6.27	0.56	0.44	0.37	0.33
14	6.83	2.38	-2.13	6.16	0.65	0.41	0.32	0.27
15	6.62	2.60	-2.39	5.57	0.59	0.40	0.24	0.41
16	6.01	2.97	-2.60	5.01	0.62	0.44	0.28	0.31
17	4.11	3.37	-3.26	3.59	1.05	0.34	0.22	0.29
18	3.93	3.60	-3.42	3.60	0.43	0.55	0.19	0.35
19	4.26	4.10	-4.61	4.35	0.41	0.54	0.30	0.36
20	4.36	4.99	-5.55	4.22	0.28	0.63	0.39	0.51
21	5.87	4.37	-4.19	5.30	0.39	0.51	0.34	0.18
22	5.81	4.28	-4.22	5.26	0.44	0.52	0.32	0.18
23	5.50	4.70	-4.90	4.93	0.29	0.83	0.36	0.24
24	4.93	5.79	-5.85	4.53	0.52	0.77	0.30	0.32
25	6.50	4.80	-4.53	6.12	0.36	0.46	0.36	0.20
26	6.73	4.74	-4.60	6.01	0.44	0.62	0.47	0.19
27	6.30	5.39	-5.20	5.66	0.32	0.59	0.44	0.46
28	5.69	6.28	-6.13	4.82	0.50	0.69	0.39	0.31
29	7.35	4.71	-4.47	6.59	0.45	0.66	0.59	0.24
30	7.47	5.11	-4.68	6.63	0.62	0.65	0.63	0.19
31	7.17	5.39	-5.08	6.44	0.59	0.52	0.39	0.33
32	6.26	6.15	-6.00	5.22	0.69	0.99	0.26	0.33

Table A.4. Continued.

Test Point	C_{XX} [kN-s/m]	C_{XY} [kN-s/m]	C_{YX} [kN-s/m]	C_{YY} [kN-s/m]	$u_{C_{XX}}$ [kN-s/m]	$u_{C_{XY}}$ [kN-s/m]	$u_{C_{YX}}$ [kN-s/m]	$u_{C_{YY}}$ [kN-s/m]
33	4.11	5.47	-5.60	3.47	0.57	0.44	0.24	0.54
34	4.24	5.65	-5.80	3.63	0.56	0.42	0.26	0.53
35	4.36	6.49	-6.50	3.97	0.41	0.75	0.23	0.68
36	-	-	-	-	-	-	-	-
37	5.88	5.37	-5.69	5.13	0.39	0.62	0.43	0.59
38	5.71	5.52	-5.75	5.09	0.35	0.51	0.29	0.54
39	6.32	6.31	-6.56	5.77	0.40	0.84	0.33	0.47
40	-	-	-	-	-	-	-	-
41	7.21	6.65	-6.99	6.30	0.35	0.62	0.39	0.25
42	6.96	6.59	-6.83	6.07	0.43	0.95	0.47	0.28
43	6.76	7.23	-7.22	5.49	0.49	1.18	0.57	0.57
44	-	-	-	-	-	-	-	-
45	7.57	7.11	-7.34	6.59	0.53	0.47	0.36	0.70
46	7.78	7.25	-7.50	6.60	0.55	0.65	0.54	0.49
47	7.40	8.13	-7.74	6.18	0.52	0.68	0.47	0.39
48	-	-	-	-	-	-	-	-
49	4.73	7.52	-7.43	3.91	0.61	0.49	0.25	0.65
50	4.87	7.59	-7.64	4.06	0.59	0.54	0.27	0.67
51	-	-	-	-	-	-	-	-
52	-	-	-	-	-	-	-	-
53	5.78	7.53	-7.62	5.02	0.53	0.40	0.32	0.53
54	5.90	7.78	-7.80	5.18	0.56	0.41	0.40	0.55
55	-	-	-	-	-	-	-	-
56	-	-	-	-	-	-	-	-
57	7.58	7.65	-7.84	6.47	0.65	0.68	0.43	0.74
58	7.56	7.51	-7.90	6.75	0.49	0.69	0.40	0.87
59	-	-	-	-	-	-	-	-
60	-	-	-	-	-	-	-	-
61	8.66	8.83	-8.87	7.88	0.55	0.86	0.63	0.45
62	8.59	8.83	-8.83	7.85	0.29	0.93	0.65	0.23
63	-	-	-	-	-	-	-	-
64	-	-	-	-	-	-	-	-

Table A.5. Virtual mass coefficients and uncertainties for the SS/GR seal with radial injection.

Test Point	M_{XX} [kg]	M_{XY} [kg]	M_{YX} [kg]	M_{YY} [kg]	$u_{M_{XX}}$ [kg]	$u_{M_{XY}}$ [kg]	$u_{M_{YX}}$ [kg]	$u_{M_{YY}}$ [kg]
1	10.11	0.06	0.27	10.91	0.20	0.11	0.13	0.28
2	10.15	-0.03	0.34	10.78	0.28	0.09	0.21	0.29
3	11.88	-0.27	0.41	11.89	0.40	0.21	0.19	0.26
4	12.47	-0.42	0.43	14.35	0.35	0.16	0.20	0.30
5	12.94	-0.72	0.53	12.03	0.44	0.18	0.15	0.29
6	13.03	-0.62	0.46	12.32	0.35	0.25	0.20	0.34
7	13.11	-0.73	0.25	13.02	0.40	0.22	0.13	0.35
8	13.53	-1.02	0.17	15.27	0.44	0.25	0.15	0.32
9	13.75	-0.45	0.30	12.83	0.40	0.24	0.18	0.24
10	13.81	-0.66	0.45	13.24	0.44	0.28	0.15	0.33
11	13.99	-0.60	0.31	14.30	0.45	0.26	0.14	0.34
12	14.38	-0.82	0.17	16.01	0.45	0.23	0.19	0.28
13	14.18	-0.43	0.49	13.41	0.52	0.27	0.24	0.29
14	14.34	-0.71	0.36	13.65	0.48	0.19	0.20	0.33
15	14.62	-0.95	0.32	14.96	0.46	0.22	0.16	0.29
16	15.08	-1.15	0.37	16.34	0.48	0.24	0.23	0.33
17	10.15	-0.04	-0.26	9.17	0.56	0.32	0.10	0.17
18	10.02	-0.20	-0.19	9.42	0.37	0.21	0.08	0.24
19	10.38	-0.80	-0.01	10.99	0.40	0.49	0.14	0.15
20	11.22	-1.38	-0.10	13.75	0.54	0.40	0.24	0.21
21	12.58	-0.91	0.35	11.78	0.33	0.23	0.13	0.22
22	12.53	-1.14	0.36	11.99	0.42	0.26	0.15	0.23
23	12.79	-1.27	-0.11	13.34	0.53	0.34	0.21	0.23
24	13.47	-1.62	-0.19	15.82	0.48	0.33	0.14	0.29
25	13.42	-0.82	0.58	12.54	0.37	0.23	0.20	0.19
26	13.74	-1.14	0.51	12.84	0.49	0.21	0.20	0.24
27	14.03	-1.29	0.19	13.67	0.43	0.40	0.27	0.27
28	14.65	-1.81	-0.04	17.24	0.49	0.36	0.18	0.33
29	14.29	-0.82	0.43	12.83	0.45	0.44	0.35	0.33
30	14.40	-1.51	0.77	13.23	0.42	0.29	0.19	0.35
31	14.72	-1.80	0.77	14.05	0.42	0.30	0.18	0.27
32	14.98	-1.84	0.06	16.94	0.49	0.26	0.20	0.30

Table A.5. Continued.

Test Point	M_{XX} [kg]	M_{XY} [kg]	M_{YX} [kg]	M_{YY} [kg]	$u_{M_{XX}}$ [kg]	$u_{M_{XY}}$ [kg]	$u_{M_{YX}}$ [kg]	$u_{M_{YY}}$ [kg]
33	10.36	-0.20	-0.14	9.52	0.41	0.28	0.09	0.19
34	10.38	-0.64	-0.12	9.86	0.34	0.22	0.14	0.16
35	10.79	-1.08	-0.08	10.98	0.44	0.42	0.16	0.19
36	-	-	-	-	-	-	-	-
37	10.45	-0.05	-0.27	9.69	0.44	0.28	0.18	0.29
38	10.68	-0.17	-0.30	10.08	0.45	0.31	0.20	0.22
39	11.20	-1.24	-0.21	11.31	0.42	0.50	0.34	0.19
40	-	-	-	-	-	-	-	-
41	13.18	-1.33	0.27	12.70	0.40	0.49	0.27	0.26
42	13.11	-1.27	0.15	12.64	0.51	0.38	0.19	0.37
43	13.09	-1.46	0.34	13.52	0.60	0.35	0.27	0.31
44	-	-	-	-	-	-	-	-
45	13.73	-0.58	0.28	13.16	0.44	0.39	0.19	0.27
46	14.06	-1.46	0.47	13.93	0.43	0.41	0.20	0.37
47	14.40	-1.84	0.48	14.31	0.44	0.30	0.26	0.27
48	-	-	-	-	-	-	-	-
49	10.23	-0.41	-0.36	9.50	0.44	0.37	0.16	0.12
50	10.47	-0.59	-0.38	9.66	0.33	0.33	0.16	0.15
51	-	-	-	-	-	-	-	-
52	-	-	-	-	-	-	-	-
53	10.89	-0.36	-0.41	10.07	0.43	0.40	0.19	0.26
54	10.92	-0.63	-0.57	10.07	0.45	0.30	0.27	0.16
55	-	-	-	-	-	-	-	-
56	-	-	-	-	-	-	-	-
57	11.11	-0.12	-0.55	10.21	0.39	0.44	0.46	0.36
58	11.08	-0.36	-0.65	10.33	0.49	0.39	0.34	0.29
59	-	-	-	-	-	-	-	-
60	-	-	-	-	-	-	-	-
61	13.32	-1.39	0.78	12.90	0.42	0.70	0.28	0.26
62	13.27	-1.85	0.52	12.59	0.49	0.51	0.31	0.30
63	-	-	-	-	-	-	-	-
64	-	-	-	-	-	-	-	-

Table A.6. WFR, C_{eff}, and uncertainties for the SS/GR seal with radial injection.

Test Point	WFR, [10]	u_{WFR}, [10]	WFR, [11]	u_{WFR}, [11]	C_{eff}	$u_{C_{eff}}$
	[-]	[-]	[-]	[-]	[kN-s/m]	[kN-s/m]
1	0.80	0.09	0.81	0.09	0.73	0.35
2	0.71	0.12	0.72	0.12	1.05	0.47
3	0.37	0.28	0.38	0.29	1.67	0.56
4	0.07	1.62	0.07	1.64	1.75	0.52
5	0.00	0.00	0.00	0.00	3.51	0.51
6	0.00	0.00	0.00	0.00	3.30	0.62
7	0.14	0.53	0.14	0.53	2.87	0.51
8	0.00	0.00	0.00	0.00	3.55	0.57
9	0.06	0.89	0.06	0.89	3.81	0.56
10	0.00	0.00	0.00	0.00	4.52	0.63
11	0.23	0.24	0.23	0.24	3.40	0.60
12	0.00	0.00	0.00	0.00	3.72	0.60
13	0.08	0.59	0.08	0.60	4.70	0.69
14	0.00	0.00	0.00	0.00	4.94	0.59
15	0.00	0.00	0.00	0.00	5.17	0.58
16	0.00	0.00	0.00	0.00	4.76	0.66
17	0.70	0.15	0.69	0.14	0.98	0.62
18	0.65	0.08	0.65	0.08	1.21	0.34
19	0.45	0.12	0.46	0.12	2.30	0.52
20	0.38	0.10	0.39	0.11	2.61	0.50
21	0.54	0.05	0.55	0.05	2.46	0.31
22	0.50	0.06	0.52	0.06	2.64	0.35
23	0.52	0.07	0.53	0.08	2.47	0.40
24	0.38	0.08	0.39	0.08	2.87	0.44
25	0.47	0.05	0.48	0.05	3.22	0.33
26	0.47	0.05	0.49	0.05	3.17	0.34
27	0.43	0.08	0.45	0.08	3.28	0.50
28	0.32	0.08	0.33	0.08	3.46	0.45
29	0.41	0.08	0.42	0.08	3.86	0.54
30	0.37	0.05	0.38	0.06	4.20	0.44
31	0.33	0.06	0.34	0.06	4.28	0.45
32	0.32	0.06	0.33	0.06	3.80	0.48

Table A.6. Continued.

Test Point	WFR, [10]	u_{WFR}, [10]	WFR, [11]	u_{WFR}, [11]	C_{eff}	$u_{C_{eff}}$
	[-]	[-]	[-]	[-]	[kN-s/m]	[kN-s/m]
33	0.68	0.08	0.68	0.08	1.20	0.43
34	0.64	0.07	0.65	0.08	1.41	0.42
35	0.51	0.08	0.54	0.09	1.97	0.47
36	-	-	-	-	-	-
37	0.74	0.06	0.73	0.06	1.40	0.40
38	0.68	0.06	0.68	0.06	1.71	0.39
39	0.48	0.07	0.50	0.07	3.02	0.47
40	-	-	-	-	-	-
41	0.60	0.05	0.63	0.06	2.68	0.38
42	0.62	0.05	0.65	0.05	2.44	0.35
43	0.52	0.05	0.55	0.06	2.91	0.46
44	-	-	-	-	-	-
45	0.62	0.05	0.63	0.06	2.68	0.50
46	0.55	0.05	0.58	0.05	3.22	0.45
47	0.46	0.04	0.48	0.05	3.63	0.40
48	-	-	-	-	-	-
49	0.68	0.08	0.68	0.08	1.37	0.48
50	0.67	0.08	0.68	0.08	1.46	0.47
51	-	-	-	-	-	-
52	-	-	-	-	-	-
53	0.72	0.06	0.71	0.06	1.52	0.42
54	0.65	0.06	0.66	0.06	1.88	0.43
55	-	-	-	-	-	-
56	-	-	-	-	-	-
57	0.70	0.06	0.69	0.06	2.07	0.56
58	0.66	0.06	0.66	0.05	2.38	0.54
59	-	-	-	-	-	-
60	-	-	-	-	-	-
61	0.59	0.05	0.64	0.06	3.35	0.48
62	0.58	0.03	0.63	0.04	3.40	0.31
63	-	-	-	-	-	-
64	-	-	-	-	-	-

Assembly 2 – Tangential Injection: Medium Pre-swirl

Table A.7. Static results of the SS/GR seal with tangential injection for medium pre-swirl.

Test Point	Target ω	Target ΔP	Target ε_0	Measured ω	Measured ΔP	Measured ε_0	ϕ	$\dot{Q}$	F_r
	[rpm]	[bar]	[-]	[rpm]	[bar]	[-]	[deg]	[LPM]	[N]
1	2000	2.068	0.00	1998.1	2.115	0.016	-110.96	16.87	4.0
2	2000	2.068	0.27	1999.4	2.088	0.278	3.93	16.94	4.2
3	2000	2.068	0.53	1999.2	2.017	0.522	3.64	17.10	-6.2
4	2000	2.068	0.80	1999.4	2.075	0.781	3.36	19.21	-18.5
5	2000	4.137	0.00	1999.5	4.089	0.041	105.12	27.11	4.3
6	2000	4.137	0.27	1999.4	4.083	0.267	12.04	27.72	2.3
7	2000	4.137	0.53	1999.4	4.073	0.522	10.54	29.35	9.0
8	2000	4.137	0.80	1999.6	4.071	0.793	7.22	32.04	-4.4
9	2000	6.205	0.00	1998.2	6.202	0.048	-78.86	36.27	5.3
10	2000	6.205	0.27	1998.3	6.128	0.270	-6.27	36.48	7.4
11	2000	6.205	0.53	1998.3	6.073	0.539	-2.13	38.72	7.1
12	2000	6.205	0.80	1998.5	6.064	0.818	0.67	41.88	2.0
13	2000	8.274	0.00	1998.2	8.145	0.072	-160.18	43.48	6.5
14	2000	8.274	0.27	1996.7	8.232	0.287	-4.12	44.80	14.1
15	2000	8.274	0.53	1997.2	8.188	0.532	0.36	46.89	14.2
16	2000	8.274	0.80	1997.5	8.277	0.756	3.08	50.16	19.3
17	4000	2.068	0.00	3998.8	2.084	0.023	-96.22	14.45	10.0
18	4000	2.068	0.27	4000.6	2.038	0.278	-3.40	14.36	41.8
19	4000	2.068	0.53	4000.5	2.051	0.560	-5.81	14.17	19.7
20	4000	2.068	0.80	4002.0	2.041	0.809	-7.99	17.01	-38.9
21	4000	4.137	0.00	3998.9	4.133	0.030	-1.81	26.90	14.2
22	4000	4.137	0.27	3999.4	4.007	0.274	0.23	26.69	-16.4
23	4000	4.137	0.53	3999.9	4.027	0.546	1.69	27.83	-30.5
24	4000	4.137	0.80	3999.8	4.173	0.816	0.71	31.22	-82.2
25	4000	6.205	0.00	3998.1	6.202	0.020	-19.14	35.59	13.3
26	4000	6.205	0.27	3999.7	6.136	0.282	-1.65	36.32	38.0
27	4000	6.205	0.53	4000.3	6.099	0.562	1.27	38.02	24.5
28	4000	6.205	0.80	4000.6	6.168	0.791	-0.48	40.93	-39.9
29	4000	8.274	0.00	3996.7	8.260	0.020	-87.07	43.04	12.7
30	4000	8.274	0.27	3997.2	8.156	0.255	5.40	43.40	4.5
31	4000	8.274	0.53	4000.9	8.143	0.543	0.73	46.02	47.2
32	4000	8.274	0.80	4000.5	8.141	0.793	1.86	49.19	15.6

Table A.7. Continued.

Test Point	Target ω	Target ΔP	Target ε_0	Measured ω	Measured ΔP	Measured ε_0	ϕ	$\dot{Q}$	F_r
	[rpm]	[bar]	[-]	[rpm]	[bar]	[-]	[deg]	[LPM]	[N]
33	6000	2.068	0.00	6004.3	2.055	0.011	57.87	10.16	-2.0
34	6000	2.068	0.27	6006.6	2.099	0.281	0.00	10.97	7.5
35	6000	2.068	0.53	6008.5	2.025	0.544	2.34	11.42	-41.4
36	6000	2.068	0.80	5999.7	2.235	0.795	-26.04	14.66	-278.1
37	6000	4.137	0.00	5999.3	4.099	0.013	-64.68	23.35	-0.3
38	6000	4.137	0.27	6000.2	4.111	0.275	1.23	24.05	35.9
39	6000	4.137	0.53	6000.0	4.078	0.534	4.00	25.57	-16.5
40	6000	4.137	0.80	5999.9	4.141	0.807	-18.86	29.47	-246.7
41	6000	6.205	0.00	6000.6	6.219	0.002	-56.01	33.48	0.0
42	6000	6.205	0.27	6001.1	6.130	0.273	7.58	33.70	30.7
43	6000	6.205	0.53	6000.6	6.172	0.535	5.91	35.61	9.4
44	6000	6.205	0.80	5999.3	6.190	0.806	-17.71	40.44	-230.7
45	6000	8.274	0.00	6001.0	8.112	0.004	-164.41	40.84	1.6
46	6000	8.274	0.27	6001.3	8.182	0.275	7.85	41.66	28.4
47	6000	8.274	0.53	6001.0	8.108	0.555	5.38	44.00	6.1
48	6000	8.274	0.80	6005.8	8.375	0.796	-1.93	49.51	-432.0
49	8000	2.068	0.00	8003.8	2.108	0.005	-30.84	8.70	0.0
50	8000	2.068	0.27	8004.5	2.074	0.265	-24.81	8.71	-80.8
51	8000	2.068	0.53	8003.9	2.083	0.511	-17.02	10.15	-150.5
52	8000	2.068	0.80	-	-	-	-	-	-
53	8000	4.137	0.00	8002.1	4.147	0.050	130.59	20.34	29.4
54	8000	4.137	0.27	8002.8	4.062	0.268	-9.96	20.45	-5.0
55	8000	4.137	0.53	8002.0	4.031	0.504	-22.78	22.02	-203.6
56	8000	4.137	0.80	-	-	-	-	-	-
57	8000	6.205	0.00	8001.8	6.114	0.005	-13.41	29.72	0.4
58	8000	6.205	0.27	8001.6	6.110	0.258	-13.67	30.50	-39.1
59	8000	6.205	0.53	7999.1	6.404	0.539	3.85	34.77	-279.7
60	8000	6.205	0.80	-	-	-	-	-	-
61	8000	8.274	0.00	8001.4	8.253	0.047	100.27	38.33	9.2
62	8000	8.274	0.27	8002.1	8.379	0.265	-3.18	40.03	-1.7
63	8000	8.274	0.53	8000.4	8.425	0.451	20.57	41.85	-173.0
64	8000	8.274	0.80	-	-	-	-	-	-

Table A.8. Additional static results of the SS/GR seal with tangential injection for medium pre-swirl.

Test Point	PSR	OSR	Inlet Temperature	Average Outlet Temperature	Re_Z	Re_θ	Re
	[-]	[-]	[°C]	[°C]	[-]	[-]	[-]
1	0.323	0.212	46.7	47.5	7.62E+02	7.98E+03	8.02E+03
2	0.305	0.263	46.3	47.1	7.60E+02	7.94E+03	7.97E+03
3	0.298	0.288	46.4	46.9	7.66E+02	7.92E+03	7.96E+03
4	0.304	0.299	46.5	47.5	8.65E+02	7.97E+03	8.02E+03
5	0.435	0.267	46.1	46.7	1.21E+03	7.89E+03	7.98E+03
6	0.421	0.284	46.5	46.7	1.24E+03	7.92E+03	8.01E+03
7	0.413	0.325	45.6	45.9	1.29E+03	7.80E+03	7.91E+03
8	0.432	0.336	46.5	46.9	1.44E+03	7.93E+03	8.06E+03
9	0.586	0.275	46.3	47.2	1.63E+03	7.94E+03	8.10E+03
10	0.543	0.293	46.3	46.4	1.62E+03	7.87E+03	8.04E+03
11	0.545	0.307	47.1	48.1	1.76E+03	8.05E+03	8.24E+03
12	0.555	0.331	46.5	46.8	1.88E+03	7.92E+03	8.14E+03
13	0.703	0.268	45.5	45.8	1.91E+03	7.78E+03	8.01E+03
14	0.676	0.336	46.8	47.8	2.03E+03	8.00E+03	8.26E+03
15	0.675	0.361	46.7	47.6	2.12E+03	7.98E+03	8.26E+03
16	0.679	0.366	46.2	46.9	2.24E+03	7.90E+03	8.21E+03
17	0.291	0.261	46.3	47.0	6.47E+02	1.58E+04	1.59E+04
18	0.287	0.259	46.0	47.3	6.43E+02	1.59E+04	1.59E+04
19	0.287	0.245	46.0	45.7	6.26E+02	1.56E+04	1.57E+04
20	0.282	0.260	46.7	48.1	7.72E+02	1.61E+04	1.61E+04
21	0.313	0.224	47.0	48.1	1.22E+03	1.61E+04	1.61E+04
22	0.307	0.260	46.5	46.9	1.20E+03	1.59E+04	1.59E+04
23	0.305	0.281	46.3	46.3	1.24E+03	1.58E+04	1.58E+04
24	0.310	0.314	46.6	47.2	1.40E+03	1.59E+04	1.60E+04
25	0.351	0.240	46.7	47.9	1.61E+03	1.60E+04	1.61E+04
26	0.342	0.261	46.8	48.1	1.65E+03	1.61E+04	1.62E+04
27	0.346	0.272	45.5	46.7	1.69E+03	1.57E+04	1.58E+04
28	0.355	0.267	46.6	47.2	1.84E+03	1.59E+04	1.60E+04
29	0.388	0.248	46.8	47.9	1.95E+03	1.60E+04	1.62E+04
30	0.377	0.269	46.4	47.4	1.95E+03	1.59E+04	1.60E+04
31	0.384	0.286	46.6	47.9	2.08E+03	1.60E+04	1.62E+04
32	0.388	0.310	46.3	46.7	2.20E+03	1.58E+04	1.60E+04

Table A.8. Continued.

Test Point	PSR	OSR	Inlet Temperature	Average Outlet Temperature	Re_Z	Re_θ	Re
	[-]	[-]	[°C]	[°C]	[-]	[-]	[-]
33	0.347	0.142	46.4	48.3	4.61E+02	2.41E+04	2.41E+04
34	0.339	0.311	47.0	49.4	5.05E+02	2.45E+04	2.45E+04
35	0.341	0.271	46.4	48.5	5.19E+02	2.42E+04	2.42E+04
36	0.326	0.260	46.2	46.3	6.51E+02	2.36E+04	2.36E+04
37	0.283	0.262	47.0	48.8	1.07E+03	2.44E+04	2.44E+04
38	0.277	0.253	46.7	48.4	1.09E+03	2.42E+04	2.42E+04
39	0.276	0.257	45.9	47.6	1.15E+03	2.39E+04	2.39E+04
40	0.296	0.259	45.9	47.8	1.33E+03	2.39E+04	2.40E+04
41	0.296	0.237	47.1	48.9	1.54E+03	2.44E+04	2.45E+04
42	0.295	0.251	46.0	47.3	1.51E+03	2.38E+04	2.38E+04
43	0.296	0.265	46.3	47.1	1.60E+03	2.38E+04	2.39E+04
44	0.315	0.295	46.4	48.1	1.83E+03	2.41E+04	2.42E+04
45	0.319	0.233	46.7	48.2	1.86E+03	2.42E+04	2.42E+04
46	0.314	0.269	45.8	46.6	1.85E+03	2.36E+04	2.37E+04
47	0.311	0.296	46.6	48.2	2.00E+03	2.41E+04	2.42E+04
48	0.322	0.319	47.1	47.7	2.25E+03	2.42E+04	2.43E+04
49	0.384	0.109	46.3	51.6	4.07E+02	3.32E+04	3.32E+04
50	0.385	0.100	46.8	51.5	4.09E+02	3.33E+04	3.33E+04
51	0.364	0.182	46.1	49.8	4.66E+02	3.26E+04	3.26E+04
52	-	-	-	-	-	-	-
53	0.313	0.317	46.7	49.3	9.34E+02	3.26E+04	3.26E+04
54	0.311	0.280	46.2	48.6	9.29E+02	3.22E+04	3.22E+04
55	0.306	0.266	46.1	48.7	1.00E+03	3.22E+04	3.22E+04
56	-	-	-	-	-	-	-
57	0.285	0.257	46.2	48.6	1.35E+03	3.22E+04	3.22E+04
58	0.281	0.250	46.2	48.1	1.38E+03	3.21E+04	3.21E+04
59	0.274	0.258	47.1	49.9	1.61E+03	3.29E+04	3.29E+04
60	-	-	-	-	-	-	-
61	0.284	0.245	46.4	48.0	1.73E+03	3.21E+04	3.21E+04
62	0.284	0.257	46.3	48.2	1.81E+03	3.21E+04	3.22E+04
63	0.281	0.260	45.8	48.5	1.89E+03	3.20E+04	3.21E+04
64	-	-	-	-	-	-	-

Table A.9. Stiffness coefficients and uncertainties for the SS/GR seal with tangential injection for medium pre-swirl.

Test Point	K_{XX} [MN/m]	K_{XY} [MN/m]	K_{YX} [MN/m]	K_{YY} [MN/m]	$u_{K_{XX}}$ [MN/m]	$u_{K_{XY}}$ [MN/m]	$u_{K_{YX}}$ [MN/m]	$u_{K_{YY}}$ [MN/m]
1	-0.15	0.79	-0.77	-0.56	0.20	0.20	0.13	0.23
2	-0.11	0.56	-0.72	-0.62	0.15	0.21	0.14	0.17
3	-0.13	0.63	-0.64	-0.56	0.16	0.26	0.10	0.18
4	-0.16	0.61	-0.48	-0.73	0.25	0.32	0.13	0.26
5	-0.11	0.66	-0.77	-0.46	0.18	0.16	0.10	0.21
6	-0.09	0.81	-0.79	-0.41	0.26	0.19	0.13	0.22
7	0.00	0.65	-0.77	-0.54	0.24	0.31	0.12	0.22
8	-0.11	0.40	-0.62	-0.70	0.29	0.34	0.13	0.29
9	0.21	0.93	-1.03	-0.21	0.16	0.24	0.19	0.18
10	0.11	0.79	-0.96	-0.47	0.23	0.28	0.16	0.26
11	0.13	0.95	-1.00	-0.27	0.22	0.27	0.12	0.25
12	0.24	0.51	-0.83	-0.68	0.23	0.32	0.11	0.25
13	0.22	1.22	-1.35	-0.21	0.22	0.21	0.20	0.24
14	0.31	0.97	-1.21	-0.29	0.21	0.21	0.17	0.18
15	0.31	1.11	-1.15	-0.30	0.18	0.24	0.15	0.18
16	0.50	0.53	-1.09	-0.74	0.25	0.30	0.12	0.24
17	-0.04	1.31	-1.32	-0.52	0.15	0.14	0.14	0.14
18	-0.33	1.06	-1.01	-0.54	0.27	0.44	0.15	0.18
19	-0.46	0.76	-1.06	-0.96	0.24	0.37	0.09	0.26
20	-0.94	1.12	-1.00	-1.24	0.24	0.53	0.18	0.32
21	-0.31	1.54	-1.56	-0.70	0.15	0.19	0.18	0.13
22	-0.46	1.85	-1.30	-0.63	0.35	0.41	0.22	0.14
23	-0.20	1.51	-1.38	-0.97	0.31	0.56	0.09	0.23
24	-0.94	1.15	-1.18	-1.32	0.52	0.87	0.22	0.46
25	-0.27	1.63	-1.74	-0.60	0.16	0.20	0.25	0.16
26	-0.15	1.88	-1.59	-0.63	0.35	0.36	0.14	0.28
27	-0.32	1.17	-1.49	-0.91	0.33	0.55	0.11	0.19
28	-0.92	1.39	-1.41	-1.40	0.68	0.67	0.19	0.28
29	-0.09	1.90	-1.91	-0.51	0.20	0.19	0.22	0.19
30	-0.27	2.00	-1.82	-0.71	0.38	0.41	0.20	0.13
31	-0.20	1.81	-1.72	-0.58	0.23	0.44	0.11	0.34
32	-0.50	1.10	-1.65	-1.08	0.64	0.56	0.26	0.40

Table A.9. Continued.

Test Point	K_{XX} [MN/m]	K_{XY} [MN/m]	K_{YX} [MN/m]	K_{YY} [MN/m]	$u_{K_{XX}}$ [MN/m]	$u_{K_{XY}}$ [MN/m]	$u_{K_{YX}}$ [MN/m]	$u_{K_{YY}}$ [MN/m]
33	-0.55	2.10	-1.48	-0.89	0.30	0.43	0.12	0.15
34	-0.81	2.22	-1.52	-1.38	0.35	0.44	0.12	0.22
35	-1.26	2.02	-1.35	-1.80	0.33	0.50	0.17	0.28
36	-2.61	2.35	-1.48	-3.09	1.12	0.88	0.56	0.67
37	-0.70	3.23	-2.42	-1.13	0.29	0.44	0.21	0.19
38	-0.43	3.08	-2.54	-1.23	0.28	0.60	0.13	0.23
39	-0.94	2.27	-2.29	-1.89	0.25	0.50	0.20	0.26
40	-1.80	1.52	-1.90	-3.21	1.31	1.34	1.04	0.91
41	-0.52	3.31	-2.60	-1.15	0.58	0.46	0.21	0.22
42	-0.68	3.51	-2.53	-1.32	0.40	0.50	0.24	0.25
43	-0.81	2.62	-2.56	-1.80	0.35	0.44	0.23	0.23
44	-2.03	1.75	-2.62	-3.14	1.77	1.29	0.68	0.93
45	-0.74	3.65	-2.75	-1.29	0.48	0.57	0.21	0.19
46	-0.62	3.69	-2.66	-1.63	0.57	0.43	0.20	0.28
47	-0.50	2.84	-2.65	-1.87	0.44	0.34	0.16	0.20
48	-0.84	1.61	-2.83	-3.49	0.56	0.68	0.53	0.75
49	0.16	3.59	-3.68	-2.45	1.30	1.59	0.95	1.08
50	-0.74	4.94	-3.26	-3.85	1.02	0.95	0.70	0.62
51	-2.61	2.86	-2.37	-3.13	0.69	0.89	0.52	0.62
52	-	-	-	-	-	-	-	-
53	0.26	4.72	-4.42	-2.38	1.25	1.29	0.94	0.84
54	-0.51	5.35	-4.10	-3.66	0.98	0.87	0.55	0.69
55	-2.04	2.74	-3.57	-3.06	0.95	0.94	0.70	0.64
56	-	-	-	-	-	-	-	-
57	1.24	6.77	-6.29	-3.32	1.23	1.45	1.17	1.05
58	-0.42	6.20	-4.82	-3.57	0.65	0.84	0.46	0.60
59	-2.67	4.63	-2.53	-4.88	2.84	1.48	2.46	1.19
60	-	-	-	-	-	-	-	-
61	1.37	6.05	-5.74	-3.10	1.11	1.20	0.80	1.05
62	-0.76	6.36	-4.86	-3.36	0.90	0.77	0.71	0.54
63	-1.79	5.13	-4.30	-3.64	1.83	1.50	1.31	0.83
64	-	-	-	-	-	-	-	-

Table A.10. Damping coefficients and uncertainties for the SS/GR seal with tangential injection for medium pre-swirl.

Test Point	C_{XX} [kN-s/m]	C_{XY} [kN-s/m]	C_{YX} [kN-s/m]	C_{YY} [kN-s/m]	$u_{C_{XX}}$ [kN-s/m]	$u_{C_{XY}}$ [kN-s/m]	$u_{C_{YX}}$ [kN-s/m]	$u_{C_{YY}}$ [kN-s/m]
1	4.27	2.08	-2.12	3.92	0.20	0.45	0.32	0.31
2	4.15	2.33	-2.22	3.69	0.30	0.43	0.30	0.42
3	4.04	2.36	-2.46	3.46	0.34	0.47	0.28	0.41
4	3.86	2.89	-2.97	3.49	0.35	0.69	0.36	0.36
5	5.46	2.58	-2.60	4.96	0.37	0.45	0.35	0.20
6	5.46	2.61	-2.62	4.85	0.30	0.52	0.30	0.20
7	5.18	2.89	-2.78	4.75	0.40	0.52	0.27	0.25
8	4.93	3.30	-3.30	4.12	0.39	0.54	0.26	0.29
9	6.24	2.84	-2.84	5.47	0.30	0.47	0.27	0.27
10	6.32	2.79	-2.92	5.48	0.32	0.53	0.33	0.24
11	6.29	2.85	-3.05	5.11	0.45	0.69	0.31	0.39
12	5.89	3.56	-3.53	4.35	0.46	0.51	0.32	0.26
13	6.97	3.06	-2.94	6.26	0.30	0.50	0.43	0.32
14	6.93	3.17	-3.04	5.94	0.36	0.49	0.34	0.20
15	6.90	3.24	-3.31	5.37	0.44	0.43	0.32	0.18
16	6.70	3.84	-3.59	4.92	0.52	0.71	0.37	0.30
17	4.16	3.56	-3.46	3.31	0.34	0.30	0.20	0.45
18	5.29	4.13	-4.48	3.94	0.88	1.04	0.54	0.31
19	5.53	4.84	-5.23	4.14	0.82	1.48	0.59	0.38
20	6.22	5.08	-6.93	4.44	1.23	1.87	0.43	0.67
21	6.43	4.28	-4.44	5.15	0.30	0.60	0.39	0.27
22	6.66	4.54	-5.61	5.03	1.33	1.10	0.68	0.32
23	7.08	5.02	-6.26	4.92	1.30	1.23	0.79	0.26
24	8.19	5.14	-8.02	4.84	2.04	2.77	1.15	0.68
25	7.18	4.90	-4.96	5.76	0.45	0.65	0.35	0.40
26	8.24	5.16	-6.75	6.27	0.88	1.45	0.81	0.74
27	8.89	5.57	-7.39	6.07	0.93	1.80	0.45	0.44
28	8.87	5.81	-8.30	4.95	1.68	3.26	0.82	0.63
29	8.00	4.98	-5.09	6.55	0.36	0.89	0.51	0.24
30	8.32	4.85	-5.31	6.23	0.65	1.23	0.47	0.37
31	9.97	5.79	-7.94	6.48	0.87	2.73	0.56	0.70
32	10.03	6.26	-8.86	5.17	1.26	2.54	0.90	0.56

Table A.10. Continued.

Test Point	C_{XX} [kN-s/m]	C_{XY} [kN-s/m]	C_{YX} [kN-s/m]	C_{YY} [kN-s/m]	$u_{C_{XX}}$ [kN-s/m]	$u_{C_{XY}}$ [kN-s/m]	$u_{C_{YX}}$ [kN-s/m]	$u_{C_{YY}}$ [kN-s/m]
33	5.57	5.87	-6.34	3.90	0.83	0.52	0.37	0.43
34	6.45	5.40	-6.95	4.46	0.99	1.84	0.67	0.53
35	6.96	6.23	-7.72	4.72	1.06	1.79	0.69	0.66
36	12.43	9.39	-15.93	2.76	2.13	2.87	2.30	2.47
37	8.13	5.58	-6.80	6.08	0.63	1.06	0.63	0.71
38	8.48	5.30	-7.03	5.92	0.91	1.67	0.70	0.43
39	9.63	6.53	-8.41	6.22	1.10	2.10	0.76	0.50
40	14.63	8.71	-17.88	4.30	3.57	3.71	4.11	3.71
41	9.70	6.56	-8.43	6.73	0.95	2.42	0.52	0.73
42	9.78	6.68	-8.70	6.50	1.50	1.79	0.91	0.43
43	10.03	7.91	-9.60	5.96	1.23	1.77	0.86	0.38
44	15.93	8.40	-19.29	5.02	3.47	2.67	2.08	2.45
45	10.87	6.44	-9.01	7.51	1.17	1.97	0.59	0.57
46	11.48	7.00	-9.61	7.30	1.78	1.76	0.97	0.48
47	11.33	8.39	-10.24	6.40	0.61	1.61	0.69	0.36
48	11.70	9.25	-16.55	4.85	1.53	3.78	1.94	3.56
49	11.30	7.16	-12.84	4.46	3.47	1.38	2.54	1.46
50	10.47	7.65	-12.50	5.17	2.78	1.70	2.01	1.47
51	11.02	11.11	-13.33	3.51	3.63	1.84	2.36	1.19
52	-	-	-	-	-	-	-	-
53	10.74	6.81	-11.96	5.65	2.91	1.54	2.42	1.22
54	11.50	7.39	-12.78	6.51	2.88	1.66	1.92	1.35
55	13.92	10.32	-14.96	4.91	4.25	1.96	3.05	1.46
56	-	-	-	-	-	-	-	-
57	13.35	5.41	-12.79	8.47	4.00	2.38	3.19	2.14
58	13.43	7.15	-13.10	7.67	2.68	1.50	1.52	0.97
59	16.47	8.81	-17.06	8.22	5.25	3.36	4.24	2.14
60	-	-	-	-	-	-	-	-
61	14.79	6.76	-15.37	10.26	3.63	1.88	3.35	1.30
62	14.38	8.92	-15.26	8.01	2.64	2.53	1.79	2.04
63	17.29	11.06	-17.71	6.63	4.68	4.07	3.32	2.60
64	-	-	-	-	-	-	-	-

Table A.11. Virtual mass coefficients and uncertainties for the SS/GR seal with tangential injection for medium pre-swirl.

Test Point	M_{XX} [kg]	M_{XY} [kg]	M_{YX} [kg]	M_{YY} [kg]	$u_{M_{XX}}$ [kg]	$u_{M_{XY}}$ [kg]	$u_{M_{YX}}$ [kg]	$u_{M_{YY}}$ [kg]
1	11.72	-0.36	0.26	10.83	0.28	0.28	0.18	0.32
2	11.85	-0.65	0.28	10.87	0.21	0.30	0.19	0.23
3	11.87	-0.69	0.13	12.16	0.22	0.36	0.14	0.25
4	12.58	-1.02	0.09	14.27	0.35	0.44	0.18	0.37
5	13.00	-0.67	0.47	12.09	0.25	0.22	0.14	0.29
6	13.07	-0.80	0.27	12.49	0.36	0.27	0.18	0.31
7	13.29	-1.16	0.10	13.13	0.34	0.43	0.16	0.30
8	13.73	-1.67	-0.19	15.58	0.41	0.48	0.18	0.40
9	13.77	-0.54	0.32	12.89	0.23	0.33	0.27	0.25
10	13.73	-0.87	0.38	13.20	0.32	0.38	0.22	0.36
11	14.09	-1.04	0.31	14.34	0.31	0.38	0.17	0.35
12	14.84	-1.65	0.12	16.52	0.31	0.45	0.16	0.35
13	14.08	-0.49	0.26	13.26	0.31	0.29	0.28	0.34
14	14.51	-0.95	0.35	13.82	0.29	0.29	0.24	0.25
15	14.88	-1.30	0.30	14.83	0.24	0.33	0.21	0.25
16	15.50	-2.00	0.08	16.11	0.35	0.42	0.16	0.34
17	10.36	-0.22	-0.23	9.38	0.21	0.20	0.19	0.19
18	10.68	-1.71	-0.11	10.78	0.75	1.22	0.41	0.51
19	11.04	-2.66	-0.11	12.10	0.68	1.02	0.26	0.71
20	12.09	-3.81	0.38	15.25	0.68	1.48	0.49	0.90
21	12.84	-1.44	0.36	11.92	0.21	0.26	0.25	0.18
22	12.55	-1.65	0.26	13.08	0.96	1.14	0.60	0.38
23	13.77	-3.32	0.06	14.73	0.85	1.57	0.25	0.64
24	14.25	-6.39	0.04	18.49	1.44	2.43	0.60	1.29
25	13.76	-1.56	0.32	12.66	0.22	0.27	0.34	0.23
26	14.40	-2.82	0.47	15.00	0.96	1.00	0.38	0.78
27	14.54	-5.32	0.41	16.05	0.91	1.53	0.31	0.54
28	14.53	-5.61	0.28	18.51	1.90	1.88	0.53	0.77
29	14.14	-1.40	0.55	13.08	0.28	0.27	0.31	0.26
30	14.08	-1.89	0.49	13.53	0.52	0.57	0.27	0.18
31	14.63	-5.45	0.62	17.19	0.65	1.23	0.31	0.94
32	15.83	-7.01	0.00	19.56	1.77	1.55	0.71	1.11

Table A.11. Continued.

Test Point	M_{XX} [kg]	M_{XY} [kg]	M_{YX} [kg]	M_{YY} [kg]	$u_{M_{XX}}$ [kg]	$u_{M_{XY}}$ [kg]	$u_{M_{YX}}$ [kg]	$u_{M_{YY}}$ [kg]
33	10.84	-1.98	-0.32	10.40	0.82	1.20	0.35	0.42
34	8.76	-2.21	0.40	10.39	0.97	1.22	0.34	0.60
35	9.95	-3.82	0.59	11.98	0.91	1.39	0.48	0.77
36	15.03	-11.08	-1.51	21.71	3.14	2.46	1.55	1.86
37	10.82	-2.35	0.01	10.86	0.81	1.23	0.58	0.53
38	10.61	-2.38	-0.37	11.21	0.78	1.68	0.37	0.64
39	11.59	-5.35	-0.09	13.75	0.70	1.39	0.55	0.73
40	16.26	-16.88	-0.07	27.13	3.67	3.73	2.91	2.53
41	13.02	-3.94	0.43	13.81	1.61	1.29	0.58	0.61
42	12.85	-3.89	0.55	14.21	1.12	1.38	0.67	0.71
43	14.07	-6.09	-0.05	15.71	0.98	1.22	0.64	0.63
44	13.91	-13.75	0.63	25.52	4.95	3.59	1.90	2.60
45	12.39	-3.59	0.82	14.06	1.33	1.59	0.58	0.52
46	13.23	-4.44	1.03	14.61	1.59	1.20	0.55	0.77
47	15.15	-7.15	0.14	16.63	1.23	0.95	0.45	0.57
48	17.15	-10.25	-0.34	22.77	1.56	1.89	1.47	2.08
49	14.13	-6.90	-3.81	15.00	1.86	2.27	1.35	1.54
50	12.18	-4.78	-1.29	13.44	2.48	2.31	1.71	1.51
51	12.10	-9.00	-1.10	17.36	1.91	2.49	1.43	1.73
52	-	-	-	-	-	-	-	-
53	13.95	-5.34	-3.62	14.66	1.78	1.85	1.34	1.20
54	12.03	-3.71	-1.27	13.79	2.39	2.11	1.34	1.69
55	15.07	-10.27	-2.95	19.09	2.64	2.61	1.96	1.77
56	-	-	-	-	-	-	-	-
57	14.34	-3.68	-4.25	14.06	2.22	2.63	2.12	1.91
58	12.96	-4.15	-1.20	14.23	1.59	2.05	1.13	1.45
59	9.91	-10.03	4.22	19.13	7.90	4.11	6.83	3.30
60	-	-	-	-	-	-	-	-
61	17.09	-7.15	-2.50	18.67	2.04	2.21	1.47	1.94
62	14.52	-6.05	-0.30	18.49	2.19	1.86	1.72	1.30
63	14.37	-12.98	-0.73	23.17	5.10	4.17	3.65	2.31
64	-	-	-	-	-	-	-	-

Table A.12. WFR, C_{eff}, and uncertainties for the SS/GR seal with tangential injection for medium pre-swirl.

Test Point	WFR, [10]	u_{WFR}, [10]	WFR, [11]	u_{WFR}, [11]	C_{eff}	$u_{C_{eff}}$
	[-]	[-]	[-]	[-]	[kN-s/m]	[kN-s/m]
1	0.88	0.15	0.89	0.16	0.37	0.59
2	0.72	0.19	0.73	0.19	0.86	0.66
3	0.76	0.20	0.78	0.21	0.73	0.71
4	0.63	0.26	0.64	0.27	1.08	0.86
5	0.64	0.10	0.65	0.10	1.80	0.49
6	0.73	0.12	0.74	0.12	1.33	0.58
7	0.64	0.19	0.65	0.19	1.57	0.83
8	0.45	0.27	0.46	0.28	2.08	0.91
9	0.78	0.13	0.79	0.14	1.17	0.76
10	0.67	0.15	0.68	0.15	1.71	0.78
11	0.80	0.14	0.82	0.14	1.04	0.77
12	0.47	0.26	0.48	0.27	1.91	0.86
13	0.91	0.11	0.92	0.12	0.47	0.73
14	0.78	0.11	0.79	0.12	1.21	0.68
15	0.85	0.12	0.87	0.13	0.73	0.71
16	0.43	0.28	0.45	0.29	1.93	0.83
17	0.83	0.09	0.82	0.09	0.60	0.37
18	0.54	0.13	0.56	0.14	2.14	0.72
19	0.43	0.11	0.46	0.13	2.66	0.64
20	0.48	0.15	0.52	0.18	2.80	0.97
21	0.64	0.06	0.66	0.07	2.08	0.37
22	0.65	0.12	0.68	0.14	2.08	0.88
23	0.56	0.14	0.60	0.16	2.54	0.95
24	0.43	0.20	0.48	0.26	3.74	1.52
25	0.62	0.07	0.64	0.07	2.45	0.48
26	0.57	0.08	0.60	0.09	3.12	0.74
27	0.41	0.11	0.45	0.13	4.31	0.85
28	0.48	0.15	0.54	0.19	3.57	1.23
29	0.62	0.05	0.65	0.06	2.72	0.41
30	0.62	0.08	0.65	0.09	2.72	0.66
31	0.51	0.08	0.57	0.10	4.01	0.78
32	0.41	0.12	0.46	0.15	4.33	1.01

Table A.12. Continued.

Test Point	WFR, [10]	u_{WFR}, [10]	WFR, [11]	u_{WFR}, [11]	C_{eff}	$u_{C_{eff}}$
	[-]	[-]	[-]	[-]	[kN-s/m]	[kN-s/m]
33	0.60	0.09	0.64	0.12	1.89	0.59
34	0.54	0.09	0.60	0.12	2.49	0.67
35	0.46	0.09	0.52	0.13	3.17	0.75
36	0.44	0.17	0.64	0.59	4.54	1.83
37	0.63	0.07	0.68	0.09	2.61	0.62
38	0.62	0.08	0.66	0.10	2.73	0.70
39	0.45	0.07	0.51	0.09	4.29	0.74
40	0.27	0.20	0.37	0.48	6.74	2.91
41	0.57	0.07	0.64	0.09	3.51	0.72
42	0.59	0.08	0.67	0.11	3.34	0.90
43	0.51	0.07	0.59	0.10	3.88	0.75
44	0.32	0.18	0.44	0.38	7.00	2.42
45	0.56	0.07	0.62	0.09	4.10	0.81
46	0.54	0.07	0.61	0.10	4.34	1.00
47	0.48	0.04	0.56	0.06	4.50	0.46
48	0.34	0.13	0.45	0.27	4.75	2.05
49	0.53	0.22	0.62	0.33	3.54	2.18
50	0.61	0.17	0.72	0.31	2.93	1.72
51	0.44	0.14	0.62	0.46	4.14	2.01
52	-	-	-	-	-	-
53	0.66	0.19	0.72	0.25	2.74	1.84
54	0.61	0.14	0.68	0.20	3.36	1.70
55	0.40	0.12	0.50	0.24	5.65	2.35
56	-	-	-	-	-	-
57	0.70	0.20	0.70	0.22	3.12	2.53
58	0.62	0.11	0.68	0.15	3.98	1.54
59	0.35	0.18	0.47	0.42	8.07	3.31
60	-	-	-	-	-	-
61	0.54	0.13	0.62	0.19	5.49	2.11
62	0.60	0.11	0.73	0.22	4.50	1.78
63	0.48	0.16	0.75	0.78	6.33	2.93
64	-	-	-	-	-	-

Assembly 3 – Tangential Injection: High Pre-swirl

Table A.13. Static results of the SS/GR seal with tangential injection for high pre-swirl.

Test Point	Target ω	Target ΔP	Target ε_0	Measured ω	Measured ΔP	Measured ε_0	ϕ	$\dot{Q}$	F_r
	[rpm]	[bar]	[-]	[rpm]	[bar]	[-]	[deg]	[LPM]	[N]
1	2000	2.068	0.00	1999.8	2.011	0.047	2.69	15.88	1.8
2	2000	2.068	0.27	1998.0	2.106	0.261	14.97	16.32	-2.6
3	2000	2.068	0.53	1997.9	2.025	0.529	30.31	16.39	-13.5
4	2000	2.068	0.80	1997.7	2.036	0.769	44.06	18.41	-26.5
5	2000	4.137	0.00	1992.1	4.017	0.014	0.83	26.03	-0.3
6	2000	4.137	0.27	1992.3	4.080	0.266	15.24	27.40	-3.7
7	2000	4.137	0.53	1992.4	3.927	0.574	32.92	28.60	-10.4
8	2000	4.137	0.80	1992.4	4.065	0.765	43.83	31.45	-19.8
9	2000	6.205	0.00	1997.4	6.086	0.034	1.93	34.99	2.0
10	2000	6.205	0.27	1998.0	6.033	0.258	14.76	35.61	0.4
11	2000	6.205	0.53	1998.1	6.077	0.515	29.51	37.84	1.4
12	2000	6.205	0.80	1998.0	6.397	0.756	43.33	41.95	-9.1
13	2000	8.274	0.00	1998.3	8.151	0.024	1.40	42.52	4.4
14	2000	8.274	0.27	1998.4	8.184	0.276	15.79	43.62	8.2
15	2000	8.274	0.53	1998.2	8.093	0.528	30.25	45.77	9.3
16	2000	8.274	0.80	1997.5	8.036	0.766	43.89	48.68	-0.3
17	4000	2.068	0.00	3999.1	2.054	0.017	0.98	13.79	0.1
18	4000	2.068	0.27	3998.8	2.001	0.274	15.70	13.80	62.8
19	4000	2.068	0.53	3999.4	1.991	0.545	31.22	14.34	30.9
20	4000	2.068	0.80	3999.9	2.062	0.815	46.68	16.26	-72.2
21	4000	4.137	0.00	3999.6	4.132	0.008	0.45	25.76	0.2
22	4000	4.137	0.27	3999.5	4.128	0.262	15.02	26.85	81.2
23	4000	4.137	0.53	3999.8	4.073	0.551	31.58	27.97	60.1
24	4000	4.137	0.80	3999.6	3.959	0.795	45.54	29.64	-24.2
25	4000	6.205	0.00	3986.9	6.120	0.006	0.32	34.54	4.2
26	4000	6.205	0.27	3994.7	6.144	0.277	15.89	35.72	43.4
27	4000	6.205	0.53	3994.9	6.088	0.560	32.07	37.44	-27.1
28	4000	6.205	0.80	3995.6	6.104	0.789	45.22	40.07	-131.2
29	4000	8.274	0.00	3999.6	8.085	0.003	0.18	41.36	2.1
30	4000	8.274	0.27	3999.7	8.160	0.281	16.09	42.90	33.1
31	4000	8.274	0.53	4000.1	8.104	0.531	30.42	45.02	18.4
32	4000	8.274	0.80	3999.1	8.109	0.775	44.38	48.10	-64.1

Table A.13. Continued.

Test Point	Target ω	Target ΔP	Target ε_0	Measured ω	Measured ΔP	Measured ε_0	ϕ	$\dot{Q}$	F_r
	[rpm]	[bar]	[-]	[rpm]	[bar]	[-]	[deg]	[LPM]	[N]
33	6000	2.068	0.00	5999.4	2.144	0.034	1.94	10.64	2.8
34	6000	2.068	0.27	5999.7	2.051	0.272	15.59	10.69	77.5
35	6000	2.068	0.53	5999.6	2.008	0.544	31.20	11.55	-12.1
36	6000	2.068	0.80	5999.0	2.101	0.838	48.00	14.25	-191.0
37	6000	4.137	0.00	6000.1	4.157	0.013	0.73	23.11	2.7
38	6000	4.137	0.27	6001.7	4.139	0.267	15.30	23.82	43.7
39	6000	4.137	0.53	6001.9	3.958	0.594	34.02	24.78	-85.2
40	6000	4.137	0.80	6001.7	4.295	0.798	45.72	29.34	-259.1
41	6000	6.205	0.00	6001.2	6.086	0.022	1.25	32.00	-3.0
42	6000	6.205	0.27	6000.5	6.085	0.269	15.42	33.17	54.9
43	6000	6.205	0.53	5999.4	6.176	0.552	31.63	35.43	-27.1
44	6000	6.205	0.80	5999.9	6.165	0.814	46.66	38.34	-202.7
45	6000	8.274	0.00	5999.7	8.238	0.011	0.64	40.05	2.4
46	6000	8.274	0.27	5999.9	8.165	0.276	15.81	41.34	39.5
47	6000	8.274	0.53	5999.6	8.095	0.550	31.51	43.45	-32.2
48	6000	8.274	0.80	5999.1	8.129	0.764	43.76	46.10	-156.3
49	8000	2.068	0.00	8002.6	2.114	0.005	0.30	7.77	3.1
50	8000	2.068	0.27	8002.4	2.058	0.271	15.55	8.31	-30.1
51	8000	2.068	0.53	8001.8	1.995	0.559	32.04	9.30	-182.9
52	8000	2.068	0.80	-	-	-	-	-	-
53	8000	4.137	0.00	8000.1	4.091	0.011	0.65	19.57	4.8
54	8000	4.137	0.27	8001.6	4.125	0.245	14.04	20.25	-21.3
55	8000	4.137	0.53	8003.1	4.100	0.516	29.56	21.18	-133.5
56	8000	4.137	0.80	-	-	-	-	-	-
57	8000	6.205	0.00	8000.4	6.067	0.019	1.08	28.70	1.0
58	8000	6.205	0.27	8001.3	6.120	0.255	14.60	29.72	26.0
59	8000	6.205	0.53	8002.3	6.089	0.550	31.52	32.90	-76.0
60	8000	6.205	0.80	-	-	-	-	-	-
61	8000	8.274	0.00	7999.3	8.236	0.013	0.72	37.62	21.9
62	8000	8.274	0.27	8000.1	8.121	0.280	16.04	38.07	60.9
63	8000	8.274	0.53	7999.2	8.067	0.575	32.95	40.73	-65.0
64	8000	8.274	0.80	-	-	-	-	-	-

Table A.14. Additional static results of the SS/GR seal with tangential injection for high pre-swirl.

Test Point	PSR	OSR	Inlet Temperature	Average Outlet Temperature	Re_Z	Re_θ	Re
	[-]	[-]	[°C]	[°C]	[-]	[-]	[-]
1	0.433	0.254	46.5	47.4	7.15E+02	7.98E+03	8.01E+03
2	0.439	0.298	46.0	46.2	7.24E+02	7.85E+03	7.89E+03
3	0.438	0.294	46.2	45.9	7.26E+02	7.85E+03	7.88E+03
4	0.458	0.300	46.3	46.9	8.23E+02	7.91E+03	7.96E+03
5	0.627	0.272	46.0	46.2	1.15E+03	7.83E+03	7.91E+03
6	0.628	0.269	46.6	46.9	1.23E+03	7.91E+03	8.01E+03
7	0.626	0.324	46.6	46.7	1.28E+03	7.91E+03	8.01E+03
8	0.630	0.315	46.3	46.8	1.41E+03	7.89E+03	8.01E+03
9	0.763	0.275	46.1	46.6	1.56E+03	7.88E+03	8.03E+03
10	0.741	0.295	45.8	46.1	1.58E+03	7.83E+03	7.99E+03
11	0.732	0.318	46.3	46.2	1.68E+03	7.87E+03	8.05E+03
12	0.750	0.349	46.6	46.5	1.88E+03	7.91E+03	8.13E+03
13	0.885	0.283	46.5	46.8	1.91E+03	7.93E+03	8.16E+03
14	0.861	0.326	46.2	46.7	1.95E+03	7.90E+03	8.14E+03
15	0.846	0.354	46.8	47.3	2.07E+03	7.99E+03	8.25E+03
16	0.850	0.373	46.2	46.7	2.17E+03	7.90E+03	8.19E+03
17	0.327	0.279	46.1	47.5	6.19E+02	1.59E+04	1.59E+04
18	0.328	0.263	45.9	47.3	6.17E+02	1.59E+04	1.59E+04
19	0.336	0.247	45.8	47.2	6.41E+02	1.58E+04	1.59E+04
20	0.348	0.261	46.2	45.6	7.19E+02	1.57E+04	1.57E+04
21	0.389	0.233	46.7	46.7	1.15E+03	1.59E+04	1.59E+04
22	0.395	0.279	46.4	47.2	1.21E+03	1.59E+04	1.60E+04
23	0.402	0.295	45.4	46.7	1.24E+03	1.57E+04	1.58E+04
24	0.416	0.301	46.3	47.1	1.33E+03	1.59E+04	1.60E+04
25	0.465	0.254	46.0	47.2	1.55E+03	1.58E+04	1.59E+04
26	0.465	0.272	46.7	47.8	1.62E+03	1.60E+04	1.61E+04
27	0.472	0.285	46.7	47.9	1.70E+03	1.60E+04	1.61E+04
28	0.484	0.287	45.1	46.1	1.76E+03	1.56E+04	1.57E+04
29	0.532	0.267	45.5	46.6	1.83E+03	1.57E+04	1.58E+04
30	0.534	0.275	45.8	46.9	1.91E+03	1.58E+04	1.59E+04
31	0.544	0.297	45.9	47.1	2.01E+03	1.58E+04	1.60E+04
32	0.563	0.312	46.4	46.8	2.15E+03	1.59E+04	1.60E+04

Table A.14. Continued.

Test Point	PSR	OSR	Inlet Temperature	Average Outlet Temperature	Re_Z	Re_θ	Re
	[-]	[-]	[°C]	[°C]	[-]	[-]	[-]
33	0.358	0.147	46.3	48.0	4.81E+02	2.41E+04	2.41E+04
34	0.358	0.255	45.5	47.9	4.80E+02	2.39E+04	2.39E+04
35	0.355	0.278	46.4	48.8	5.27E+02	2.43E+04	2.43E+04
36	0.345	0.270	44.9	46.8	6.30E+02	2.35E+04	2.35E+04
37	0.327	0.272	46.3	48.0	1.04E+03	2.40E+04	2.41E+04
38	0.333	0.256	45.9	47.7	1.07E+03	2.39E+04	2.39E+04
39	0.342	0.261	45.7	46.1	1.10E+03	2.35E+04	2.36E+04
40	0.358	0.263	46.2	48.0	1.33E+03	2.40E+04	2.41E+04
41	0.363	0.244	45.6	46.2	1.41E+03	2.35E+04	2.36E+04
42	0.368	0.271	46.6	48.1	1.50E+03	2.41E+04	2.42E+04
43	0.375	0.288	46.4	47.2	1.59E+03	2.39E+04	2.39E+04
44	0.386	0.294	46.2	46.4	1.71E+03	2.37E+04	2.37E+04
45	0.396	0.240	46.4	46.8	1.79E+03	2.38E+04	2.39E+04
46	0.399	0.289	46.5	48.0	1.87E+03	2.41E+04	2.42E+04
47	0.408	0.298	46.2	47.6	1.96E+03	2.39E+04	2.40E+04
48	0.419	0.309	45.5	45.6	2.02E+03	2.34E+04	2.34E+04
49	0.392	0.112	46.5	50.9	3.62E+02	3.31E+04	3.31E+04
50	0.394	0.097	45.8	51.0	3.85E+02	3.29E+04	3.29E+04
51	0.395	0.148	46.9	51.7	4.38E+02	3.34E+04	3.34E+04
52	-	-	-	-	-	-	-
53	0.336	0.329	46.4	49.0	8.93E+02	3.24E+04	3.24E+04
54	0.335	0.305	46.2	48.7	9.20E+02	3.22E+04	3.22E+04
55	0.335	0.280	45.7	47.1	9.45E+02	3.17E+04	3.17E+04
56	-	-	-	-	-	-	-
57	0.324	0.274	46.0	47.8	1.29E+03	3.19E+04	3.19E+04
58	0.327	0.260	45.4	46.4	1.31E+03	3.14E+04	3.14E+04
59	0.337	0.260	46.4	49.1	1.50E+03	3.24E+04	3.25E+04
60	-	-	-	-	-	-	-
61	0.346	0.257	46.3	48.7	1.71E+03	3.23E+04	3.23E+04
62	0.347	0.259	45.8	48.3	1.72E+03	3.20E+04	3.21E+04
63	0.350	0.268	46.1	48.5	1.85E+03	3.21E+04	3.22E+04
64	-	-	-	-	-	-	-

Table A.15. Stiffness coefficients and uncertainties for the SS/GR seal with tangential injection for high pre-swirl.

Test Point	K_{XX}	K_{XY}	K_{YX}	K_{YY}	$u_{K_{XX}}$	$u_{K_{XY}}$	$u_{K_{YX}}$	$u_{K_{YY}}$
	[MN/m]	[MN/m]	[MN/m]	[MN/m]	[MN/m]	[MN/m]	[MN/m]	[MN/m]
1	-0.43	0.71	-0.59	-0.47	0.25	0.11	0.22	0.21
2	-0.22	0.52	-0.55	-0.49	0.24	0.12	0.18	0.20
3	-0.12	0.42	-0.59	-0.68	0.30	0.12	0.28	0.23
4	-0.23	0.45	-0.55	-0.87	0.29	0.11	0.24	0.27
5	-0.42	0.71	-0.63	-0.51	0.25	0.10	0.23	0.22
6	-0.25	0.95	-0.72	-0.45	0.28	0.11	0.17	0.27
7	-0.11	0.36	-0.69	-0.74	0.48	0.14	0.30	0.28
8	-0.10	0.45	-0.53	-0.90	0.50	0.13	0.57	0.22
9	-0.15	1.02	-0.87	-0.38	0.36	0.16	0.26	0.18
10	-0.04	1.05	-0.93	-0.47	0.26	0.11	0.19	0.25
11	0.09	1.05	-1.07	-0.48	0.30	0.12	0.29	0.27
12	0.11	0.63	-1.02	-0.99	0.31	0.13	0.22	0.27
13	-0.04	1.38	-1.28	-0.25	0.28	0.17	0.30	0.21
14	-0.02	1.14	-1.27	-0.37	0.19	0.10	0.20	0.20
15	0.25	1.53	-1.36	-0.30	0.28	0.15	0.27	0.23
16	0.15	0.76	-1.25	-1.00	0.24	0.12	0.21	0.22
17	0.14	1.18	-1.50	-0.52	0.14	0.16	0.21	0.12
18	-0.16	1.07	-1.34	-0.60	0.21	0.17	0.23	0.18
19	-0.04	0.62	-1.40	-0.82	0.25	0.22	0.23	0.19
20	-0.30	0.71	-0.99	-1.20	0.29	0.31	0.29	0.26
21	0.10	1.52	-1.88	-0.80	0.17	0.15	0.27	0.13
22	0.09	1.67	-1.82	-0.75	0.22	0.20	0.29	0.15
23	0.34	1.16	-1.87	-0.80	0.18	0.23	0.29	0.19
24	0.22	0.52	-1.40	-1.04	0.21	0.27	0.30	0.25
25	0.01	1.79	-2.01	-0.78	0.25	0.13	0.17	0.12
26	-0.26	2.05	-1.96	-0.97	0.31	0.21	0.30	0.16
27	0.31	1.41	-2.03	-0.91	0.23	0.21	0.29	0.24
28	0.99	0.69	-1.94	-1.13	0.25	0.28	0.26	0.23
29	-0.09	2.20	-2.36	-0.84	0.27	0.23	0.33	0.14
30	-0.07	2.05	-2.33	-0.86	0.34	0.18	0.34	0.15
31	0.18	1.56	-2.24	-0.76	0.31	0.23	0.32	0.25
32	0.30	0.99	-2.05	-0.90	0.32	0.33	0.26	0.19

Table A.15. Continued.

Test Point	K_{XX}	K_{XY}	K_{YX}	K_{YY}	$u_{K_{XX}}$	$u_{K_{XY}}$	$u_{K_{YX}}$	$u_{K_{YY}}$
	[MN/m]	[MN/m]	[MN/m]	[MN/m]	[MN/m]	[MN/m]	[MN/m]	[MN/m]
33	-0.07	1.75	-1.94	-1.07	0.18	0.14	0.22	0.18
34	-0.69	1.93	-1.75	-1.35	0.33	0.28	0.28	0.26
35	-0.70	1.35	-1.93	-1.72	0.39	0.22	0.33	0.27
36	-0.77	1.26	-1.59	-2.18	0.26	0.46	0.23	0.24
37	-0.11	2.74	-2.88	-1.18	0.36	0.24	0.29	0.18
38	-0.71	2.76	-2.66	-1.24	0.28	0.18	0.22	0.18
39	-1.26	1.74	-2.34	-1.95	0.30	0.29	0.31	0.30
40	-1.16	1.18	-2.06	-1.89	0.31	0.34	0.21	0.21
41	-0.36	3.12	-3.05	-1.38	0.38	0.28	0.35	0.27
42	-0.42	3.07	-3.01	-1.43	0.30	0.21	0.24	0.22
43	-0.42	2.08	-2.80	-1.68	0.24	0.23	0.33	0.23
44	-0.42	1.15	-2.43	-2.19	0.26	0.31	0.20	0.28
45	-0.23	3.50	-3.37	-1.49	0.34	0.33	0.27	0.32
46	-0.60	3.35	-3.25	-1.61	0.38	0.37	0.31	0.29
47	-0.63	2.64	-3.18	-1.76	0.24	0.23	0.27	0.35
48	-0.54	1.40	-2.70	-2.03	0.22	0.27	0.21	0.28
49	-1.11	3.05	-2.80	-2.15	0.17	0.17	0.20	0.17
50	-1.47	2.85	-2.75	-2.30	0.37	0.27	0.17	0.14
51	-1.35	2.31	-2.48	-2.78	0.31	0.20	0.26	0.19
52	-	-	-	-	-	-	-	-
53	-0.72	3.69	-3.67	-1.83	0.25	0.19	0.22	0.22
54	-1.34	3.30	-3.40	-2.06	0.23	0.21	0.24	0.18
55	-2.01	2.45	-3.14	-2.68	0.28	0.28	0.20	0.26
56	-	-	-	-	-	-	-	-
57	-0.61	4.81	-4.47	-2.11	0.32	0.23	0.24	0.25
58	-1.18	4.19	-4.16	-2.09	0.29	0.28	0.23	0.19
59	-1.79	2.98	-3.91	-3.02	0.27	0.43	0.25	0.28
60	-	-	-	-	-	-	-	-
61	-0.59	4.92	-4.71	-2.45	0.31	0.23	0.26	0.27
62	-0.88	4.58	-4.48	-2.39	0.24	0.16	0.31	0.25
63	-0.81	2.81	-4.12	-3.26	0.32	0.28	0.32	0.33
64	-	-	-	-	-	-	-	-

Table A.16. Damping coefficients and uncertainties for the SS/GR seal with tangential injection for high pre-swirl.

Test Point	C_{XX} [kN-s/m]	C_{XY} [kN-s/m]	C_{YX} [kN-s/m]	C_{YY} [kN-s/m]	$u_{C_{XX}}$ [kN-s/m]	$u_{C_{XY}}$ [kN-s/m]	$u_{C_{YX}}$ [kN-s/m]	$u_{C_{YY}}$ [kN-s/m]
1	3.63	2.18	-2.39	3.60	0.63	0.31	0.19	0.31
2	3.70	2.52	-2.37	3.55	0.38	0.40	0.30	0.40
3	3.44	2.64	-2.69	3.48	0.54	0.36	0.34	0.32
4	3.21	3.13	-3.38	2.93	0.55	0.31	0.22	0.41
5	4.86	2.83	-2.86	4.78	0.51	0.50	0.31	0.21
6	4.98	2.89	-2.84	4.72	0.53	0.27	0.32	0.25
7	4.80	3.32	-3.22	4.47	0.91	0.37	0.27	0.18
8	4.61	3.67	-4.00	3.79	1.14	0.30	0.65	0.28
9	5.71	3.20	-3.21	5.49	0.61	0.33	0.23	0.23
10	5.70	3.26	-3.24	5.40	0.62	0.35	0.31	0.30
11	5.52	3.44	-3.44	5.12	0.71	0.29	0.32	0.26
12	5.15	4.13	-4.16	4.09	0.90	0.28	0.22	0.26
13	6.32	3.32	-3.36	6.15	0.42	0.40	0.31	0.25
14	6.32	3.68	-3.54	5.80	0.56	0.36	0.32	0.21
15	6.10	3.67	-3.82	5.33	0.99	0.27	0.28	0.31
16	5.50	4.49	-4.47	4.25	0.84	0.21	0.16	0.26
17	4.69	3.37	-4.93	3.49	0.33	0.36	0.39	0.46
18	4.80	3.78	-5.00	3.34	0.41	0.52	0.38	0.47
19	5.35	4.58	-5.77	3.55	0.52	0.57	0.43	0.29
20	4.88	5.43	-7.21	3.79	0.58	0.72	0.41	0.44
21	7.20	4.22	-6.36	5.44	0.40	0.69	0.39	0.16
22	6.71	4.47	-6.50	5.04	0.40	0.46	0.37	0.33
23	6.97	5.28	-7.05	4.64	0.66	0.55	0.49	0.33
24	6.22	6.36	-8.13	3.99	1.02	0.73	0.42	0.29
25	7.95	5.02	-7.33	6.34	0.37	0.69	0.39	0.24
26	7.84	5.11	-7.30	6.14	0.43	0.72	0.32	0.32
27	8.08	5.57	-8.00	5.47	0.69	0.78	0.45	0.36
28	7.42	6.62	-8.84	4.51	1.22	0.67	0.50	0.38
29	8.78	5.29	-7.75	7.05	0.55	0.68	0.41	0.39
30	8.93	5.48	-8.17	6.90	0.54	0.89	0.46	0.51
31	9.13	6.15	-8.78	6.10	0.86	0.91	0.53	0.39
32	7.87	6.77	-9.71	4.82	1.10	0.71	0.63	0.46

Table A.16. Continued.

Test Point	C_{XX} [kN-s/m]	C_{XY} [kN-s/m]	C_{YX} [kN-s/m]	C_{YY} [kN-s/m]	$u_{C_{XX}}$ [kN-s/m]	$u_{C_{XY}}$ [kN-s/m]	$u_{C_{YX}}$ [kN-s/m]	$u_{C_{YY}}$ [kN-s/m]
33	5.26	5.42	-7.12	3.53	0.60	0.80	0.44	0.32
34	5.42	5.57	-7.23	3.70	0.40	0.55	0.31	0.37
35	5.98	6.68	-8.01	3.69	0.60	0.88	0.33	0.24
36	5.68	8.49	-10.23	3.82	0.89	1.24	0.49	0.69
37	7.40	5.11	-7.62	5.61	0.41	0.74	0.42	0.37
38	7.57	5.28	-8.00	5.50	0.37	0.65	0.39	0.38
39	8.56	6.59	-9.51	5.82	0.47	0.98	0.58	0.44
40	8.32	8.78	-11.53	4.77	0.85	1.17	0.63	0.44
41	9.40	5.95	-9.44	7.18	0.67	1.22	0.35	0.77
42	9.09	6.30	-9.72	6.32	0.50	0.99	0.41	0.45
43	9.02	7.63	-10.62	5.68	0.63	1.04	0.46	0.43
44	8.24	9.68	-12.15	4.56	0.85	1.18	0.44	0.32
45	9.95	6.67	-10.27	7.48	0.44	1.06	0.47	0.55
46	10.02	6.79	-10.57	7.04	0.54	1.17	0.42	0.60
47	9.89	7.89	-11.38	6.19	0.77	1.21	0.52	0.67
48	9.55	9.35	-13.05	5.16	0.84	1.20	0.71	0.43
49	6.68	7.22	-9.67	4.14	0.90	0.61	0.54	0.78
50	6.52	7.77	-9.81	4.05	0.84	0.46	0.48	0.61
51	6.74	8.93	-10.46	4.11	0.68	0.90	0.40	0.46
52	-	-	-	-	-	-	-	-
53	7.45	7.61	-9.67	4.88	0.47	0.53	0.33	0.36
54	7.43	8.26	-9.89	4.80	0.71	0.45	0.33	0.46
55	8.43	9.15	-11.28	4.96	0.55	0.68	0.49	0.43
56	-	-	-	-	-	-	-	-
57	9.32	7.48	-10.23	6.44	0.61	0.52	0.61	0.43
58	9.09	7.98	-10.41	6.21	0.56	0.41	0.37	0.54
59	10.13	9.39	-11.84	6.38	0.60	1.26	0.43	0.40
60	-	-	-	-	-	-	-	-
61	11.22	8.19	-11.96	8.70	0.53	1.17	0.72	0.61
62	10.60	9.34	-11.92	7.19	0.53	0.84	0.46	0.53
63	10.49	11.30	-13.39	6.16	0.73	0.97	0.44	0.37
64	-	-	-	-	-	-	-	-

Table A.17. Virtual mass coefficients and uncertainties for the SS/GR seal with tangential injection for high pre-swirl.

Test Point	M_{XX} [kg]	M_{XY} [kg]	M_{YX} [kg]	M_{YY} [kg]	$u_{M_{XX}}$ [kg]	$u_{M_{XY}}$ [kg]	$u_{M_{YX}}$ [kg]	$u_{M_{YY}}$ [kg]
1	11.01	0.08	0.36	10.78	0.34	0.15	0.30	0.30
2	11.36	-0.25	0.37	11.05	0.34	0.18	0.26	0.28
3	11.65	-0.26	0.26	12.37	0.44	0.17	0.41	0.33
4	12.19	-0.16	0.26	14.96	0.42	0.16	0.35	0.39
5	12.24	-0.16	0.62	11.87	0.37	0.15	0.34	0.32
6	12.48	-0.10	0.45	12.49	0.40	0.16	0.25	0.39
7	12.82	-0.66	0.34	13.96	0.70	0.20	0.44	0.41
8	13.20	-0.44	0.12	15.86	0.72	0.18	0.83	0.32
9	13.07	-0.04	0.62	12.56	0.51	0.22	0.37	0.26
10	13.22	-0.27	0.35	13.31	0.38	0.16	0.28	0.37
11	13.63	-0.34	0.19	14.29	0.44	0.17	0.43	0.39
12	14.12	-0.52	-0.06	16.41	0.45	0.19	0.32	0.40
13	13.46	-0.02	0.46	13.11	0.40	0.24	0.43	0.31
14	13.71	-0.47	0.41	13.96	0.27	0.14	0.29	0.29
15	14.21	-0.19	0.22	15.20	0.41	0.21	0.40	0.33
16	14.53	-0.44	-0.01	16.99	0.35	0.17	0.30	0.32
17	10.97	-1.25	-1.65	10.87	0.20	0.22	0.29	0.17
18	11.17	-1.36	-1.49	11.17	0.29	0.23	0.32	0.25
19	11.74	-1.26	-0.54	12.19	0.34	0.31	0.32	0.26
20	12.94	-0.45	0.53	14.39	0.41	0.43	0.40	0.36
21	13.76	-2.46	-1.60	13.83	0.24	0.21	0.38	0.18
22	13.99	-2.15	-1.62	14.04	0.30	0.28	0.41	0.21
23	14.42	-1.91	-0.88	15.27	0.25	0.31	0.41	0.27
24	15.02	-1.34	0.02	17.25	0.29	0.38	0.42	0.35
25	14.41	-2.42	-0.91	14.46	0.35	0.18	0.24	0.17
26	14.44	-2.04	-1.06	14.76	0.43	0.29	0.41	0.23
27	14.76	-2.31	-0.76	16.06	0.32	0.29	0.40	0.34
28	15.40	-1.98	-0.41	18.28	0.34	0.38	0.37	0.31
29	14.89	-2.40	-1.24	15.08	0.38	0.32	0.46	0.19
30	15.43	-2.87	-0.88	16.20	0.48	0.24	0.47	0.21
31	15.71	-2.57	-0.40	16.61	0.43	0.31	0.45	0.34
32	16.81	-1.58	0.05	18.31	0.45	0.45	0.37	0.26

Table A.17. Continued.

Test Point	M_{XX} [kg]	M_{XY} [kg]	M_{YX} [kg]	M_{YY} [kg]	$u_{M_{XX}}$ [kg]	$u_{M_{XY}}$ [kg]	$u_{M_{YX}}$ [kg]	$u_{M_{YY}}$ [kg]
33	10.89	-1.58	-1.51	10.95	0.26	0.20	0.31	0.25
34	10.66	-1.60	-1.10	11.41	0.46	0.39	0.39	0.37
35	11.02	-1.76	-0.41	12.42	0.54	0.31	0.47	0.37
36	12.17	-1.49	0.12	15.07	0.37	0.65	0.33	0.35
37	11.08	-1.61	-1.32	11.49	0.51	0.34	0.41	0.26
38	10.86	-1.57	-1.16	12.05	0.39	0.25	0.31	0.25
39	12.09	-2.04	-0.40	13.70	0.42	0.40	0.43	0.41
40	14.50	-2.36	0.03	17.84	0.44	0.49	0.30	0.30
41	13.28	-2.98	-0.96	14.65	0.53	0.39	0.49	0.37
42	13.80	-2.88	-1.15	15.05	0.42	0.29	0.33	0.31
43	14.42	-3.16	-0.61	16.45	0.33	0.32	0.46	0.32
44	15.37	-2.87	-0.51	18.69	0.37	0.45	0.29	0.39
45	14.16	-2.73	-0.95	14.98	0.47	0.47	0.38	0.45
46	14.36	-3.05	-0.86	15.70	0.54	0.51	0.44	0.41
47	14.94	-3.24	-0.66	17.09	0.33	0.32	0.38	0.48
48	15.69	-3.27	-0.33	19.10	0.31	0.39	0.30	0.39
49	10.63	-1.36	-1.51	10.75	0.25	0.24	0.28	0.25
50	10.77	-1.51	-1.12	11.26	0.52	0.39	0.25	0.20
51	11.56	-2.11	-0.24	12.40	0.44	0.29	0.37	0.28
52	-	-	-	-	-	-	-	-
53	11.53	-1.68	-1.95	11.60	0.36	0.27	0.31	0.31
54	11.45	-1.76	-1.67	11.88	0.32	0.29	0.34	0.26
55	11.56	-2.09	-0.65	13.10	0.40	0.40	0.28	0.36
56	-	-	-	-	-	-	-	-
57	11.53	-1.47	-1.77	11.77	0.46	0.33	0.35	0.36
58	11.37	-1.48	-1.53	12.21	0.41	0.40	0.32	0.28
59	12.47	-2.09	-0.62	13.66	0.39	0.62	0.35	0.39
60	-	-	-	-	-	-	-	-
61	13.25	-3.20	-0.54	14.15	0.44	0.33	0.36	0.39
62	14.14	-3.61	-0.88	15.20	0.34	0.23	0.44	0.36
63	15.09	-4.05	-1.12	16.85	0.46	0.40	0.45	0.47
64	-	-	-	-	-	-	-	-

Table A.18. WFR, C_{eff}, and uncertainties for the SS/GR seal with tangential injection for high pre-swirl.

Test Point	WFR, [10]	u_{WFR}, [10]	WFR, [11]	u_{WFR}, [11]	C_{eff}	$u_{C_{eff}}$
	[-]	[-]	[-]	[-]	[kN-s/m]	[kN-s/m]
1	0.86	0.19	0.87	0.19	0.50	0.68
2	0.69	0.16	0.70	0.16	1.07	0.58
3	0.62	0.25	0.63	0.26	1.05	0.80
4	0.68	0.27	0.69	0.27	0.68	0.72
5	0.66	0.14	0.67	0.14	1.63	0.67
6	0.81	0.12	0.82	0.12	0.86	0.57
7	0.45	0.24	0.45	0.25	2.12	0.92
8	0.42	0.46	0.43	0.47	1.84	1.52
9	0.80	0.14	0.81	0.15	1.07	0.80
10	0.84	0.12	0.84	0.12	0.82	0.63
11	0.92	0.17	0.93	0.17	0.26	0.85
12	0.69	0.22	0.70	0.22	0.67	0.78
13	1.02	0.14	1.02	0.14	-0.12	0.85
14	0.94	0.10	0.95	0.10	0.31	0.60
15	1.19	0.18	1.20	0.18	-1.19	0.91
16	0.84	0.18	0.85	0.18	0.07	0.72
17	0.76	0.09	0.75	0.09	0.89	0.42
18	0.69	0.10	0.69	0.10	1.19	0.46
19	0.47	0.11	0.49	0.11	2.05	0.48
20	0.43	0.14	0.44	0.14	2.30	0.62
21	0.62	0.06	0.64	0.07	2.26	0.43
22	0.69	0.08	0.71	0.08	1.71	0.50
23	0.57	0.09	0.59	0.10	2.19	0.58
24	0.35	0.13	0.36	0.13	2.81	0.71
25	0.63	0.04	0.65	0.05	2.59	0.34
26	0.68	0.07	0.70	0.07	2.20	0.51
27	0.56	0.07	0.58	0.08	2.66	0.58
28	0.35	0.14	0.36	0.14	2.83	0.79
29	0.68	0.07	0.70	0.07	2.47	0.59
30	0.65	0.06	0.68	0.07	2.69	0.59
31	0.57	0.07	0.59	0.08	3.09	0.67
32	0.50	0.11	0.52	0.12	2.71	0.78

Table A.18. Continued.

Test Point	WFR, [10]	u_{WFR}, [10]	WFR, [11]	u_{WFR}, [11]	C_{eff}	$u_{C_{eff}}$
	[-]	[-]	[-]	[-]	[kN-s/m]	[kN-s/m]
33	0.65	0.07	0.66	0.08	1.47	0.40
34	0.64	0.08	0.66	0.09	1.63	0.42
35	0.51	0.08	0.54	0.09	2.23	0.45
36	0.45	0.11	0.47	0.13	2.48	0.69
37	0.68	0.06	0.69	0.06	2.03	0.41
38	0.67	0.05	0.68	0.05	2.22	0.35
39	0.44	0.05	0.46	0.06	3.94	0.46
40	0.37	0.06	0.39	0.07	3.97	0.57
41	0.59	0.06	0.63	0.07	3.38	0.62
42	0.63	0.04	0.67	0.05	2.87	0.42
43	0.51	0.05	0.55	0.06	3.47	0.50
44	0.39	0.07	0.41	0.07	3.55	0.54
45	0.63	0.05	0.66	0.06	3.24	0.49
46	0.62	0.06	0.66	0.07	3.28	0.56
47	0.56	0.05	0.61	0.06	3.41	0.58
48	0.40	0.05	0.43	0.06	4.08	0.54
49	0.64	0.08	0.64	0.08	1.92	0.62
50	0.63	0.07	0.65	0.08	1.94	0.55
51	0.51	0.05	0.56	0.07	2.57	0.46
52	-	-	-	-	-	-
53	0.71	0.04	0.70	0.05	1.77	0.34
54	0.65	0.05	0.66	0.06	2.12	0.46
55	0.49	0.04	0.52	0.05	3.36	0.40
56	-	-	-	-	-	-
57	0.70	0.04	0.70	0.04	2.34	0.42
58	0.65	0.04	0.65	0.05	2.67	0.44
59	0.49	0.04	0.51	0.05	4.14	0.47
60	-	-	-	-	-	-
61	0.57	0.03	0.62	0.04	4.21	0.45
62	0.60	0.03	0.66	0.05	3.49	0.43
63	0.46	0.04	0.51	0.05	4.19	0.48
64	-	-	-	-	-	-

APPENDIX B: WHIRL FREQUENCY RATIO

As mentioned in Section 7.2.3 cross-coupled mass terms of opposite sign are destabilizing. The traditional definition of WFR given in Eqs. (4)-(5) does not account for M_{XY} and M_{YX}. From San Andrés [11], WFR (Φ) that accounts for cross-coupled virtual mass is

$$\Phi^4 I_4 + \Phi^2(I_2 - 1) + \Phi_0^2 = 0 \tag{B.1}$$

where

$$\Phi_0^2 = \frac{(K_{eq} - K_{XX})(K_{eq} - K_{YY}) - K_{XY}K_{YX}}{\omega^2(C_{XX}C_{YY} - C_{XY}C_{YX})} \tag{B.2}$$

and

$$K_{eq} = \frac{K_{XX}C_{YY} + K_{YY}C_{XX} - K_{XY}C_{YX} - K_{YX}C_{XY}}{C_{XX} + C_{YY}} \tag{B.3}$$

I_4 is

$$I_4 = \omega^2 \frac{I_1^2 - M_{XY}M_{YX}}{C_{XX}C_{YY} - C_{XY}C_{YX}} \tag{B.4}$$

where

$$I_1 = \frac{C_{YX}M_{XY} + C_{XY}M_{YX}}{C_{XX} + C_{YY}} \tag{B.5}$$

Finally, I_2 is

$$I_2 = \frac{K_{XY}M_{YX} + K_{YX}M_{XY} - I_1(K_{XX} + K_{YY}) + 2K_{XY}I_1}{C_{XX}C_{YY} - C_{XY}C_{YX}} \tag{B.6}$$

APPENDIX C: UNCERTAINTY ANALYSIS

Instrument error is assumed to be negligible and only repeatability is calculated for the uncertainty of measurements. A 95% confidence interval is used to calculate the uncertainties for static measurements and the dynamic stiffness values. The true mean, μ, of a set of sample measurements, x_i, lies within the confidence interval

$$\bar{x} - t_{\alpha/2,\nu}\frac{S_x}{\sqrt{n}} < \mu < \bar{x} + t_{\alpha/2,\nu}\frac{S_x}{\sqrt{n}} \tag{C.1}$$

where $\bar{x}$ is the sample mean, $t_{\alpha/2,\nu}$ is the Student's *t*-distribution value, the level of significance is $\alpha = 1 - c$, c = 0.95 is the level of confidence, the degrees of freedom are $\nu = 1 - n$, and n is the number of samples. The standard deviation is

$$S_x = \sqrt{\frac{(\sum_{i=1}^{n} x_i^2) - n\bar{x}^2}{n-1}} \tag{C.2}$$

Recalling Eqs. (15)-(18) of Section 5.2 used to calculated the rotordynamic coefficients from curve fits to the dynamic stiffness data, the confidence intervals on the rotordynamic coefficients are determined using a statistical test described in [30]. The true slope of a least-squares regression lies within the *c*% confidence interval

$$b \pm t_{\alpha/2,\nu}\frac{s_{y/x}}{S_{xx}} \tag{C.3}$$

where the standard error of the y-data about the curve fit is

$$s_{y/x} = \left(\frac{1}{n-2}\sum_{i=1}^{n}[y_i - y(x_i)]^2\right)^{1/2} \tag{C.4}$$

and the total squared variation of the independent variable, x_i, is

$$S_{xx}^2 = \sum_{i=1}^{n} (x_i - \bar{x})^2 \tag{C.5}$$

Finally, the true intercept lies within the interval

$$a \pm t_{\alpha/2,\nu} s_{y/x} \sqrt{\frac{1}{n} + \frac{\bar{x}^2}{S_{xx}^2}} \tag{C.6}$$

Confidence intervals of the rotordynamic coefficients are propagated into the confidence intervals on the WFR and C_{eff} values. Uncertainty propagation is defined as

$$u_y = \sqrt{\left(\frac{\partial y}{\partial x_1} u_1\right)^2 + \left(\frac{\partial y}{\partial x_2} u_2\right)^2 + \cdots + \left(\frac{\partial y}{\partial x_n} u_n\right)^2} \tag{C.7}$$